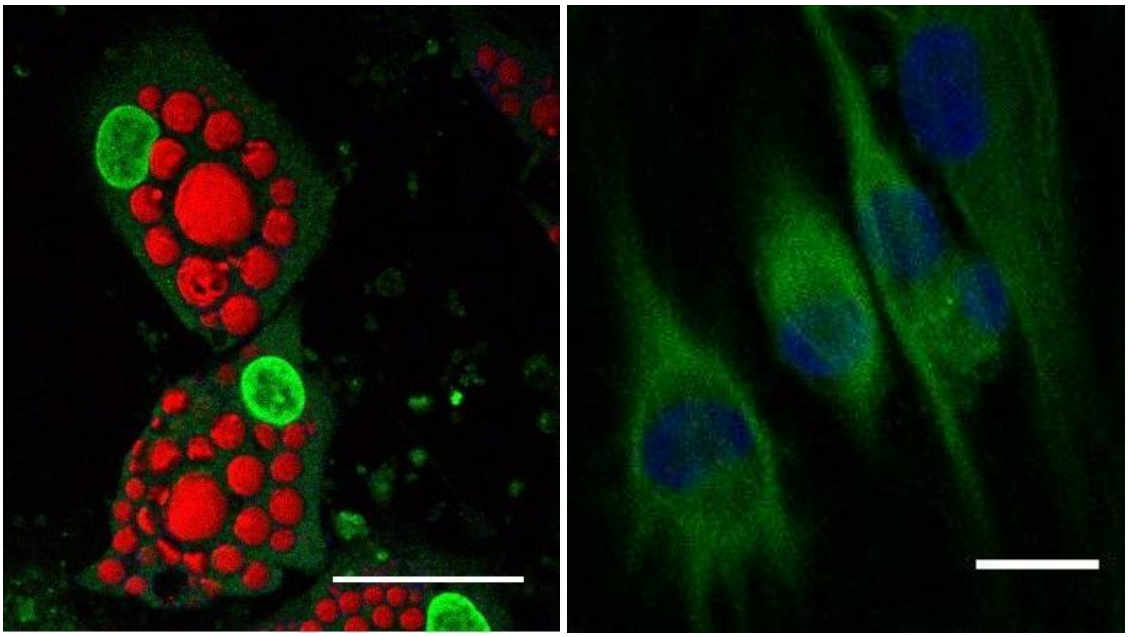

# Evaluation of ELP, collagen and laminin hydrogel composites to support *in vitro* differentiation of hADSCs toward adipocytes and β-cells

MARIA ÅSTRÖM
ROBIN DAHLÉN

Chalmers University of Technology, Gothenburg
AstraZeneca R&D Discovery Sciences, Mölndal
Sweden, 2015

MASTER'S THESIS

# Evaluation of ELP, collagen and laminin hydrogel composites to support *in vitro* differentiation of hADSCs toward adipocytes and β-cells

Master's Thesis within the *Biotechnology* programme

MARIA ÅSTRÖM
ROBIN DAHLÉN

SUPERVISORS
Alexandra Paul
Chalmers University of Technology, Gothenburg
Diana Ribeiro
Chalmers University of Technology, Gothenburg and
AstraZeneca R&D, Discovery Sciences, Mölndal

EXAMINER
Annika Enejder
Chalmers University of Technology, Gothenburg

Department of Biology and Biological engineering
CHALMERS UNIVERSITY OF TECHNOLOGY
Gothenburg, Sweden 2015

# Evaluation of ELP, collagen and laminin hydrogel composites to support *in vitro* differentiation of hADSCs toward adipocytes and β-cells

Master's Thesis within the Biotechnology Masters Programme

MARIA L. ÅSTRÖM
ROBIN T. DAHLÉN



Department of Biology and Biological engineering
Chalmers University of Technology
SE-412 96 Gothenburg
Sweden
Telephone + 46 (0)31-772 10 00

In collaboration with AstraZeneca AB
R&D, Discovery Sciences
SE-431 83 Mölndal
Sweden
Telephone: +46 (0)31-776 10 00

Cover:
Left image: Cells visualized with multimodal microscope after 13 days of differentiation from hADSCs toward adipocytes. Lipid droplets in red (CARS), Hoechst in green (MPEF) and perilipin in blue (MPEF). Scale bar 30 µm.
Right image: Cells visualized with 20x confocal microscope after 16 days of differentiation from hADSCs toward β-cells. Nucleus in blue (Hoechst) and insulin in green (Alexa Fluor 488). Scale bar 30 µm.

Printed at the department of Biology and Biological engineering,
Chalmers University of Technology, Gothenburg, Sweden 2015

Evaluation of ELP, collagen and laminin hydrogel composites to support *in vitro* differentiation of hADSCs toward adipocytes and β-cells

MARIA ÅSTRÖM
ROBIN DAHLÉN

Department of Biology and Biological engineering
Chalmers University of Technology

# ABSTRACT

Drug discovery typically involves studies on animal models as proxies for human beings followed by three phases of clinical studies, which result in frequent late rejections due to interspecies differences, present moral issues and requires extensive administration. Hence, large efforts are made to develop *in vitro* drug screening assays based on human cells, which provide detailed information on intracellular processes and enable high-throughput analysis of multiple drugs in parallel. Assays mimicking metabolic diseases such as diabetes and obesity are of particular interest, due to their increasing prevalence and due to important interspecies differences in metabolic pathways. However, it becomes increasingly clear that cells grown *in vitro* on conventional flat surfaces have difficulties maintaining their native, mature functionalities and eventually develop artificial phenotypes. For that reason, we have evaluated tissue-mimicking, protein-composite hydrogels for three-dimensional growth and differentiation of human adipocytes-derived stem cells (hADSCs) toward (i) adipocytes and (ii) β-cells. The proteins collagen I, laminin isoforms 411 and 511 and recombinant-engineered elastin-like proteins (ELP) have been investigated in detail, individually as well as in mixes. Their different amino-acid sequences coding for cell attachment/interaction, attractive material properties (i.e. soft and hydrated) together with the three-dimensional encapsulation are intended to mimic the native microenviroment, and thereby drive the differentiation and cellular maturation. The metabolic activity, viability and function of the differentiated cells were analyzed with cellular assays. Further, the tissue-mimicking samples were evaluated with non-linear microscopy; multi-photon excitation fluorescence (MPEF, autofluorescence and stains), coherent anti-Stokes Raman scattering (CARS, cellular lipid content) and second harmonic generation (SHG, collagen fibers). The assays and MPEF microscopy revealed that cells do not thrive in the ELP hydrogels crosslinked with amine-reactive THPC, probably due to cytotoxicity of the crosslinker and as the hydrogel seems not to permit cellular expansion. In contrast, cells in collagen and collagen/ELP matrices were successfully differentiated into adipocyte-like cells, confirmed by the presence of excessive amounts of lipid stores co-localized with perilipin. Insulin-positive cells were found in the collagen and collagen/laminin matrices. Hence, different collagen mixes seem to be promising hydrogel materials for three-dimensional growth of hADSCs for metabolic drug screening.

**Keywords:** 3D scaffold, Adipocytes, β-cells, collagen, diabetes, ELP, hADSCs, laminin, non-linear microscopy, obesity

# ABBREVIATIONS

| | |
|---|---|
| HAc | Acetic acid |
| CARS | Coherent Anti-Stokes Raman Scattering |
| DMEM | Dulbecco's Modified Eagle Medium |
| ECM | Extracellular matrix |
| ELISA | Enzyme-linked immunosorbent assay |
| ELP | Elastin-like protein |
| EthD-1 | Ethidium homodimer-1 |
| GSIS | Glucose stimulated insulin secretion |
| hADSCs | Human adipose-derived stem cells |
| ICC | Immunocytochemistry |
| LM | Laminin |
| mAb | Monoclonal antibody |
| MPEF | Multiphoton excitation fluorescence |
| NaOH | Sodium hydroxide |
| OPO | Optical parametric oscillator |
| pAb | Polyclonal antibody |
| SHG | Second harmonic generation |
| THP | Trishydroxymethyl phosphine |
| THPC | Tetrakis(hydroxymethyl)phosphonium chloride |
| Wt% | Weight percent |

# CONTENTS

# 1. INTRODUCTION

Throughout the history of modern medicine, scientists have tried to understand diseases that cause discomfort or eventually could lead to death for the patients if remained untreated. With all diseases that are still uncured today it is easy to overlook the improvements that have been accomplished for human health. By global immunization, Smallpox has been eradicated[1] and vaccination coverage of diseases such as Diphtheria, Measles and Poliomyelitis reached 84% in 2013.[2] Further, alleviating medicines have been developed for many other diseases enabling the patients to live a long and high quality life.

Diabetes Mellitus, or short diabetes, is an example of such a disease that has not yet been cured but is treatable nowadays. In 1869, diabetes was still a dreaded disease with deadly outcome. It was at that time Paul Langerhans, a German medical student, examined a sample of pancreatic tissue and observed clusters of cells within the tissue which had an unknown function. Later, it was revealed that these cell clusters played a huge role in the understanding of diabetes since they contain β-cells, the insulin secreting cell type.[3]

The next breakthrough in diabetes research was attained in 1921 by the Canadian doctor Frederick Banting and his assistant Charles Best who conducted experiments on dogs.[4] By removing the pancreas of one dog, the animal started to develop typical diabetes symptoms i.e. excessive drinking and urinating while also having high blood sugar levels. Simultaneously they extracted and isolated a substance from the pancreas of a healthy dog. As the substance was injected into the diabetic dog, Dr. Banting and Mr. Best could observe how the blood sugar in the diseased dog dropped and the overall health improved. Through further purification and intensive work the team enabled the first diabetic person in history to be treated by insulin shots in the beginning of 1922.[4] This was a major breakthrough and the starting point of modern diabetic treatment.[5] The discoveries in the 1920´s have saved millions of lives during the years but since diabetes is such a complex disease it is not completely understood and many people still die of it as a primary cause. In 2012 this number were estimated to 1.5 million world-wide.[6] More knowledge about the disease has revealed that even though insulin injections help with the primary symptoms, it does not prevent secondary diseases. These secondary diseases can be cardiovascular diseases such as heart attacks and strokes or kidney failures due to excessive blood filtration during high blood sugar levels.[7]

Diabetes can be grouped into different types, with only type I and type II discussed in this work, and are categorized by the cause of hyperglycemia (high blood sugar). The causes of type I diabetes are still debated but characteristic for these patients is that they rely on exogenous insulin replacement due to lack of own production. In the majority of the cases this is because of an autoimmune response caused by a series of defect functions inside of their bodies in places such as the thymus, bone marrow, immune system and the insulin producing β–cells.[8,3] Type II diabetes comprises 90% of all cases of diabetes and is characterized by the incapability for the body to utilize insulin in the blood stream and failure of the pancreas to compensate for this inability.[9] This disease type has been considered as a disease only affecting adults but in recent years, cases of children with the disease have also been reported.[10] Obesity and inactivity are risk factors highly associated with type II diabetes[9] and therefore also a trigger for secondary diseases. As obesity and type II diabetes accelerates all over the world more scientists focus their research on studying the adipose tissue and their adipocytes.[11] In 2014, the World Health Organisation estimates that 600 million people suffer from obesity with a body mass index above 30.[12] Even though many of the cellular mechanisms connecting obesity to the effects on insulin resistance and diabetes have been

investigated[13], medicine to reverse the illness remain to be discovered. A healthy lifestyle based on diet and physical activity has shown to be the most effective way to reduce the symptoms and improve glucose tolerance.[14] Treatment with substances that manage hyperglycemia have also been investigated and shown positive results on cardiovascular diseases connected with diabetes type I, but remain sparse regarding diabetes type II.[15] The adipocyte cells in adipose tissue increase in size during weight gain and triggers a state of chronic inflammation with metabolic changes as result.[16] To study these changes and enable drug screenings on these cells, improved models to attain mature adipocytes *in vitro* are crucial.

To get a better understanding of how drugs affect diabetes and related diseases *in vivo*, it is desirable to develop reliable *in vitro* drug screening platforms which enable characterisation of disease-related drugs. Normal two-dimensional (2D) substrates for cell studies do not provide the complex *in vivo* microenvironmental effects, such as the extracellular matrix (ECM) and matrix-cell interactions. Both adaptation and lack of stimuli from all directions in this non-native topography have shown to change the cellular behaviour and structure.[17] With three-dimensional (3D) scaffolds, the ECM can be more explicitly mimicked and more tissue-like results can be obtained.[17]

In this project evaluation of how 3D hydrogel scaffolds formed by mixtures of elastin-like protein (ELP), collagen and laminin affect human adipose-derived stem cells (hADSCs) were performed. ELPs provide mechanical and biological similarities to the elastin-rich ECM, as well as containing cell binding sites.[18] This sequence is a fibronectin derived motif with three specific amino acids R-G-D (arginine, glycine and aspartic acid) which provides attachment sites for cells.[19] Collagen is a major component in the ECM for adipocyte tissue meanwhile collagen IV is the most abundant isoform in pancreas.[20] Laminins are glycoproteins which are a major component in the basement membrane in the pancreas and an important regulator for cellular function.[21]

### 1.1. Aim

By mixing different amounts of ELP, collagen and laminin the aim of the project is to evaluate the best suited composition for proliferation and differentiation of hADSCs into adipocytes and β-cells. Structural examination of hydrogels and cells will be performed with microscopy techniques (CARS, SHG, MPEF and confocal) complemented with cell-biological assays to verify cell viability, metabolic activity, tissue-like functionalization and differentiation.

## 2. BACKGROUND

This section describes the tissues involved with the cell types investigated and proteins important to these tissues. The differentiation process of the cell types are also described, as well as the microscopy techniques used to analyze the results.

### 2.1. The adipose tissue

The human body contains two types of adipose tissues with distinctly different tasks[22], brown adipose tissue (BAT) and white adipose tissue (WAT). BAT exists to keep a balanced body temperature and produce heat when the body is experiencing cold temperatures, by metabolizing fat. WAT is instead responsible for energy storage. BAT is morphologically different from WAT mainly by the lipid droplet structure in the cells. BAT adipocytes contain

several smaller droplets while adipocytes in WAT contain one single lipid droplet covering almost the entire cytosol. The focus in this project will be on WAT, which is more abundant in obesity related aspects and also the main target for drug discovery. This type of adipose tissue, as mentioned, is to store fat when intake is larger than then the metabolic output. Storage is accomplished by either lipogenesis or uptake of fatty acids and in times of deprivation of energy, WAT mobilizes the fatty acids by lipolysis. WAT is located in different areas in the body as intra-abdominal tissue (surrounding organs) or subcutaneous tissue (under the skin). Excess fat storage is linked to diabetes type II[23] and inflammation in the adipose tissue. This inflammation alters the behavior of the adipocytes and other constituents of the adipose tissue. Obesity is lately considered to be an inflammatory disease of the white adipose tissue[24] and questions regarding how inflammation starts and how to cure this state on a cellular level need to be answered. Large scale gene-expression studies have shown that typical macrophage genes are transcribed in adipocytes of obese mice[25] and that macrophage recruitment during weight gain may lead to altered adipocyte function such as insulin resistance.[26] A drug screening model with mature adipocytes might play an important role in better understanding the regulatory mechanisms and effects of possible drugs.

## 2.2. The human pancreas

The pancreas is an organ which is considered both an endocrine and an exocrine gland in the human body.[27] Its exocrine function is to aid the digestive system by secreting enzyme-containing pancreatic fluid into the small intestine.[27] The endocrine compartment only contributes to 1-2% of the pancreas but is governed by cell clusters, called islets of Langerhans.[28] These islets secrete hormones which are responsible for the maintenance of blood sugar homeostasis.[28] There are five different cell types in the islets of Langerhans, all characterized by their secreted hormone. The α-cells produce glucagon, β-cells secrete insulin, δ-cells generate somatostatin, ε-cells secrete ghrelin and PP-cells produce pancreatic polypeptides.[29] The principal constituents of the islets are the β-cells and α-cells which approximately constitute 54% and 34% respectively of the total cell mass in human islets.[30] All these cells work together in a highly regulatory manner by activating and inhibiting cellular secretion upon exogenous signaling.[28] A high blood glucose concentration activates insulin production which in turns activates glucose uptake by cells in the peripheral such as liver, muscle and adipose tissues.[28] The endocrine pancreas also expresses vascular endothelial growth factor-A (VEGF-A) which promotes capillary growth within the tissue supplying the endocrine compartment with up to 5-7 times as much capillaries as the neighboring exocrine compartment.[31] The highly vascularized network also provides an environment where β-cells are closely interacting with 1-2 adjacent capillaries.[32] Each of these capillaries is surrounded by a basement membrane (BM) which provides structural support and influences cellular functions. The BM is a thin layer composed mainly of laminins and collagen IV, which self-assemble into a network and are connected with each other by nidogens.[33] It has been found that the BM embedding capillaries in humans differs from the BM found in mice.[21] Otonkoski *et al*. found that each vessel in mice is surrounded by a single membrane but in humans each vessel is actually embedded by two layers of BM, each with a specific composition of proteins. The endocrine BM sheath in humans is solely expressing laminin isoform 511 while the vascular sheath expresses both laminin 511 and 411.[21]

## 2.3. Extra cellular matrix protein overview

To mimic the native ECM, three proteins have been used in this project. Collagen and laminin are two extracellular proteins and ELP is a bioengineered protein with similarities with native elastin. These three proteins are more thoroughly described in this section.

### *2.3.1. Collagen*

There are more than 20 natural collagen types, and even more proteins exists that expresses collagen-like domains.[34] Collagen constitutes to almost 30% to the total protein content in in our body and is the major insoluble protein.[19] Collagen I, IV and VI are the most abundant in adipose tissue[22], where collagen I is a fibril forming collagen, collagen IV forms multi tetramer complexes and collagen VI forms beaded filaments. Disregarding the structure of the collagen type, the main purpose of collagens is to help various body compartments to tolerate and cope with stretching of the tissue.[35] Collagen I polypeptides forms triple-stranded molecules in the cell and are thereafter transported to the extracellular space where they spontaneously forms fibrils after C and N-terminus cleavage by proteases.[34] Because of its abundance in adipose tissue, collagen I is regarded as a suitable protein for hydrogel formation for adipocyte studies, since it mimics the ECM and therefore provides similar extracellular cues. Collagen I is widely used in hydrogel fabrication[36,37] since it is easily extracted from animal tissue. With its fibrous structure that is detectable with non-linear microscopy[38] (SHG) it is well suited for hydrogel matrices in this project.

### *2.3.2. Laminins*

Rupert Timpl *et al.* first discovered laminins (LM) as a constituent of BM in 1979[39] when investigating protein content of mouse sarcomas. Laminins have since then also been identified in humans[21] and in lower species such as worms and fruitflies.[40] The preservation of laminins throughout evolution indicates its importance for normal development and function which is confirmed by experiments with knockout mice possessing severe defects.[41] Laminins are hetrotrimeric glycoproteins consisting of one α-, β- and γ-chain. To date, at least 19 isoforms have been identified[40] and each isoform is named according to its composition of these chains e.g. laminin 111 is composed of α1, β1 and γ1 chains.[41] The N-terminus differs depending on isoform but generally they can be described to possess a globular domain (LN) followed by a tandem laminin epidermal growth factor-like domain. However, they all share a characteristic C-terminal end composed of five homologous global domains located at the α-chain. The three chains entwine and form a coiled-coil resulting in a T-shaped structure. An interruption of a few amino acids within the coiled-coil has been located on the β-chain which therefore is called the laminin β knob.[40] Laminins self-assemble and form a 2D network by mutual binding of LN-domains.[33] Even though the first protein in the laminin family was discovered 36 years ago, it was only in 1997 that Laminin 411 and 511 were characterized.[42] Laminin 411, a 569 kDa[43] protein, has been identified as a truncated protein lacking the LN-domain on the α-chain, effectively reducing the number of possible binding sites and may therefore negatively influence the self-assembled structure.[41] Laminin 511 on the other hand is a 766 kDa[43] isoform which seems to have an elongated N-terminus of the α-chain.[41]

### *2.3.3. Elastin-Like Protein (ELP)*

Elastin is an important extracellular protein giving flexibility in body tissues. Elastin-like proteins (ELPs) are recombinant proteins with varying properties that are becoming of interest for biomaterial production. Advantages include the possibility to produce tunable hydrogels with determined stiffness depending on cell type investigated.[44] Another advantage is the full

control from gene to product which reduce the batch-to-batch differences found in other hydrogel materials such as Matrigel.[45] The risk of contaminated samples due to animal harvested proteins is also removed with this production control. ELP, developed at Stanford University (Heilshorn biomaterials group), offers these possibilities. Several cell types have been investigated within this scaffold[18] of which some show promising results in both proliferation and differentiation. The adhesion site for cells normally found in fibronectin[46], the RGD sequence, consists of the three amino acids Arginine(R)- Glycine(G)- Aspartic acid(D), is inserted into the protein sequence. These motifs have shown to promote viability and a more spread morphology of different cell types.[47,48] A type of membrane proteins in cells, integrins, recognize the RGD sequence and this provides the cells with anchor points, signals for migration and polarity, differentiation and other signals.[49]

## 2.4. Tissue specific differentiation

Two different differentiations of hADSCs have been performed in this project, one toward adipocytes and one toward β-cells. Background explaining both events are presented below.

### *2.4.1. Adipocyte differentiation*

Two steps in the differentiation process from stem cell to adipocyte have been characterized.[22]
Determination phase: Stem cell conversion into cell lineage committed to adipose cells. At this point the ability to differentiate into other cell types than adipocytes is lost, but typical adipocyte characteristics are not yet developed.[22] Different words to describe the stem cells isolated from adipose tissue have been used, which may lead to confusion. The word preadipocyte has been used in the field leading to misinterpretations, since the cells are multipotent and can differentiate into several cell types.[50,51] Therefore the terminology in this thesis will be kept to hADSCs for the stem cells used. Cells with some degree of differentiation toward adipose cells will be referred to as adipocyte-like cells.
Terminal differentiation phase: Mature adipogenic markers are developed. Morphologically, lipid droplets forms and the shape of the cells turn more round. They start to produce molecules needed for adipogenic processes as transport, insulin recognition and secretion of specific proteins.[52] Over 2000 genes are connected to adipocyte behavior and regulation which have to be activated or silenced by a cascade of events during differentiation.[22] The most important transcriptional changes include the proteins C/EBP-β and C/EBP-δ that are early induced in adipocyte differentiation.[53] These then induce PPAR-γ and C/EBP-α which are responsible for the consequent activation of several downstream factors that are important for adipocyte behavior.[54] PPAR-γ is though confirmed as the main protein for adipogenesis since no adipocyte behavior is seen if it is not present.[22] There are both similarities and differences between *in vitro* differentiated adipocytes and adipose cells matured *in vivo.* Lipolysis, insulin stimulated glucose uptake and lipid accumulation occur in both *in vitro* and *in vivo* adipocytes.[55] One major morphological difference between *in vitro* differentiated adipocytes and mature adipocytes is the lipid droplet arrangement. *In vitro* adipocytes have multiple lipid droplets and comparably large cytoplasmic volume, where as a mature adipocyte usually have one large single lipid droplet covering almost the entire cytoplasm.[11] This difference suggests that protocols to fully differentiate adipose derived stem cells to mature adipocytes needs improvement. This could lead to the understanding of the mechanisms behind adipogenesis and drive cellular experiments for drug screening forward. Terminology in this thesis will be *in vitro* adipocytes or adipocyte-like cells when the morphology resembles that with multiple lipid droplets. If compared to *in vivo* adipocytes the

term mature adipocytes will be used to refer to cells with one large single lipid droplet. Figure 1 shows an illustration of lipid accumulation from stem cell to mature adipocyte. In the last stage, one large lipid droplet covers almost the entire cell and the third stage resembles the phenotype of *in vitro* differentiated adipocytes.

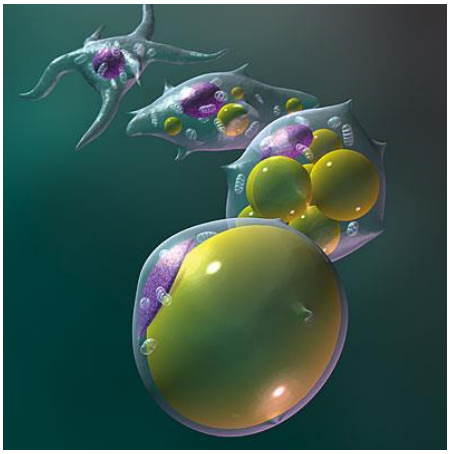

**Figure 1.** Illustration "Adipogenesis" by Gary Carlson. Nucleus (purple) and lipid droplets (yellow). © 2013 Gary Carlson, permission to use given 2015-03-05. www.gcarlson.com

### *2.4.2. β-cell differentiation*

The differentiation of hADSCs towards β-like cells has been characterized in a stepwise differentiation[56] since the hADSCs are multipotent mesenchymal stroma cells[57] and needs to be driven towards endodermal cells in order to become insulin producing cells.[58] This has been achieved by first growing the cells in three different media, in this report referred to as M1, M2 and M3. In the first phase of the differentiation these cells needs to become definite endoderm and are therefore exposed to M1. In this stage, the cells start to express HNF-3/FoxA2 which is a typical endoderm marker. At day three of differentiation, media is changed to the taurine supplemented M2 medium. Taurine is a non-essential amino acid which has been shown to be an important factor for β -cell development and maturation.[59] By this phase of the differentiation, the cell will start to express PDX1 and NKX6.1[60] which indicates pancreatic endoderm stage. After two days of culture with M2 another media change is made exposing the cells to M3 medium throughout the remaining time of the differentiation. By the end of differentiation the hADSCs have become β-like cells with upregulated expression of the transcription factor PDX1, which is involved in pancreatic development, while also expressing their own insulin upon exogenous glucose stimuli. In Figure 2 an overview of the differentiation scheme is presented.

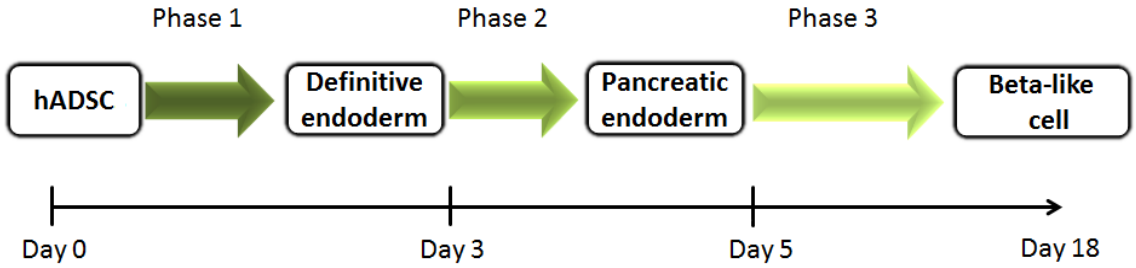


**Figure 2.** An overview of the differentiation scheme of hADSCs toward β-like cells. The time line defines the days of culture. The three different phases during differentiation all involves a specific growth medium.

## 2.5. Microscopy techniques

This section explains the different microscopy techniques used in this report in more detail. First Multiphoton excitation fluorescence (MPEF) is explained, followed by Coherent anti-Stokes Raman scattering (CARS) and lastly Second harmonic generation (SHG). Figure 3 describes, with Jablonski diagrams, how electrons are excited and how measureable photons are generated in each method.

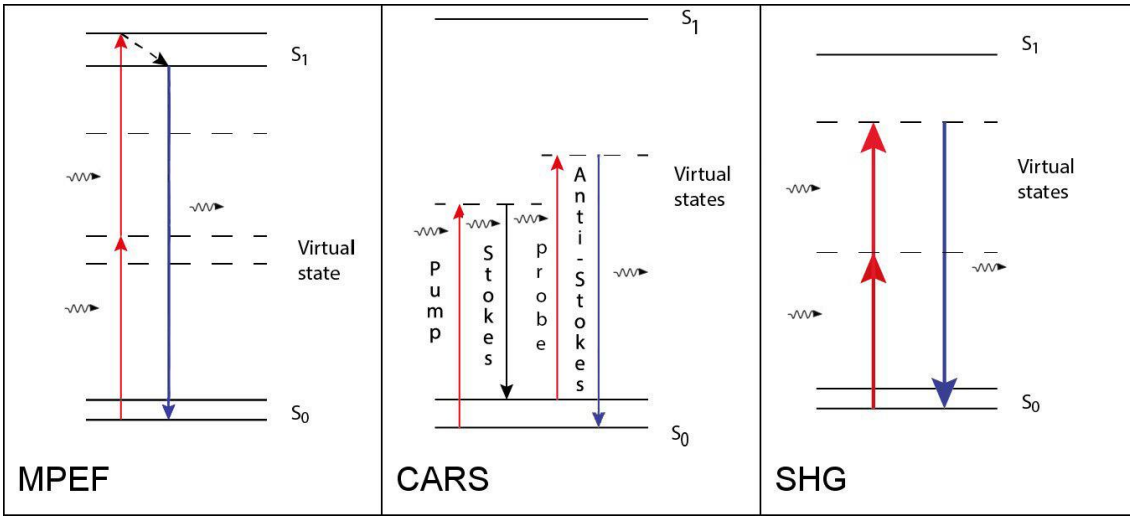


**Figure 3**. Jablonski diagram for the multiphoton excitation fluorescence (MPEF), Coherent Anti-Stokes Raman Scattering (CARS) and Second harmonic generation (SHG). The ground state and excited state of the electron is denoted $S_0$ and $S_1$ respectively. The dashed lines illustrate virtual states. The waved arrows represent the incoming and outgoing photons.

### *2.5.1. MultiPhoton Excitation Fluorescence (MPEF)*

In conventional fluorescence microscopy the illuminating light passes through a filter which selectively only passes wavelengths which excites the fluorophore of choice. The emitted wavelengths from the molecule pass through another filter selective for the emission wavelengths. Internal conversion within the molecule causes energy losses resulting in lower energy photons emitted than those which excite the molecule, a phenomena called the Stokes shift.[61] Confocal microscopes only detect light which is emitted by the fluorophores at the focal plane within the specimen. This is achieved by pinholes placed in the focal plane of the rays emitted from the specimen.[62] Due to these pinholes, rays that are not in focus in the sample will not be in focus at the pinholes either and therefore mostly excluded from the detector.[62] Another advantage with the pinholes is that the point spread function is reduced

which improves the resolution.[63] In this kind of setup, a fluorophore is excited with one photon of specific wavelength, which is called one-photon excitation fluorescence.

In MPEF on the other hand, two or more photons are absorbed and excite an electron within the fluorophore. Less energetic photons in the infrared range can be used to reach a similar excitation compared to the single photon excitation. This technique allows for higher depths of penetration and less scattering in the sample. Additionally, photo damage and bleaching are reduced.[64] The emission process after internal conversion is the same as for conventional fluorescence microscopy and hence when the electron returns to its ground state a photon is emitted with lower energy than the sum of the ingoing photons.[65] Many endogenous cellular components emits fluorescent signals when exposed to light of a distinct wavelength.[66] According to Monici, organelles such as lysosomes and mitochondria contribute most to this autofluorescence since they contain molecules of certain properties such as the pyridinic NADPH. Zipfel *et al.* have reported several endogenous molecules excited in two-photon microscopy that also emits photons with wavelengths in the green spectra.[67]

### *2.5.2. Coherent anti-stokes Raman Scattering (CARS)*

Chemical bonds have characteristic vibrational frequencies, which depend on the atoms as well as the type of bond between them. In Raman microscopy these properties are measured as a change of frequency of an incident photon, called inelastic Raman scattering. A laser illuminates the sample and some of the light shifts in frequency. If a molecule absorbs energy from the photon the outgoing light is red-shifted compared to the ingoing light, and called Stokes scattering. If the photon absorbs energy from the molecule the light is blue-shifted compared to the ingoing light, and called anti-Stokes Raman scattering. The shift measured over a spectral range can be seen as a chemical fingerprint of the molecules in the sample.[68] Since most of the light is unaffected and transmitted through the sample, Raman microscopy requires long integration times and high laser powers which for living systems is a major drawback.[69] CARS microscopy overcomes the problems of weak signals since the molecular vibrations are coherently driven by a wave mixing process consisting of a pump beam ($\omega_p$), Stokes beam ($\omega_s$) and probe beam ($\omega_{pr}$) which usually have the same wavelength as the pump beam. If the difference between $\omega_p$ and $\omega_s$ correspond to the energy of a Raman active vibrational bond, an anti-Stokes signal ($\omega_{as}$) is generated according to:

$$\omega_{as} = \omega_p + \omega_{pr} - \omega_s \qquad \text{(Eq. 1)}$$

This signal is considerably stronger than Raman scattering allowing visualization of unlabeled samples with high chemical sensitivity. CARS is specifically good at imaging lipids commonly found in cells and tissues which are often hard to visualize due to their small size and difficulties in labelling without altering their properties. Adipose tissue, for example, contains a lot of lipids with multiple $CH_2$-groups which have a vibrational signature at 2845 $cm^{-1}$.[70] With CARS, both transmission and reflectance setups are possible and 3D sectioning is possible, granting visualization of thick samples, up to 400 µm.[70] The outgoing light is easily distinguishable from fluorescence and Second Harmonic Generation (SHG) due to its higher wavelength where it has low disturbance from other light. One limiting aspect of the method is the so called non-resonant background, giving low signal to background ratio in the detection. Weak signals from objects smaller than the optical wavelength are therefore better detected in the epi direction where backscattered light gives a strong signal.[71] Early improvements of the CARS microscopy technique was performed by Zumbusch *et al.*[72] when introducing near-infrared pulses, high numerical apertures and an optical oscillator/amplifier. These longer wavelengths, compared to earlier lasers in the visible range, softened the phase-

matching condition making CARS microscopy possible.[70] This also reduce the Rayleigh scattering, making it possible to image thicker samples.[72]

### *2.5.3. Second Harmonic Generation (SHG)*

SHG is a light-matter interaction, where the matter facilitates a frequency doubling of the incoming light waves. Frequency-doubling results in half the wavelength of the origin photon according to the formula:

$$\lambda = \frac{c}{\nu} \qquad \text{(Eq. 2)}$$

where λ corresponds to the wavelength, c is the speed of light and ν is the frequency. The nonlinear signal of the SHG is in the order of the square of the incoming laser intensity, which gives signal mainly in the focus of the objective since the power is highest there. This enables high depth 3D imaging.[73] From quantum mechanical equations it can be understood that resonance only occurs in non-centrosymmetric structures[74] and it is therefore suitable for visualisation of non-labelled collagen fibers which comprise these characteristics.

# 3. METHOD AND MATERIALS

This section first describes the methods and materials used for the differentiation processes. Afterwards, each of the cellular assays performed in this project are explained. Finally, the multimodal microscope, used for visualizing the samples, is described.

## 3.1. Adipocyte differentiation

Differentiation of hADSCs towards adipocytes was performed in two stages (Figure 4).[11] Two time points have been performed for each seeding. The first one was done before differentiation media was added at day 2, to analyze cell proliferation at an early stage. The second time point was performed at the end of the protocol at day 13 to evaluate differentiation and viability.

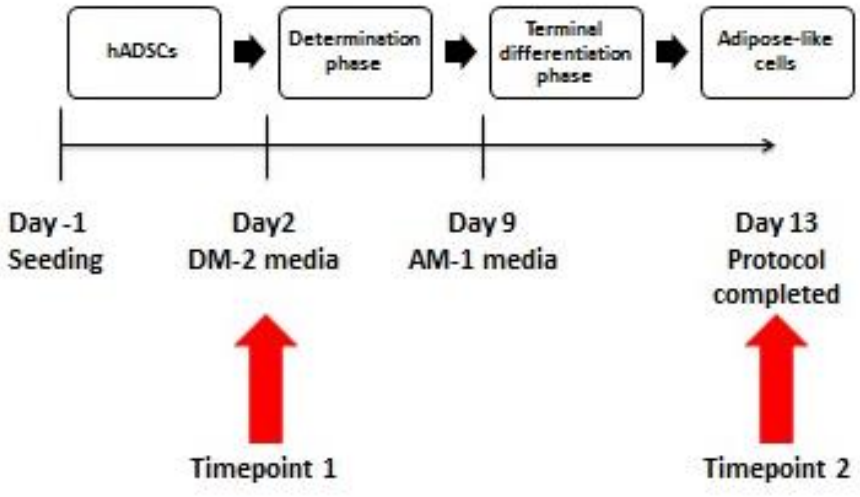


**Figure 4.** Schematic overview of the procedure for differentiation of hADSCs toward adipocytes.

### *3.1.1. First seeding – ELP/Collagen hydrogels*

The first seeding evaluates the impact on cell proliferation and differentiation of hydrogel compositions consisting of different ratios of collagen and ELP. The conditions for this differentiation study are presented in Table 1. Twelve wells per condition were used for the different assays. These assays include live/dead staining, metabolic activity assay (MTS) and Pico-Green DNA assay. Hydrogels for nonlinear microscopy were also included. Glass-bottom plates (Invitro Scientific, catalogue number: P384-1.5H-N) were used for the two time points, due to multimodal microscopy requirements. hADSCs (Batch 140304 P=3) were seeded in enriched endothelial growth medium-2 (EBM-2) (Lonza, catalogue number CC-3156). A cell suspension was counted in Cedex HiRes cell counter (Innovartis). A cell concentration of 2000 cells/µl was prepared prior to seeding and hydrogels, each of 5 µl, were used.

Collagen I Rat Tail tendon (2.92 mg/mL, Merck Millipore, catalogue number: 08-115, lot number: 243504) was used in collagen coating as well as for all hydrogels composed of collagen. For coating, collagen I diluted in 0.02 M acetic acid (HAc) was filter sterilized prior to 1 hour incubation time at room temperature. This procedure was performed one day prior to seeding to reduce the laboratory time for the seeding. Coating was included in the experiment as a 2D control to assess viability and differentiation. All wells for hydrogels were also pre-coated with the same concentration. For collagen I hydrogels, sodiumhydroxide (NaOH) was included before seeding to increase the pH of the storage solution leading to spontaneous formation of collagen fibres. Two different crosslinking temperatures were examined to investigate the effect of fiber diameter and pore size on differentiation. Lower crosslinking temperatures have been shown to increase pore size and diameter of the collagen fibers.[75] Collagen I was mixed with cell media and NaOH on ice and instantly pipetted into well to avoid gelation prior to pipetting.

For ELP hydrogels, the crosslinker Tetrakis(hydroxymethyl)phosphonium chloride (THPC) was used. This compound crosslinks the amine groups of ELP creating a hydrogel composed of a protein network.

Mixtures of collagen I and ELP at ratios 25/75, 50/50, 75/25 and pure ELP 5wt% were used. These mixes were chosen to explore how hADSCs proliferate and differentiate while increasing ELP concentration/RGD content stepwise. A stock solution of 10wt% UV-sterilized ELP (Stanford University), dissolved overnight in 1x Dulbecco's phosphate-buffered saline (1xDPBS) was prepared prior to seeding. Collagen I, ELP, cell media, NaOH and THPC were mixed on ice and instantly pipetted into well for gelation. Cells were added after gelation of hydrogels to investigate survival on top of the matrices. Studies have shown that the ratio between ELP and THPC determine the stiffness of the hydrogel.[76] For the first differentiation, a ratio of 1:2.4 between amine groups in ELP and reactive groups of THPC was used. The first differentiation medium was added to wells at day 2, and media changes with this medium were performed every second day. At day 9, the second differentiation medium was added followed by one media change prior to completion of the differentiation protocol at day 13.

**Table 1. Conditions used for first seeding**

| Compound/Mix | Concentration | Gelation temperature |
|---|---|---|
| Collagen coating | 50 µg/ml | - |
| Collagen I hydrogel | 1.5 mg/ml | 4°C |
| Collagen I hydrogel | 1.5 mg/ml | 37°C |
| ELP/Collagen hydrogel (25/75) | 1.25wt% / 0.375 mg/ml | 37°C |
| ELP/Collagen hydrogel (50/50) | 2.5wt% / 0.75 mg/ml | 37°C |
| ELP/Collagen hydrogel (75/25) | 3.75wt% / 1.125 mg/ml | 37°C |
| Pure ELP 5wt% hydrogel | 5wt% | 37°C |

### *3.1.2. Second seeding*

Based on the result from the first differentiation, several changes were made in the hydrogel compositions (Table 2). Cells were encapsulated inside the hydrogels in an effort to mimic the natural surroundings of *in vivo* adipocytes. The weight percent of ELP in the hydrogels were lowered from 5wt% to 3wt% to provide a less stiff material more suitable for adipogenic differentiation. The ratio of THPC reactive groups to ELP amines was therefore also lowered from 1:2.4 to 1:1.4. This lower THPC concentration should give an elastic moduli closer to 1.5 kPa in a 3wt% ELP hydrogel.[44] Another possible advantage with the lower crosslinker concentration is reduced toxicity from this compound. Cell concentration was increased from 2000 cells/µl to 6000 cells/µl for all conditions except the cells incorporated in ELP hydrogel. For these hydrogels a concentration of 50,000 cells/µl was used, based on information attained by personal communication with prof. Sarah Heilshorn, Biomaterials Group, Stanford University. No coating was used prior to casting hydrogels to prevent misleading positive results rising from cells attaching to the coating instead of being incorporated in the hydrogel. ELP was used as 2D coating instead of collagen to investigate its properties on cellular differentiation on flat surfaces. Collagen I and ELP were allowed to adsorb in mixture overnight and crosslinked with NaOH. Collagen I hydrogel prepared as in seeding 1 (3.1.1) and the differentiation protocol was performed in the same manner as before. Wells for perilipin and stem cell surface marker CD105 immunostaining as well as neutral lipid staining (Bodipy) were included.

**Table 2. Conditions used for second differentiation**

| Compound/Mix | Concentration | Gelation temperature |
|---|---|---|
| ELP coating | 1 mg/ml | - |
| Collagen/ELP hydrogel | 1.5 mg/ml / 1.7wt% | 37 °C |
| Collagen I hydrogel | 1.5 mg/ml | 37 °C |
| ELP hydrogel (50,000 cells/µl) | 3wt% | 37 °C |
| ELP hydrogel (cells seeded on top) | 3wt% | 37 °C |

## 3.2. β-cell differentiation

Differentiation of hADSCs towards β-like cells were performed in three different phases with media formulation based on Chandra *et al*..[56] Two time points have been performed on each seeding, one at day 5 and one at the last day of differentiation. Assays used during time points are more thoroughly described in the sections below.

### *3.2.1. First seeding – ELP/Collagen hydrogels*

The initial seeding for this project was performed in order to evaluate how different compositions of ELP and collagen affected the cellular function and differentiation. Table 3 present the eight conditions examined.

**Table 3. Conditions for first seeding. Compounds, concentrations and gelation temperatures are stated.**

| Compound/Mix | Concentration | Gelation temperature |
|---|---|---|
| Collagen I coating | 50 µg/ml | - |
| ELP pure | 5wt% | 4 °C |
| Collagen I | 1.5 mg/ml | 4 °C |
| Collagen I | 1.5 mg/ml | 37 °C |
| ELP/Collagen I | 50/50 | 4 °C |
| ELP/Collagen I | 25/75 | 4 °C |
| ELP/Collagen I | 75/25 | 4 °C |
| Matrigel | 4.2 mg/ml | 37 °C |

ELP 10wt% stock solutions were prepared from UV-sterilized ELP powder (provided by Stanford, 80 min in UV light) mixed in 1xDPBS. The solution was stored at 4 °C overnight to ensure full solvation before use. Glass-bottom plates (Invitro Scientific, catalogue number: P384-1.5H-N), one for the first time point at day 5 and another for the second time point at day 18 were used during this experiment. Wells used in the experiment were coated one day prior to seeding with 30 µl of 50 µg/ml UV sterilized collagen I Rat Tail tendon (2.92 mg/mL, Merck Millipore, catalogue number: 08-115, lot number: 243504), diluted in 0.02 M HAc, for 45 minutes in room temperature. Thereafter, PBS (Life technologies, catalogue number: 10010) was added to each well and the plates were stored at 4 °C overnight. The wells were rinsed with PBS twice before seeding of cells. Thawed hADSCs (Batch 140304 P=3) were suspended in additive enriched endothelial growth medium-2 (EBM-2) (Lonza, catalogue number CC-3156), referred to as seeding medium. The cell number was counted in a Cedex HiRes cell counter (Innovartis) which also provided viable cell concentration, percentage viability, average diameter and aggregate percentage. A final cell concentration of 2000 viable cells/µl was prepared in microcentrifuge tubes for use in the hydrogels. All components were stored on ice when not used during the hydrogel mixing step to minimize the risk of gelation before casting. Collagen I, ELP and Matrigel (BD, CAT: 354230, Lot 3270647) were added to each microcentrifuge tube according to calculations. Lastly, 0.1 M NaOH and 13.95 mg/ml of the crosslinker THPC were added to each tube. The added amount of NaOH in each tube was 23 % of the collagen I volume – to promote fibrillogenesis by adjusting the pH – while the molar ratio between amine groups of ELP and hydroxyl groups of THPC was 1:2.4. Hydrogels of 5 µl were casted in each of the pre-coated wells. The plates were incubated on

cooling packs for 30 minutes prior to incubation in incubator (37 °C, 5% $CO_2$, 95% rH) for additionally 30 minutes. Fresh seeding medium, 50 µl, was added to each well after gelation and the plates were placed into incubator.

The day of seeding was nominated as day minus one, and differentiation protocol was initiated on the followed day. On day zero, as a first step in the differentiation towards endodermic cells the seeding medium was exchanged to a new medium (M1) which contained DMEN/F12 with sodium butyrate, penicillin streptomysin, Activin A and basic fibroblast growth factor (bFGF). The medium was renewed every day during the differentiation. At day three, the medium was changed to the second differentiation medium (M2) which contained Taurine in order to promote pancreatic endoderm. On day 5, the medium was exchanged again to a new medium (M3) which contained Taurine, GLP-1 and Nicotinamide to achieve mature β-like cells. The rest of the components in M1-M3 are stated in the reference.

Two time points were included in the differentiation, one at day 5 and one on day 18. In the first time point metabolic activity of the cells were analysed with a cell proliferation assay (Promega). A Picogreen assay was used to examine the double stranded DNA (dsDNA) content in wells used for the metabolic activity assay. The cellular morphology and viability were examined with Life technologies Live/dead kit. The cells used for live/dead staining and the cells in remaining wells were fixed by incubation in 4 % formaldehyde for 15 minutes at room temperature. After fixation imaging with non-linear microscopy were performed. For the second time point live/dead assay, proliferation assay and imaging with non-linear microscopy were performed. Image analyses have been performed in ImageJ.

### *3.2.2. Second seeding – Laminin hydrogels*

The second seeding was performed as the first seeding but with changes explained in this section. The hydrogels composition was changed based on experimental results from the first seeding and ELP optimization trials. The aim of this seeding was to investigate if laminins enhanced differentiation towards β-like cells and if isoform or mixes affected the end commitment result.

The additional laminin isoforms were LM 411 and LM 511 both purchased from Biolamina (product numbers: LN411-02, LN511-02). The collagen I concentration was reduced to 1.15 mg/ml in order to retain the hydrogel volume during LM incorporation. All hydrogels, including those with LM, have the same collagen I concentration in order to evaluate the effect of LM incorporation. The compositions and concentrations of the new hydrogels are stated in Table 4. For LM mixed hydrogels the concentration denotes the final concentration with isoforms in equal amount. The cell concentration was increased to 6000 cells/µl based on published data from Heilshorn's Lab.[77] The differentiation time was reduced and the second time point was performed at day 16 instead of day 18. During time points, the cell number and viability were examined with the CedexHiRes cell counter instead of the picogreen assay. An immunocytochemistry assay was performed for both time points. For the time point at day 16, cells were also stained with Bodipy and two additional assays were performed namely, glucose-stimulated insulin assay (GSIS) and C-peptide enzyme-linked immunosorbent assay (C-peptide ELISA).

**Table 4. Overview of second seeding hydrogels with concentration and gelation temperature stated. For the LM mixed hydrogels the concentration denotes the final concentration with each isoform in equal amounts.**

| Compound/Mix | Concentration | Gelation temperature |
|---|---|---|
| Collagen I | 1.15 mg/ml | 37 °C |
| Collagen I/ Laminin 411 | 1.15 mg/ml / 50 µg/ml | 37 °C |
| Collagen I/ Laminin 511 | 1.15 mg/ml / 50 µg/ml | 37 °C |
| Collagen I/ Laminin mix | 1.15 mg/ml / 50 µg/ml | 37 °C |
| Collagen I/ Laminin 411 | 1.15 mg/ml / 10 µg/ml | 37 °C |
| Collagen I/ Laminin 511 | 1.15 mg/ml / 10 µg/ml | 37 °C |
| Collagen I/ Laminin mix | 1.15 mg/ml / 10 µg/ml | 37 °C |
| ELP coating | 1 mg/ml | - |

## 3.3. ELP optimization

Between the first and second cell specific differentiation, a seeding to evaluate how different weight percentages of ELP and THPC concentrations impacted the cellular survival in the scaffolds was performed. To investigate cell viability and proliferation on 2D growth, well were also coated with the protein. Two different cellular concentrations, 6000 cells/µl and 4000 cells/µl, were included in this seeding in order evaluated how the cellular density affected the cellular survival in the 3D matrices. Collagen coating were included as controls for both of these cellular densities. Table 5 summarizes the conditions used in this seeding. The cells were cultured 3 days prior to examination with metabolic activity assay and live/dead staining.

**Table 5. An overview of the seeding details for the ELP optimization experiment. Cellular concentration, condition and crosslinker ratio are presented.**

| Cell concentration (cells/µl) | Condition | Crosslinker ratio (ELP: THPC) |
|---|---|---|
| 6000 | ELP coating | - |
| 6000 | 3wt% ELP | 1:1.4 |
| 6000 | 3wt% ELP | 1:0.7 |
| 6000 | 1wt% ELP | 1:1.4 |
| 6000 | Collagen coating | - |
| 4000 | ELP coating | - |
| 4000 | 3wt% ELP | 1:1.4 |
| 4000 | 3wt% ELP | 1:0.7 |
| 4000 | 1wt% ELP | 1:1.4 |
| 4000 | Collagen coating | - |

## 3.4. Toxicity evaluation

To evaluate the toxicity of the crosslinker THPC and to compare it to other crosslinkers, a toxicity seeding was performed after the second differentiation. At this point of the project, it was of interest to investigate if a crosslinker change could be beneficial for future studies. The three crosslinkers THPC, trishydroxymethyl phosphine (THP) (Sigma-Aldrich, product number: 177881) and Glutaraldehyde (Acros organics, product code: G/0518/PB08) were examined in both collagen and ELP hydrogels. These crosslinkers were chosen since they previously have shown to form hydrogels which supports cellular survival.[78,48] Both collagen hydrogel without crosslinker and an ELP coating was included in the experiment as controls. A stock solution of THPC was prepared from the 80wt% storage flask with 1.5 µl diluted in 345 µl PBS. THP was prepared with 2.3 mg in 205.7 µl PBS from a solution with concentration 8.05 mg/ml. Glutaraldehyde from a 25 % solution was diluted as 0.75 µl in 50 µl PBS to give a final hydrogel concentration of 0.075 %. For the live/dead assay, 2.4 µl Ethidium homodimer-1 (EthD-1) and 0.6 µl calcein-AM was diluted in 1197 µl PBS. The compounds, concentration and gelation temperatures are stated in Table 6. Results from Cedex measurement are included in APPENDIX E.

**Table 6: An Overview of the toxicity evaluation seeding. Compounds, concentrations and gelation time are stated for each condition.**

| Compound/Mix | Concentration | Gelation temperature |
|---|---|---|
| Collagen I | 1.5 mg/ml | 37 °C |
| Collagen I + THPC | 1.5 mg/ml | 37 °C |
| ELP + Glutaraldehyde | 3wt% | 37 °C |
| ELP + THPC | 3wt% | 37 °C |
| ELP + THP | 3wt% | 37 °C |
| ELP Coating | 1 mg/ml | - |

## 3.5. Metabolic activity assay

The metabolic activity assay is a colorimetric method which measures the absorbance of formazan at 490 nm, a bioreduced product converted from the reagent MTS tetrazolium. The product quantity obtained in the assay is proportional to the amount of living cells in the sample. The solution was mixed by adding 20 µl MTS reagent to each 100 µl of phenol red-free Dulbecco's Modified Eagle Medium (DMEM) in dark environment. After mixing, 100 µl of solution were added to each well in the 384-well plate and the plate was incubated at 37 °C for 1.5 and 2 hours for the first and second seeding respectively. Media was transferred to a 96-well plate, covered by aluminum foil, followed by absorbance measurement in a microplate reader.

## 3.6. Proliferation assay

The kit for this assay were purchased from Invitrogen (catalogue number: P7589). This assay quantifies the dsDNA content in a solution. Initially, 100 µl of water was added to each well for cellular lysis after which the plate was incubated for 1.5 hours at 37 °C. After incubation, 28.7 µl of lysate from each well was mixed with 71.3 µl PicoGreen reagent solution and transferred into a 96-well plate. For this assay, two wells per condition were examined with

three replicates each. Calibration concentrations of lambda-DNA ranging between 0 µg/µl – 2 µg/µl were prepared by dilutions with 1xTris-EDTA (1xTE) buffer according to Table 7. The calibrators were also analyzed with three replicates per concentration. Fluorescence intensity at 520 nm was measured. The linear regression of calibrators obtained in the software GraphPad Prism 6 was used for the calculation of DNA concentration in the samples.

**Table 7. Concentration of calibrators used in proliferation assay.**

| Concentration (µg/µl) | Lambda-DNA (µl) | 1xTE buffer (µl) |
|---|---|---|
| 0 | 0 | 1000 |
| 0.2 | 2 | 998 |
| 0.5 | 5 | 995 |
| 1 | 10 | 990 |
| 1.5 | 15 | 985 |
| 2 | 20 | 980 |

## 3.7. Live/Dead assay

The cells were investigated with Life technologies LIVE/DEAD Viability/Cytotoxicity kit ( catalogue number: L-3224). In a microcentrifuge tube, 2 µl of EthD-1 and 0.5 µl calcein-AM were diluted with PBS to a final volume of 1 ml. The wells were washed with 100 µl PBS before 100 µl of EthD-1/calcein-AM solution was applied. The plate was covered in aluminium foil and incubated in room temperature for 10 minutes. The wells were rinsed again with 100 µl PBS and stored in PBS during measurements with confocal microscope. All time points have been analysed with Nikon Eclipse TE2000-U except for the time point at day 18, for the first seeding of β-cells, where the cells were visualized with Nikon Eclipse TE2000-E. EthD-1 is a reagent which enters cells with damaged cell membrane and upon binding to DNA fluoresces with emission maximum around 617-635 nm. Calcein-AM is a reagent which can penetrate through the intact cell membrane but is only converted intracellular in living cells by the presence of esterase into the fluorescence product calcein which has a emission maximum at 515-517 nm.

## 3.8. Glucose-Stimulated Insulin Secretion Assay (GSIS)

Insulin secretion is the primary function of β-cells. The cells release insulin upon elevated glucose concentrations, which can be stimulated in an *in vitro* assay and used to investigate the cellular response.

Kreb buffer stock solution containing 25 mM HEPES, 115 mM NaCl, 24 mM $NaHCO_3$, 5 mM KCl, 1 mM $MgCl_2*6H_2O$, 0.1% BSA, $dH_20$ and 2.5 mM $CaCl_2*2H_2O$ were mixed with glucose into two different microcentrifuge tubes to a final glucose concentration of 2.8 mM and 28 mM respectively. Cells were washed with 50 µl PBS prior to 30 minutes incubation with 2.8 mM glucose containing kerb-buffer at 37 °C. Supernatant were removed and 120 µl 2.8 mM or 28 mM glucose kreb-buffer solution was added. Cells were incubated at 37 °C for one hour followed by collection of supernatant and transfer to a 96-well plate. Supernatant were stored at -20 °C until analysis with C-peptide enzyme-linked immunosorbent assay. Cell number for each wells were analysed with Cedex HiRes cell counter (Innovartis). An established β-cell line, EndoC-βH1, was used as a positive control for this assay but examined with 25 mM of glucose as the higher concentration.

## 3.9. C-peptide Enzyme-Linked Immunosorbent Assay (ELISA)

C-peptide concentration in collected supernatant from section 3.8 was investigated with Mercodia Ultrasensitive C-peptide ELISA kit (catalogue number: 10-1141-01) according to suppliers instruction. Briefly, samples were thawed at the laboratory bench and duplicates of calibrators, controls and samples were added to separate wells in the ELISA plate. Assay buffer was added to each well, followed by incubation on a shaker (850 rpm, 20 °C) for one hour. Wells were washed 6 times with 300 µl 1x wash buffer prior to addition of 1x conjugated solution to each well. The plate was then re-placed on the shaker (850 rpm, 20 °C) for an additional hour. Another washing step, repeated 6 times, was performed prior to 3,3',5,5'-tetramethylbenzidine (TMB) substrate addition to wells. Because of the light sensitivity of TMB the plate was covered in aluminium foil and incubated in room temperature for 30 minutes. The reaction was terminated by addition of stop solution to each well. Optical density measurements at 450 nm were performed within the suggested time span.

Modifications of the analysis protocol had to be done due to low detection of samples. The calibration curve was modified by removing the two highest concentrations and adding the zero concentration value as a data point for the calibration. Furthermore, the curve was constrained at the first data point of the calibrators. The concentration for calibrators can be seen in Table 8. The linear regression model and following diagram were achieved in GraphPad Prism 6.

**Table 8. Concentration for calibrators used in analysis of C-peptide content of each condition. *=Calibrator 0 is not a part of the original calibrators.**

| Calibrator | Concentration (pmol/L) |
|---|---|
| 0* | 0 |
| 1 | 4.71 |
| 2 | 16.2 |
| 3 | 67.2 |

## 3.10. Immunocytochemistry assay (ICC)

Fixed cells were permeabilized with 0.1% Triton X-100/PBS for 10 minutes, followed by a wash with PBS. Samples were incubated in 3% BSA/PBS for 1 hour to prevent unspecific binding of antibodies. Specific primary antibodies used are stated in sections below. Primary antibodies were diluted to specific concentrations and a total of 20 µl antibody solution was added to each well. Samples where then incubated overnight at 4 °C. Afterwards, cells were permeabilized with 0.1% Triton X-100/PBS and rinsed in PBS for 10 minutes. Secondary antibodies were diluted and 20 µl of solution was added to wells with primary antibodies. The secondary antibody mix which consisted of goat anti-mouse Alexa Fluor 488 (1:400, Life technologies, pAb) and goat anti-rabbit Alexa Fluor 594 (1:650,Life technologies, pAb) were diluted in a 1% BSA/PBS solution. After 2 hour incubation in dark environment, wells were washed with PBS for 10 minutes. Hoechst (33342, Life technologies) at concentration of 0.2 µg/ml was added as nuclei stain for 15 minutes and washed with PBS for 15 minutes. Samples were stored in PBS at 4 ºC until visualization. Controls for unspecific binding of secondary antibodies were hADSCs at passage 0.

### *3.10.1. Adipocyte differentiation markers*

For detection of the mesenchymal stem cell marker CD105, mouse anti-CD105 (1:100, Abcam, ab114052, mAb) was used and measured at 495-530 nm with non-linear microscopy. Perilipin, an intracellular lipid droplet protein, was detected with rabbit anti-Perilipin (1:500, Abcam, ab3526, pAb) and fluorescence measurements at different wavelengths (578-640 nm, 650-720 nm) was performed with non-linear microscopy.

### *3.10.2. β-cell differentiation markers*

In the β-cell differentiation protocol the following primary antibodies were mixed and applied on the first time point plate: rabbit anti-HNF3β/FoxA2 (1:100, Merck Millipore, 07-633, pAb) was mixed with mouse anti-Sox17 (1:60, R&D systems, MAB1924, mAb). The same anti-Sox17 were also mixed with rabbit anti-PDX1 (1:750, abcam, ab47267, pAb) and placed in a separate well. For the last time point plate, antibodies were mixed accordingly; anti-PDX1 (mentioned above) was mixed with mouse anti-insulin (1:1000, Sigma Aldrich, I2018, mAb). Another mixture with anti-PDX1 and anti-Sox17 (both mentioned above) was also applied to a separate well.

## 3.11. Bodipy

Neutral lipid staining was performed with Bodipy (1:1000, Life technologies, D-3922) (4,4-difluoro-3a,4a-diaza-s-indacene). Each well was covered with 20 µl Bodipy solution followed by incubation of the plate for 15 minutes. The staining solution was removed and PBS was added. Fluorescence at 514 nm was examined in microscope.

## 3.12. Multimodal Microscope

A multimodal microscope was used in these projects, which is detailed in Figure 5. A picosecond laser generates two different laser beams, one with a wavelength of 1064 nm and the other one with a wavelength of 532 nm. The latter beam enters the optical parametric oscillator (OPO) which enables tuning of the wavelength. In these projects wavelengths between 811-817 nm have been used. The 1064 nm beam is time delayed in the retroreflector while lambda half-plates are used to adjust the power of the outcoming beam from the beamsplitter (BS). The different optical tools enable the two beams to be overlapped in time and space before reaching the samples which is necessary for detection. Three different detectors are incorporated into the set-up, one for detection in forward direction, denoted F in the picture, and two for detection in epi direction, denoted E. The epi detectors are referred to as epi-straight and epi-side with separate wavelength ranges due to optical set-up.

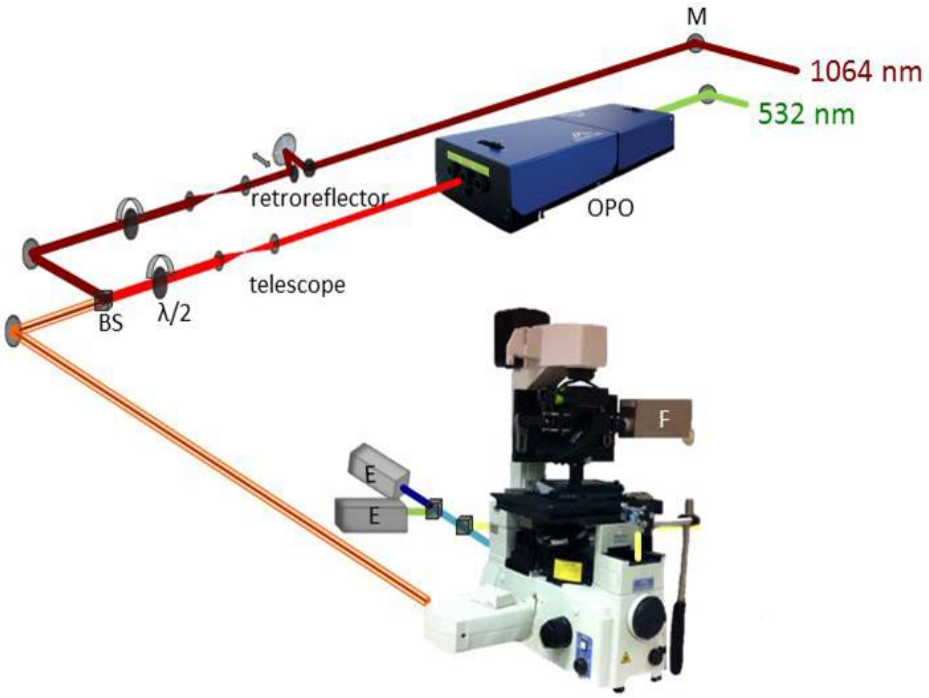


**Figure 5.** Schematical overview of the non-linear multimodal microscope. Ingoing laser beams are denoted as 1064 nm and 532 nm. The blue device is the optical parametric oscillator denoted (OPO) while the beam splitter is denoted (BS). The three detectors of the microscope marked as F, E, E in the picture. (Group internal picture, used with permission from Enejder lab, Chalmers University of Technology.)

Laser powers ranging from 60 mW to 120 mW have been used throughout the experiments. Image size of 512 x 512 pixels and pixel dwell of 5.04 µs has been used if not explicitly stated otherwise. All images compared in figures will have same settings on gain, exposure times and laser powers if nothing else is stated. The software EZ-C1 (Nikon) has been used to control the microscope. The software DCC (Becker & Hickl) and SPCM (Becker & Hickl) were used to manage the detectors and signal collection respectively. For bright field images the software Micro Manager 1.4. (Vale Lab UCSF) was used.

# 4. RESULTS AND DISCUSSION

The first results obtained in this thesis for the adipocyte and β-cell differentiation are presented and discussed in section 4.1. Thereafter, the results from the ELP optimization trial are discussed. The second differentiation of the adipocyte and β-cell differentiation are presented and discussed in section 4.3. Lastly, the results from the crosslinker toxicity is presented and discussed.

## 4.1. First differentiation

Hydrogels without cells are referred to as pure hydrogels in this report. The results from pure hydrogels used in first seeding, imaged with non-linear microscopy techniques will first be described. Later results from adipocyte differentiation are presented and lastly results from the β-cell differentiation will be presented and discussed.

### *4.1.1. Pure hydrogels*

Non-linear images of hydrogels without cells used in first differentiation were taken to assess the structure of the proteins in the hydrogels (Figure 6). Collagen fibers are clearly visible in forward detection with second harmonic generation (filter 405/10 nm) with excitation wavelength of 811 nm set by OPO, image A. ELP domains are visualized in image B-C, with both detection of autofluorescence (filter 514/30 nm) and with CARS (filter 661/20 nm). Excitation wavelengths used for this investigation was 817 nm and 1064 nm. ELP structure obtained in these images are comparable with earlier experiments with ELP.[48]

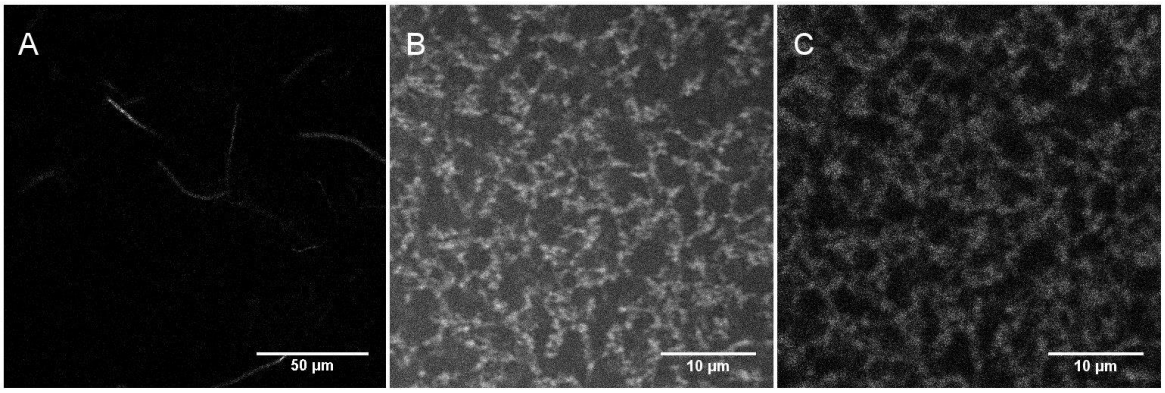


**Figure 6.** Pure hydrogels imaged with nonlinear microscopy**.** A: Pure collagen hydrogel, z-stacks projected into same plane, scalebar:50µm. Collagen fibers are clearly visible with Second Harmonic Generation. B: CARS signal of pure ELP hydrogel detected in epi-straight direction with 661/20nm filter, C: Autofluorescence signal collected in epi-side detector with 514/30nm filter. Both ELP hydrogels have a scalebar of 10µm.

### *4.1.2. ADIPOCYTE DIFFERENTIATION*

In this section results from the initial seeding of hADSCs towards adipocytes will be presented. Confocal overview images and more detailed nonlinear images will be presented. The assays performed will also be discussed. Data from the Cedex measurements prior to seeding is included in Appendix A.

#### 4.1.2.1. Time point day 2

Confocal microscopy images (Figure 7) stained with Live/Dead fluorescent markers (Calcein and EthD-1) from day 2 show that cells on collagen coating and in collagen hydrogels proliferate well and have high cell density. Cell morphology is spread and EthD-1 DNA-stain of non-viable cells is low. No cellular morphological difference between the two crosslinking temperatures of collagen visible. Cells on hydrogels containing ELP show low or no spread morphology and non-viable cell concentration is higher. Figure 8 show nonlinear images with a more detailed cellular morphology.

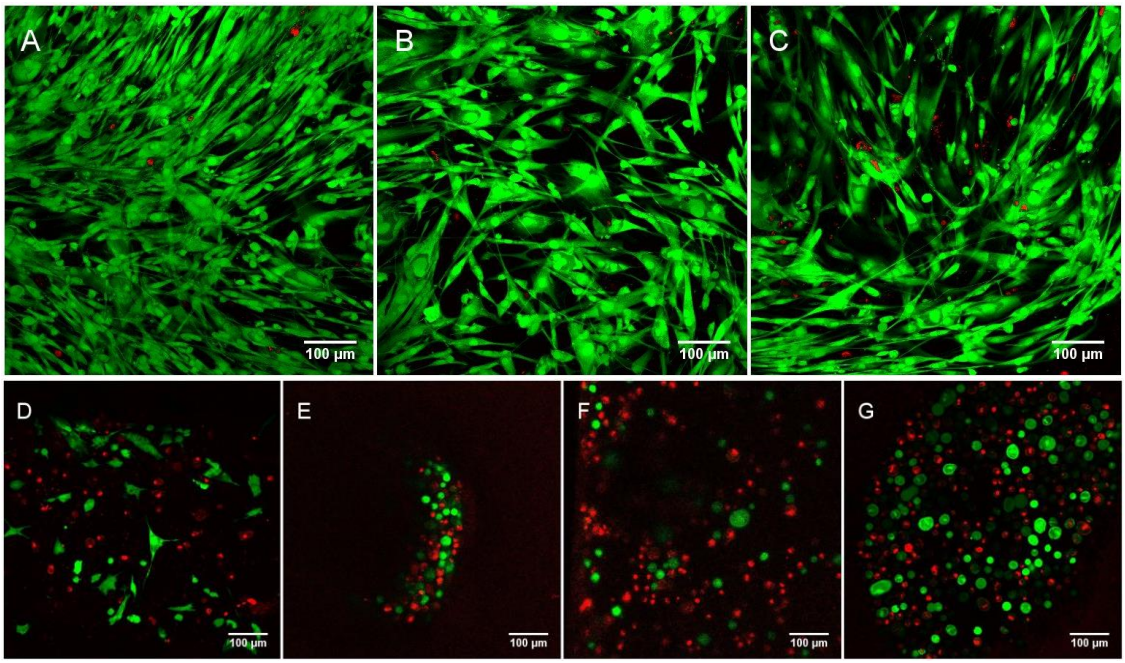


**Figure 7.** Confocal images of live/dead stained cells at day 2 with calcein in green (live) and EthD-1 in red (dead). A - Collagen coating. B - Collagen hydrogel 4°C. C - Collagen hydrogel 37°C. D - 25% ELP – 75% collage hydrogel. E - 50% ELP – 50% collagen hydrogel. F - 75% ELP – 25% collagen hydrogel. G - Pure ELP 3wt% hydrogel. (Scalebar: 100µm, image sizes 710x710µm)

A possible factor influencing these results is toxicity of the amine-reactive crosslinker THPC used for ELP hydrogel formation. This crosslinker reacts with amine groups in ELP in a fast Mannich type reaction leading to gelation times around 10 minutes.[76]

After the reaction the THPC toxicity is lowered due to the linkage with primary and secondary amines of proteins. A toxicity assay where THPC was added to cells growing on 2D collagen coating showed high increase in cell death giving strength to the conclusion of toxicity. Since the cells were added after gelation at this first assay, toxicity should be low since most THPC molecules have crosslinked before cell addition and less reactive groups are present. Results suggest that unreacted THPC molecules might still be present which affects the proliferation of the cells. If the assumption is made that all THPC molecules are crosslinked when the cells are added, other factors explaining the viability/morphology are present. The ELP hydrogel might not provide a suitable surface for the cells, at current concentration. Further investigations with new conditions are determined to be made to further assess reason for differences in morphology (second differentiation). Since the decision to use 5wt% ELP hydrogels based on research showing spread morphology in fibroblasts[48] does not seem to be appropriate for hADSCs, an approach to lower the matrix stiffness was implemented. Heilshorn *et al.*[79] managed to enhance neurite outgrowth in hydrogels with a lower concentration of ELP (3wt%) which formed the basis for the next differentiation.

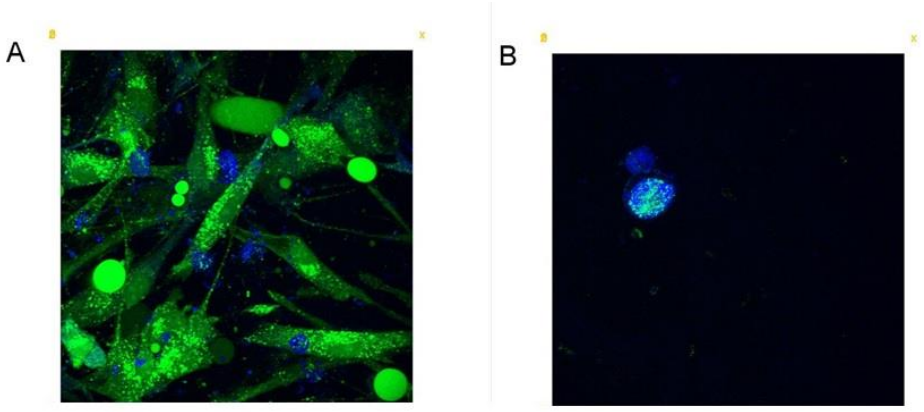


**Figure 8.** Non-linear images showing 3D rendering viewed from above. Live/dead staining with calcein in green and EthD-1 in blue. A – Cells on collagen hydrogel. B – Cells on 25% ELP / 75% collagen hydrogel. Image size A - 159,1x159,1x66µm. B - 159,1x159,1x31µm.

A viability investigation from the live/dead stained cells where the area of live cells (green) and the area of total staining (green and red) were divided to give a comparable quantitative value of cell survival (Figure 9). This is not a value representing proper cell viability but a way to visualize relative live staining from dead staining in the samples. Since calcein stains the whole cytoplasm and EthD-1 only stains nuclei the area is not comparable for actual difference between amount of cells that are alive or dead, but presents a more visually understandable comparison of amount live/dead stain. This calculation confirms the impression given by Figure 7 of a higher ratio of dead stain present in all conditions where ELP crosslinked with THPC is present.

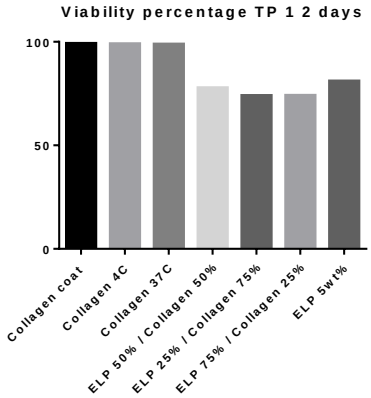


**Figure 9.** Live stain divided by total stain in confocal images at day 2

## Metabolic activity

Live/dead staining, even though widely used, can lead to misinterpretation of viability due to overall incorporation of calcein in not spread cells (most likely dead cells). Complementary assays need to be performed to improve the understanding of cellular metabolism. MTS results varied heavily both between conditions and within the same condition compromising the interpretation of the results (Figure 10). Cells on hydrogels containing ELP show

comparable values in metabolic activity after 2 days as cells seeded on collagen. When the values are normalized to the dsDNA content (fluorescence of DNA stained with Pico-Green), similar results are obtained. The high variance of the results leading to large error bars can be depending on: few replicates, cells detaching from the hydrogels, hydrogel detachment during media change and washing leading to loss of cells. That the cells on ELP have a high arbitrary MTS value despite the round morphology that suggest low viability, indicates that there are issues with the MTS assay when performed on cells in hydrogels. The ELP hydrogels are opaque with a brownish color similar to that of the MTS reagent that is used to measure the metabolic activity. This might affect the value from the colorimetric absorbance measurement since parts of the hydrogel might be transferred into the measuring wells, giving a higher value. Due to these issues with the assay, results are determined not to bear large input to the cellular state.

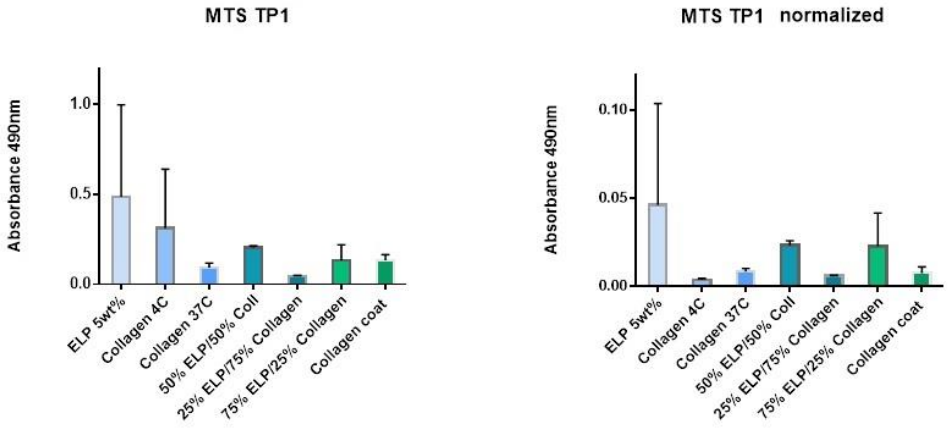


**Figure 10**. Metabolic activity at day 2. A - Overall average value/well and B - normalized value to dsDNA content.

#### 4.1.2.2. Time point day 14

After completion of the differentiation it is visible, that the trend predicted on day 2 continued. Cells incubated on collagen coating and collagen hydrogels have a morphology indicating that differentiation towards (*in vitro)* adipocytes has been successful. Crosslinking temperatures of collagen hydrogels show no impact on differentiation. Cells incubated on ELP-containing hydrogels show no lipid droplets and cell number is greatly reduced. Lipid droplets in cells on collagen are clearly present in all wells. No distinguishable differences in lipid droplet size or cell morphology were found in cells on the different collagen scaffolds (Figure 11).

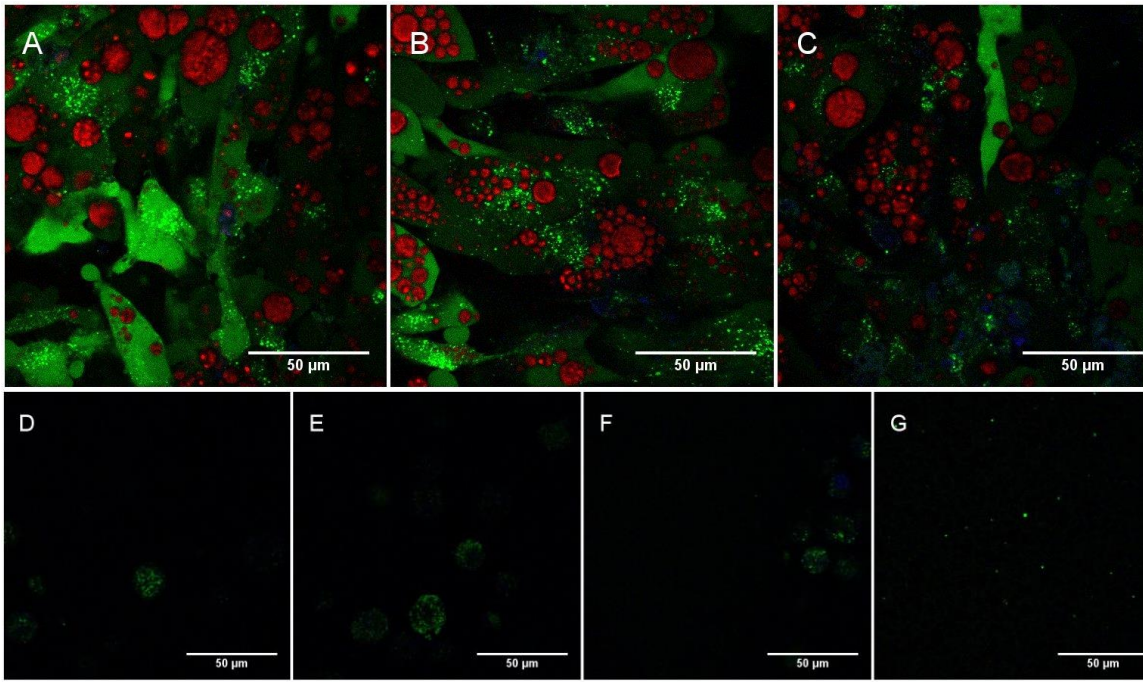


**Figure 11**. Non-linear microscopy images of cells after 14 days with lipid droplets in red (CARS) and cytoplasm in green. A - Collagen coating. B - Collagen hydrogel 4 °C. C - Collagen hydrogel 37 °C. D - 25% ELP – 75% collage hydrogel. E - 50% ELP – 50% collagen hydrogel. F - 75% ELP – 25% collagen hydrogel. G - Pure ELP 3wt% hydrogel. Image size 159.1x159.1 µm. (Scalebar: 50µm, image sizes 710x710 µm)

## Lipid droplet analysis

A small lipid droplet analysis was performed in the three conditions where lipid droplets formed (Table 9). Lipid/cell area calculated to around 30% in all conditions and no major differences in lipid size was found between the conditions. The amount of lipid droplets per cell increases with cell size. A more thorough lipid analysis of second differentiation is included in later chapter. Figure 12 describes the method of the calculation.

**Table 9. Lipid size analysis**

| Condition | Number of lipid droplets/cell > 4 µm | Cell diameter | Mean lipid droplet diameter > 4µm | Lipid area percent of whole cell |
|---|---|---|---|---|
| Collagen coating | 7 | 44,6 µm | 6,87 µm | 34,6% |
| Collagen 37 °C | 11 | 50,3 µm | 6,08 µm | 30% |
| Collagen 4 °C | 14 | 57,3 µm | 5,67 µm | NA due to issues with cell area |
| ELP 25% | - | 17,6 µm | - | - |
| ELP 50% | - | 18,8 µm | - | - |
| ELP 75% | - | 15,3 µm | - | - |
| ELP | - | No cells | - | - |

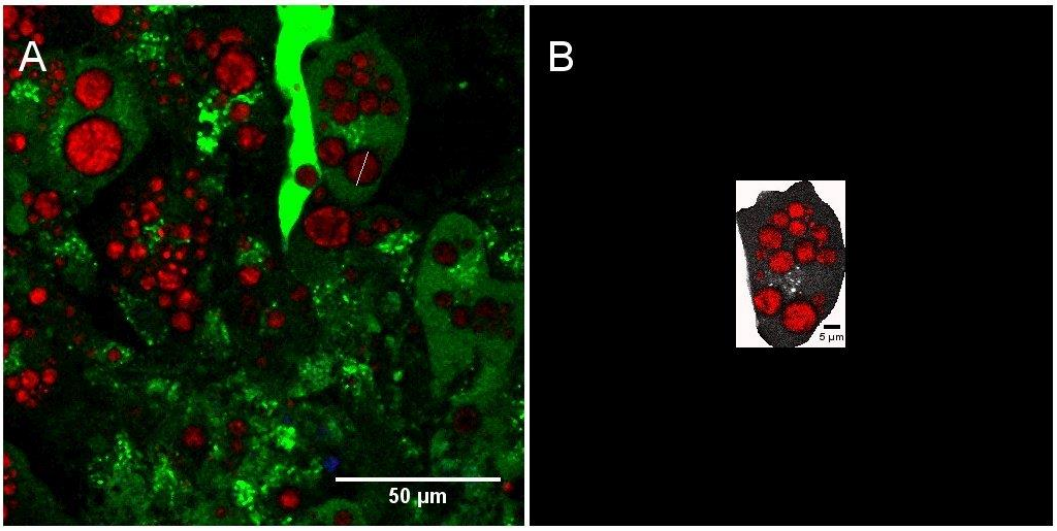


**Figure 12.** Lipid droplet and cell size calculation (collagen hydrogel 37 °C). A. Lipid diameter assessment (white line). B. Lipid volume / cell volume calculated by color thresholding of lipid droplets (red) divided by total cellular area by manual border sectioning of cell in ImageJ. (Scalebar: 50 µm, image sizes 159.1x159.1 µm)

## Metabolic activity

After 14 days, the metabolic activity on ELP hydrogels have decreased versus collagen, indicating that the cells cannot survive on this material during differentiation protocol (Figure 13). Figure 11 show that no cells are present on the ELP 5wt% hydrogel. This show that improvement of the MTS assay is needed when performed in hydrogels composed of ELP, since the MTS value should be close to zero if no cells are present. One possible explanation, as mentioned earlier, is that debris from the hydrogel is transferred from the seeding well into the 96-well plate used for measuring absorbance and that this debris affects the obtained value from the absorbance measurement.

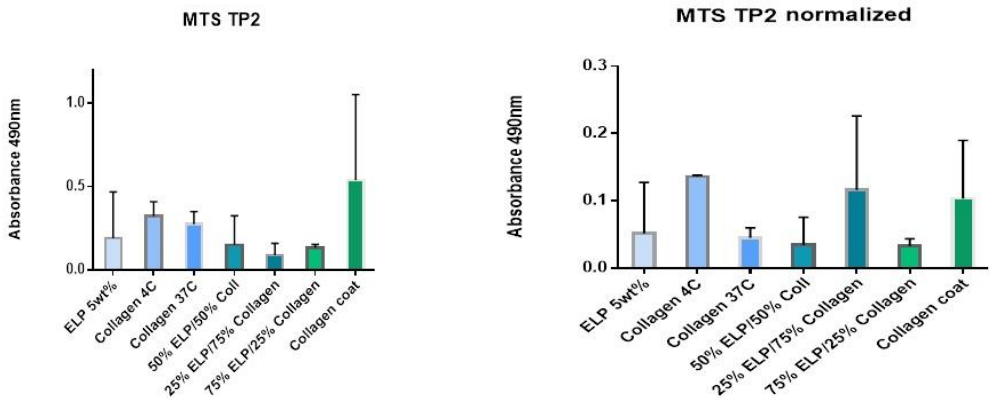


**Figure 13.** Metabolic activity at day 14. Overall average MTS value/well and normalized value to ds DNA content.

### *4.1.3. β-CELL DIFFERENTATION*

In this section results from the initial seeding of hADSCs toward β-like cells will be presented. First, results from the metabolic activity assay and proliferation assay will be discussed. Secondly, confocal images of live/dead stained cells are presented and lastly non-linear results of cells in hydrogels are presented. Data for the Cedex measurements prior to seeding are provided in APPENDIX C.

#### 4.1.3.1. Metabolic activity assay

The preparation and measurements were performed accordingly to the methods described in section 3.5 and the results are visualized in Figure 14. Here, the first bar for each condition represent the absorbance value for the first time point while the second bar represent the absorbance measurements for the second time point. Undifferentiated cells are only measured at the first time point since the hADSCs have high proliferation and are almost totally confluent at this time point. The high proliferation of these cells also results in a high absorbance value for formazan and therefore the y-axis has been divided into two parts to illustrate the other results better. Overall, a slight tendency of increased metabolic activity can be seen for cells grown on collagen coating, collagen hydrogel 4 °C and matrigel. Even though cells grown in collagen 37 °C hydrogels have relatively large error bars at second time point, the result indicate that the observation of increased activity might also be applicable for this condition.

The collagen coating (2D) results in higher absorbance than all the different compositions of collagen hydrogels (3D), which initially seem to indicate that cells grown in 3D matrices, has an additional stress factor. However, one should keep in mind that this assay is formulated for 2D seeded cells and the recommended incubation time spans between one to four hours. Because the plate is incubated with the reagent in a humidified and temperature controlled incubator, the process of how the reagent penetrates the hydrogels and the subsequent metabolical conversion to formazan is purely diffusion driven. For that reason, the incubation time of 1.5 hours might be too short for cells in hydrogels and favorable towards 2D seeded cells since in that case the reagent is applied directly on the cells and the diffusion process is not significant. When comparing between 3D seeded cells, the cells grown in matrigel give rise to the highest metabolic activity followed by cells grown in collagen hydrogels.

It is known that cells can be grown in matrigel hydrogels. Yet, this is a material that is extracted from Engelbreth-Holm-Swarm mouse sarcoma, meaning that the material is chemically undefined with batch-to-batch variation[80], which may lead to incomparable results when different batches are used. Since more stable hydrogels are desirable to find in this project, matrigel hydrogels can be seen as a control that the cells grow in 3D.

Lastly, all hydrogels with ELP result in very low absorbance values hence low metabolic activity. This observation can be seen already at time point day 5, which indicates poor proliferation of the cells at an early stage of differentiation.

#### 4.1.3.2. Proliferation assay

The results from this assay are typically used as normalization for the metabolic activity assay. This approach could thereby generate a result of metabolic activity per dsDNA content which then would minimize variations due to different cell number in between wells. The linear regression was obtained in GraphPad prism 6.

Each calibrator has been analyzed three times, result and error bars with standard deviation for each calibrator is presented Figure 15. These measurements show very low variation for

each calibration which indicates low effect of sample handling. However, when analyzing the sample results presented in Figure 16, large variation of dsDNA content in measurement within the same well can be observed for some of the conditions. Additionally, hydrogels with ELP mixtures have negative dsDNA content according to the results presented in the diagram. Intuitively, this is not possible since $10^4$ cells have theoretically been seeded in each hydrogel. The large variation within samples might be due to lack of mixing before pipetting aliquots into the reader plate resulting in higher concentration of dsDNA in some wells. However, since the samples have been treated the same way as the calibrators, with aspect of sampling handling, the impact of pipetting should not be that significant. Another explanation for the result of these hydrogels is that the cells might already have died. As a consequence the cellular integrity was compromised allowing some of the dsDNA to be washed away in medium changes. This reasoning should result in a low amount of dsDNA, but not a negative value. For some of the hydrogels it is also possible that they were accidentally removed during the washing step in between metabolic activity assay and the proliferation assay but this should not result in hydrogel losses for all ELP mixtures. Another possible explanation is that the dsDNA content in these hydrogels was not extracted from the hydrogels and that the negative amount is a result of error in the linear regression at that low concentration of DNA.

#### 4.1.3.3. Live/dead assay

Live/dead staining of cells enable visualization of cellular viability and morphology since calcein fluoresces in the cytoplasm of live cells and also gives information of the cellular integrity since EthD-1 is not able to penetrate cells with intact cellular integrity.

For the images presented in Figure 17, two different confocal microscopes have been used for the two different time points. Therefore the data analyses of the different time points have been done with different methods. All images from the first time point at day 5 have been normalized to the same gain with 0-4095 photons per pixel for the green channel and 0-1800 photons per pixel for the red channel. This allows for direct cross evaluation of the conditions. For the second time point at day 18, the images did not have the same contrast to the background. Therefore, the channels for hydrogels containing ELP have been modified by using the threshold function in ImageJ and then constraining the area to the outline of the cells before adjusting the gain. After merging channels, the gain was adjusted to 0-150 photons per pixel for the green channel and 0-170 photons per pixels for the red channel. Bright field images of these cells have also been included due to the low contrast. This assay confirmed the results obtained in the proliferation assay but did not provide any additional information. The threshold operation was complicated to perform for the rest of the hydrogels and the coating, where the cells were spread. For that reason, these images have been presented without any changes.

By examinations of the cellular morphology, one can observe that the cells in ELP containing hydrogels are round at both time points and high abundance of red staining indicates that these cells have lost their cellular integrity. Even cells which fluoresce in the green channel but have EthD-1 staining in the nucleus should be considered as unhealthy cells. The undifferentiated hADSCs are almost fully confluent at day 5. The collagen coating, collagen hydrogels and matrigel hydrogel visualizes cellular spreading which indicates that the cells have adhered and interacts with the matrices. Some red staining, indicating dead cells, can be seen in these images, which is expected in any cell culture. Cluster formation can also be seen in collagen coating and matrigel hydrogel which is a desirable result because of its similarity to previous published results.[56] By examining the collagen hydrogels no significant difference in appearance can be concluded at day 5. Unfortunately, the collagen 37

°C hydrogel was lost for the second time point and therefore no comparison can be done at this time point.

#### 4.1.3.4. Non-linear images

Images taken with multimodal non-linear microscopy have provided additional information in the analyses. In this section, images of ELP 5wt% and ELP/collagen mix (50/50) will be presented in Figure 18 and Figure 19 respectively but similar results were obtained for the rest of the ELP mixed hydrogels. Collagen 4 °C will also be discussed.

The upper image of ELP 5wt% hydrogel in Figure 18 shows the cellular distribution within the hydrogel. Most of the cells have descended to the bottom of the hydrogel with only a few cells still remaining within the hydrogel. This result indicates that the gelation time was not short enough and therefore that the cells sunk during the gelation process. Another explanation is that the hydrogel was too soft and that the cells have sunken due to that reason. When examining a cross section of the hydrogel as in the bottom image, additional information for the analyses was obtained. The images taken with this microscope have a much narrower field of view, 159.1x159.1 µm in comparison to the 710x710 µm of the live/dead stained images. This cross section image confirms that the cells are round and that the EthD-1 has stained the nucleus (blue). When analyzing the green signal, one should keep in mind that autofluorescence from endogenous fluorophores is also collected in this channel since the filter (514/30 nm) has a transmission window between approximately 495-533 nm. It can clearly be seen that one cell has initiated cellular expansion within the hydrogel but could not survive and therefore has developed to a necrotic cell which has decreased in size. Another interesting feature of the images is that the ELP containing matrix also autofluoresces, which gives information about how much each cell has expanded and contracted the hydrogel. However, only a large cell and a cell on the left side seem to have contracted the hydrogel. When examining seven cells, which can clearly be distinguished in the hydrogel, the average diameter was 18.6 µm. Comparing this result with the initial average diameter at the day of seeding which was 17.6 µm also indicated that the cells has not expanded significantly in size.

The results from the 50/50 mixed hydrogel in Figure 19 also indicate that some of the cells on the bottom have tried to expand. The distribution is presented in the upper image and analyzed with trilinear interpolation in volume viewer. A cross section and enlargement of the bottom left cell in the upper image are displayed in the middle image. This cell has a clear halo around it of contracted hydrogel. Measurement of the halo results in a diameter of 32-35 µm which indicates that the cell has expanded during the differentiation. In the bottom image the same cell with surrounding matrix is displayed with intensity ranging from low (blue) to high (yellow). It seems that the intensity of the border of the halo has a slightly higher intensity than the bulk hydrogel which indicates that the hydrogel has been compressed.

The cells in collagen 4 °C hydrogel in Figure 20 have a totally different morphology than the cells in ELP hydrogels. The upper image shows the cellular distribution throughout the hydrogel and spread cells can be observed along with round cells. In the lower image a cross section of the hydrogel is displayed which also shows elongated cells. Collagen fibers, detected with SHG, can be observed in the red channel which confirms that the cells are located within the hydrogel.

The last figure in this section, Figure 21, presents a comparison of the two collagen hydrogels and the results was considered to be silimar in both images. Therefore, the comparision did not reveal any additional information which would favor one hydrogel over the other.

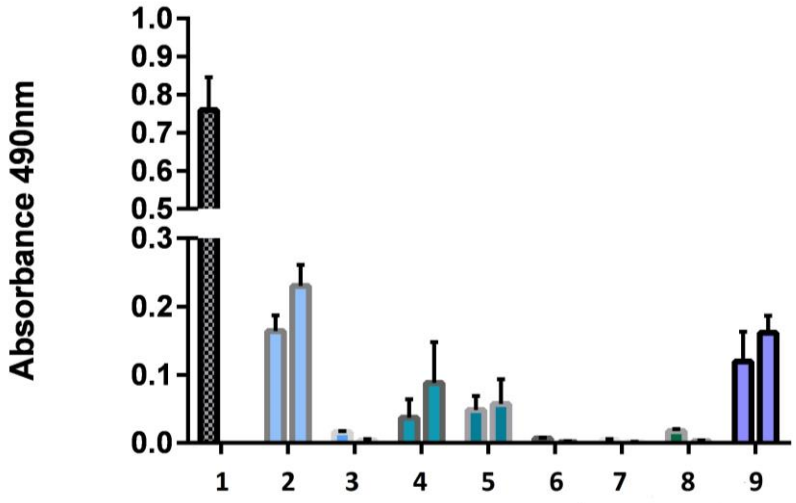


**Figure 14.** Absorbance measurement at 490 nm of formazan, a product of MTS tetrazolium. The first bar represent data from time point day 5 and the second bar represent data from time point day 18. Each condition has been measured with three adjacent wells. Undifferentiated cells have only been measured at day 5. 1: Undifferentiated cells, 2: Collagen coating, 3: 5wt% ELP hydrogel, 4: Collagen 4 °C hydrogel, 5: Collagen 37 °C hydrogel, 6: ELP/Collagen 50/50 hydrogel, 7: ELP/Collagen 25/75 hydrogel, 8: ELP/Collagen 75/25 hydrogel, 9: Matrigel hydrogel.

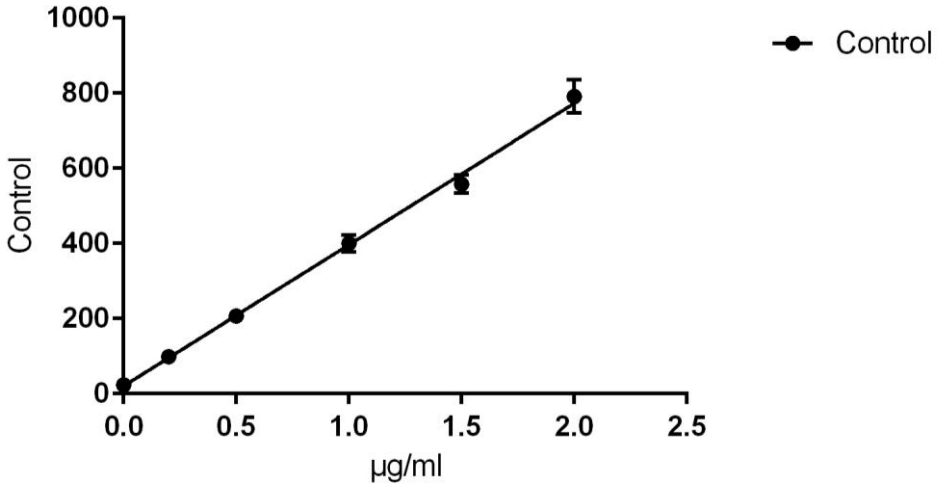


**Figure 15.** Regression model for proliferation assay based on lambda-DNA calibrators. Each calibrator has three replicates.

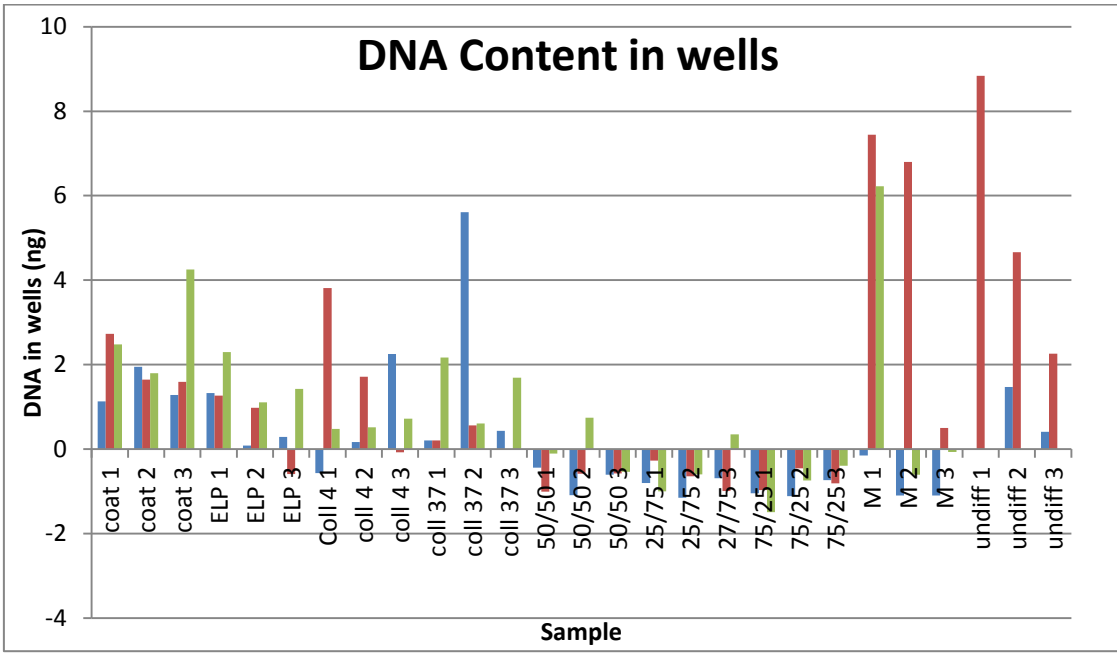


**Figure 16.** Results from proliferation assay at time point day 5. The bars represent the DNA content (ng). Each condition has been analyzed in three wells with three replicates from each well. Measurements with known errors, collagen 37 °C (3) and undifferentiated cells (1), have been subtracted.

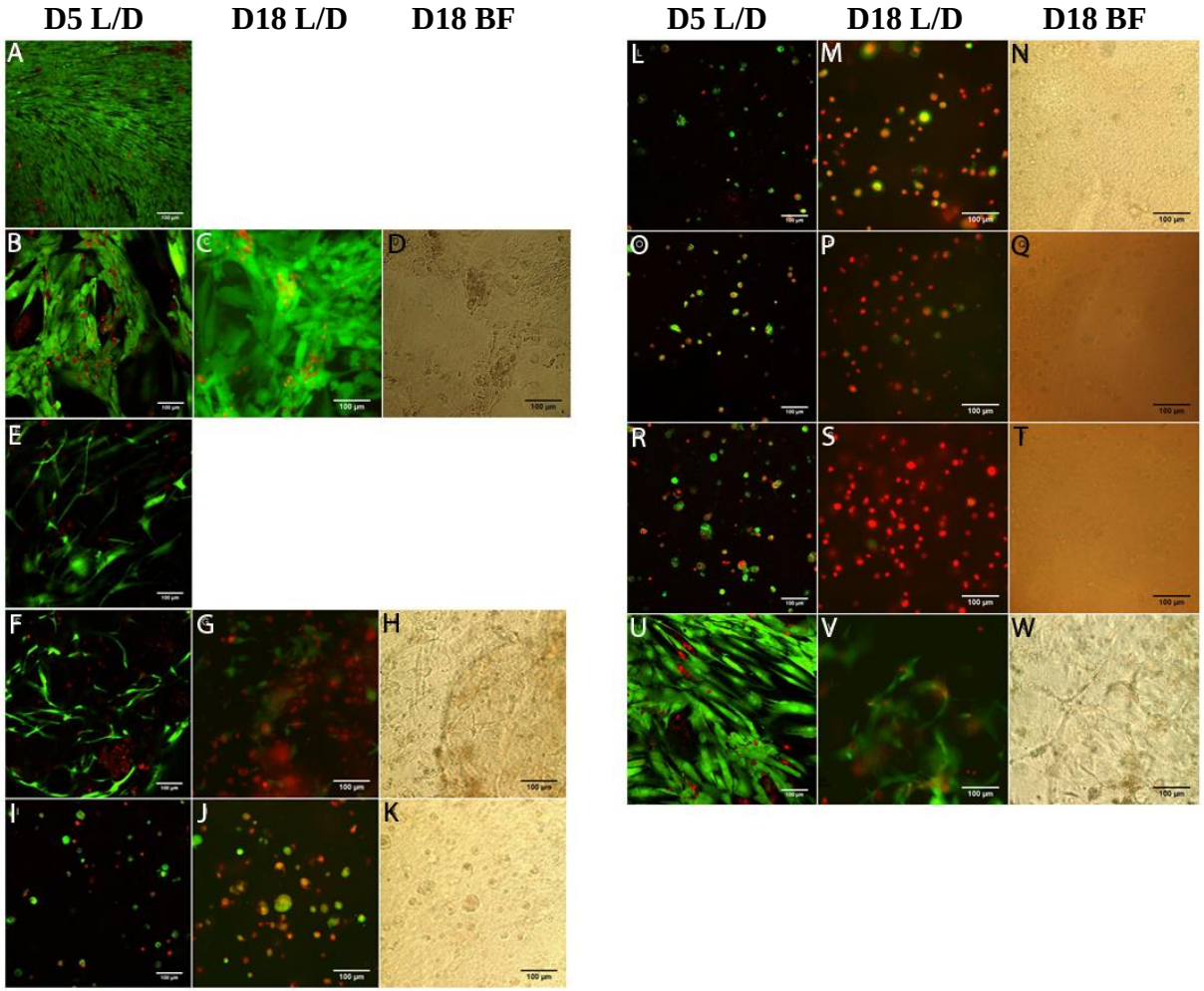


**Figure 17.** 20x confocal images of live/dead stained cells at day 5 and day 18. Live cells stained with calcein (green) and dead cells stained with EthD-1 (red). A, B, E, F, I, L, O, R and U are images from time point day 5. C, G, J, M, P, S and V are images from time point day 18 analyzed by thresholding in ImageJ. D, H, K, N, Q, T and W are bright field images of the conditions taken at time point day 18. A: Undifferentiated cells, B-D: collagen coating, E: collagen 37 °C, F-H: collagen 4 °C, I-K: ELP/Collagen 25/75, L-N: 50/50, O-Q: 75/25, R-T: 5wt% ELP, U-W: Matrigel. Scale bar 100µm.

**ELP 5wt%**

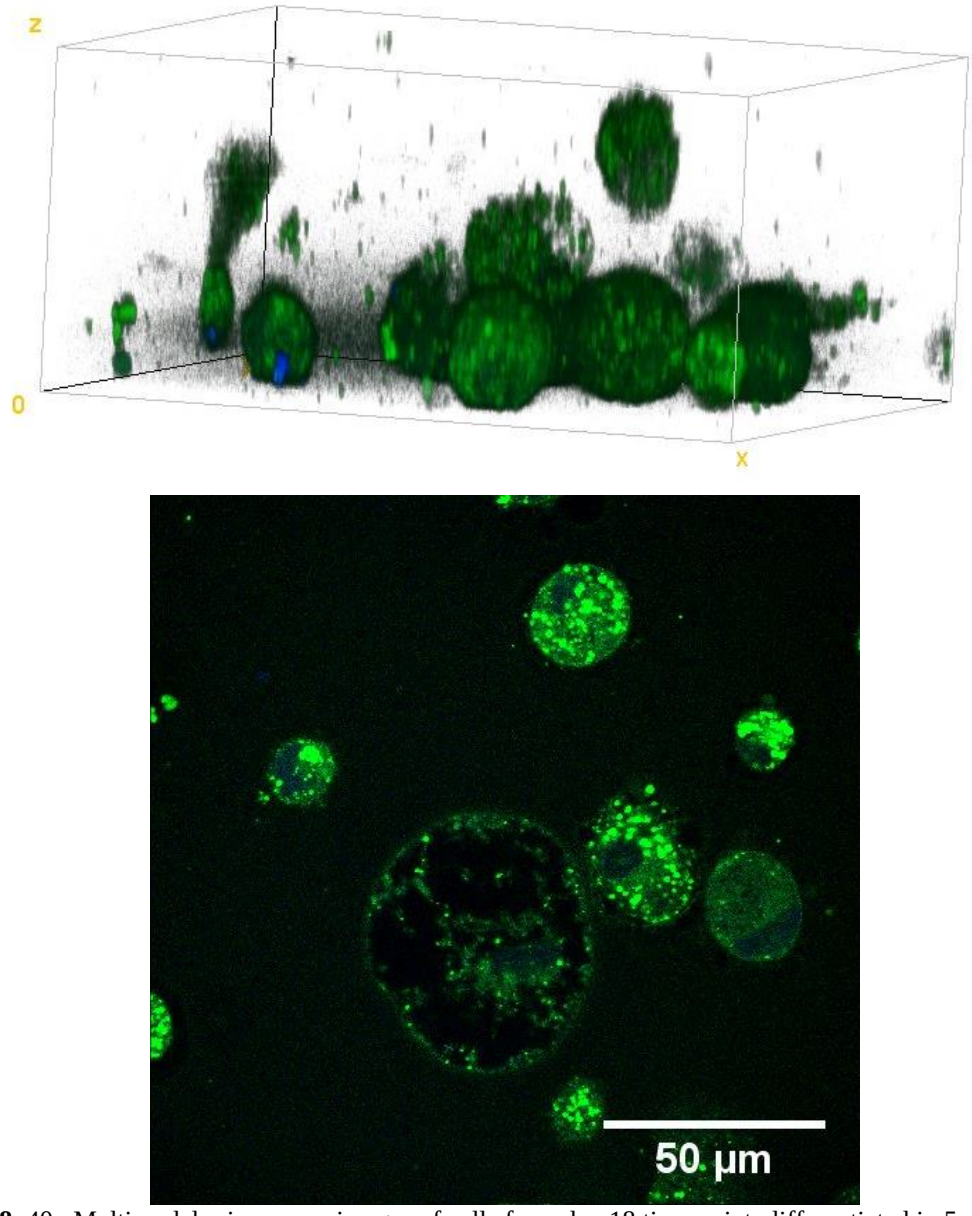


**Figure 18.** 40x Multimodal microscope images of cells from day 18 time point, differentiated in 5wt% ELP. Images have been taken two days past live/dead staining. Calcein staining and autofluorescence in green (MPEF) and EthD-1 staining in blue (MPEF). Upper image: Volume view of cells, analyzed with trilinear interpolation. Scale x-axis: 159.1 µm. z-axis: 76 µm. Bottom image: 2D image of cells, 15 µm from glass surface. Epi-straight filter 661/20 nm (blue), Epi-side filter 514/30 nm (green). Color gain G:0-45, B:0-33 counts per pixel.

**ELP Collagen 50/50**

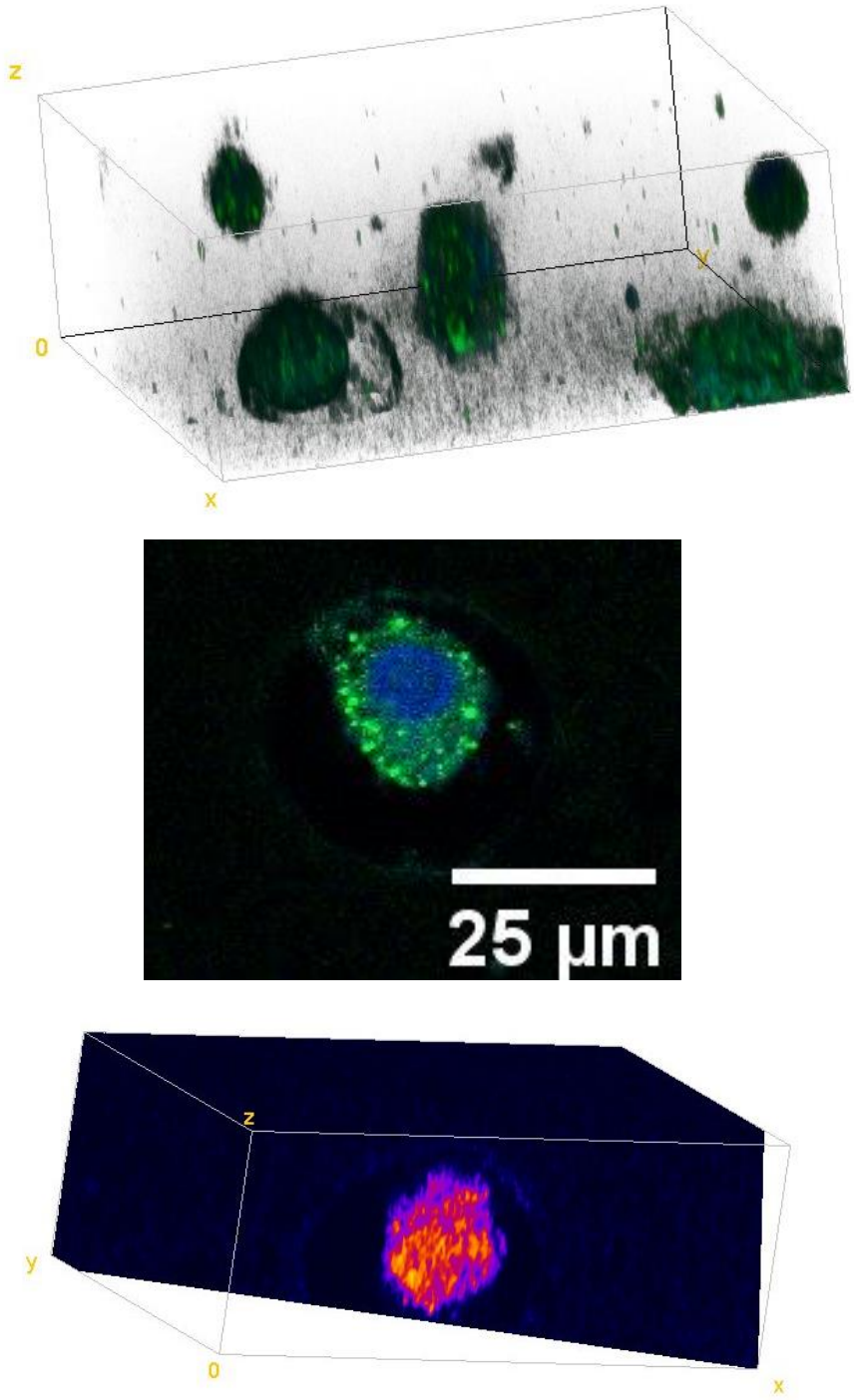


**Figure 19.** 40x Multimodal microscope images of cells from day 18 time point, differentiated in collagen/ ELP 50/50 hydrogel. Images have been taken two days past live/dead staining. Upper image: Volume view of cells in hydrogel. Scale x-axis: 158.48 µm, y-axis: 144.81 µm, z-axis: 56 µm. The image has been analyzed with trilinear interpolation. Middle image: 2D view of cell in hydrogel. Calcein staining and autofluorescence displayed as green (MPEF), EthD-1 staining as blue (MPEF). Bottom image: Volume view of the same cells as in the middle image. Image has been analyzed with trilinear interpolation and the intensity is ranging from low (blue) to high (yellow). Scale: x-axis: 89.18 µm, y-axis: 56.56 µm, z-axis: 34 µm. Epi-straight filter 661/20 nm (blue), Epi-side filter 514/30 nm (green). All images has the same gain, G:0-45, B:0-33.

**Collagen 4°C**

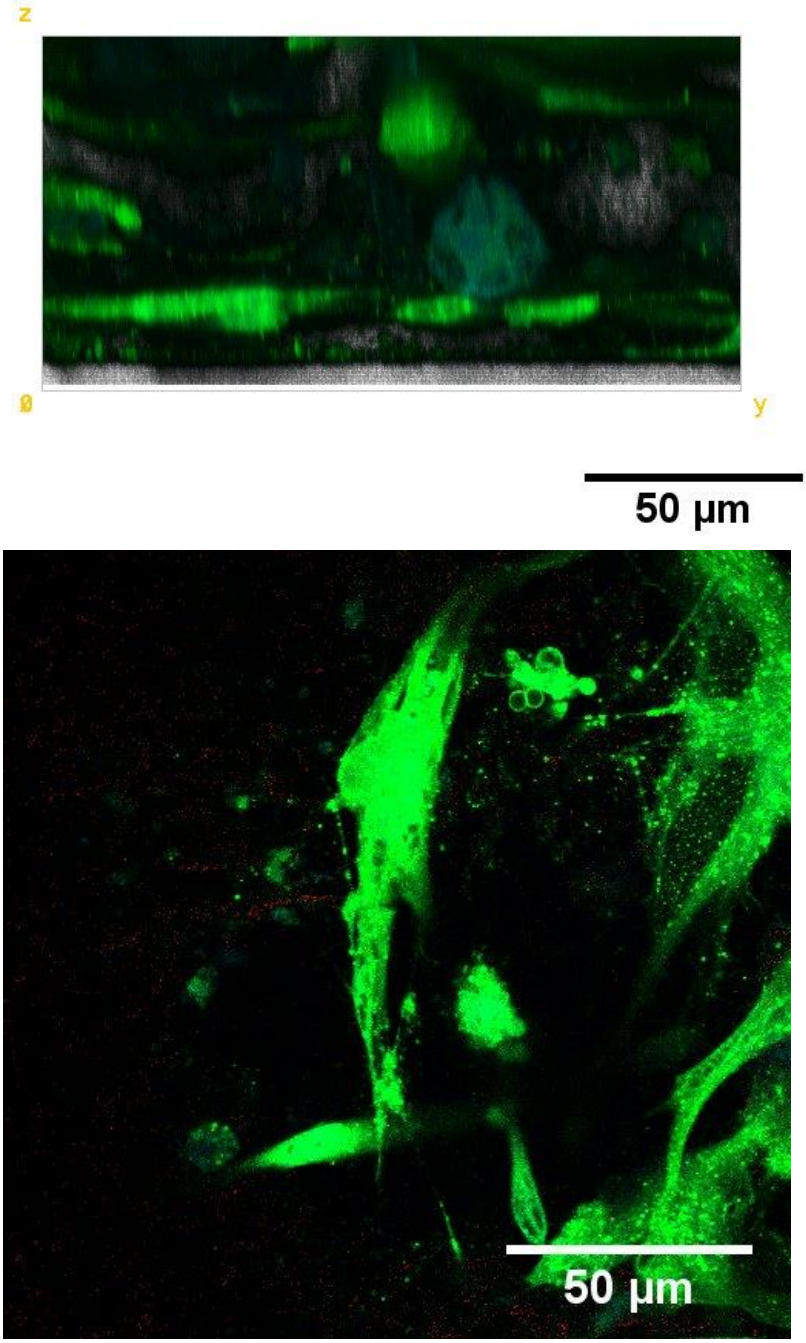


**Figure 20.** 40x Multimodal microscope images of cells from day 18 time point, differentiated in collagen 4 °C hydrogel. Images have been taken two days past live/dead staining. Calcein and autofluorescence in green (MPEF), EthD-1 in blue (MPEF) and collagen fibers in red (SHG). Upper image: A vertical cross section of the hydrogel. Image has been analyzed with trilinear interpolation. Bottom image: 2D image of cells in hydrogel. Forward filter: 405/10 nm, Epi-straight filter 661/20 nm (blue), Epi-side filter 514/30 nm (green). Both images have the same gain.

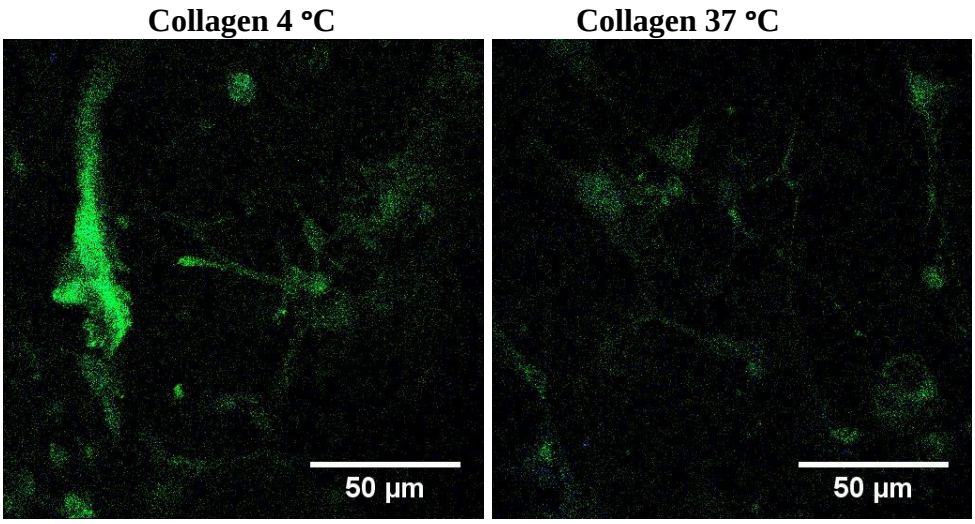


**Figure 21**. 40x Multimodal microscope images of cells from day 5 time point, differentiated in collagen hydrogels. Left: Collagen 4 °C hydrogel. Right: Collagen 37 °C hydrogel. Epi-straight filter 661/20 nm (blue), Epi-side filter 514/30 nm (green). Both images have the same gain.

## 4.2. ELP optimization

A survival study was performed in order to investigate how ELP, crosslinker and cell concentration affects proliferation. Viability was evaluated by cellular morphology and with a metabolic activity assay.

Table 10 summarizes which cells that have spread and which cells that have not after 3 days of culture. A new coating condition with ELP was included to investigate if the cells could proliferate on the protein. All coating conditions with no cell spreading were subjected to THPC during hydrogel incubation. Only one condition of ELP hydrogels (6000 cells/µl, 3wt% ELP, 1:1.4 ratio of THPC) showed cell spreading in 50% of the wells. No explanation for cell survival in these three wells can be given since they were seeded from the same vial and subjected to the same treatment as the three subsequent wells where cells did not spread.

The results from the metabolic activity assay are displayed in Figure 22. ELP coating show similar cell spreading and MTS value as the collagen coating which indicate that the protein is not toxic to the hADSCs. The results show that cells grown on 2D conditions, regardless of substrate, have much higher metabolic activity than cells grown in hydrogels. This result indicates that the issue with cell death has to do with the hydrogel composition. When comparing the absorbance values between the hydrogel seeded cells, none show a significant result which would favor that condition over the others. Also, no correlation between less ELP or lower crosslinker ratio and cell viability can be seen. Another observation is that the cell concentration does not seem to influence the results significantly since the absorbance value for each condition is similar for both concentrations. However, no examination of actual cell number in each well has been performed for this seeding.

Results from live/dead staining of the cells are presented in Figure 23. Cells cultured on collagen coating for three days can be seen in Image A. These cells clearly show spread morphology and have high esterase activity since the majority of the cells contain the green fluorescence calcein. A few dead cells with incorporated EthD-1 (red) were also observed in this condition. Cells grown on collagen coating subjected to THPC during hydrogel gelation time show significant difference in morphology as can be seen in image B. Even though the cells fluoresce in the green channel they are clearly round which indicates unhealthy cells.

Staining of spread cells in 3wt% ELP hydrogel with 1:1.4 crosslinker ratio are shown in image C. These cells, although encapsulated in a 3D matrix, show similar morphology as cells grown on collagen coating. Further, almost no cells with EthD-1 could be observed. The last image, D, visualizes cells grown in 1wt% ELP hydrogel with the same crosslinker ratio as in image C. This image is representable for all other conditions were no cellular spreading was observed. The round morphology and the relatively high detection of EthD-1 suggest low viability.

Figure 24 presents a 3D rendering of cells grown in 3wt% ELP investigated with 40x multimodal microscope. Both live/dead stain and morphology show that cells near the bottom of the hydrogel are more viable (green) than cells further up in the hydrogel (blue).

**Table 10. Cell viability after 3 days of culture.**

| Cell concentration (cells/µl) | Condition (crosslinker ratio) | Well 1 | Well 2 | Well 3 | Well 4 | Well 5 | Well 6 |
|---|---|---|---|---|---|---|---|
| 6000 | ELP coating | x | cell spreading | cell spreading | cell spreading | cell spreading | cell spreading |
| 6000 | 3wt% ELP (1:1.4) | cell spreading | cell spreading | cell spreading | x | x | x |
| 6000 | 3wt% ELP (1:0.7) | x | x | x | x | x | x |
| 6000 | 1wt% ELP (1:1.4) | x | x | x | x | x | x |
| 6000 | Collagen coating | x | cell spreading | cell spreading | cell spreading | cell spreading | cell spreading |
| 4000 | ELP coating | x | cell spreading | cell spreading | cell spreading | cell spreading | cell spreading |
| 4000 | 3wt% ELP (1:1.4) | x | x | x | x | x | x |
| 4000 | 3wt% ELP (1:0.7) | x | x | x | x | x | x |
| 4000 | 1wt% ELP (1:1.4) | x | x | x | x | x | x |
| 4000 | Collagen coating | x | cell spreading | cell spreading | cell spreading | cell spreading | cell spreading |

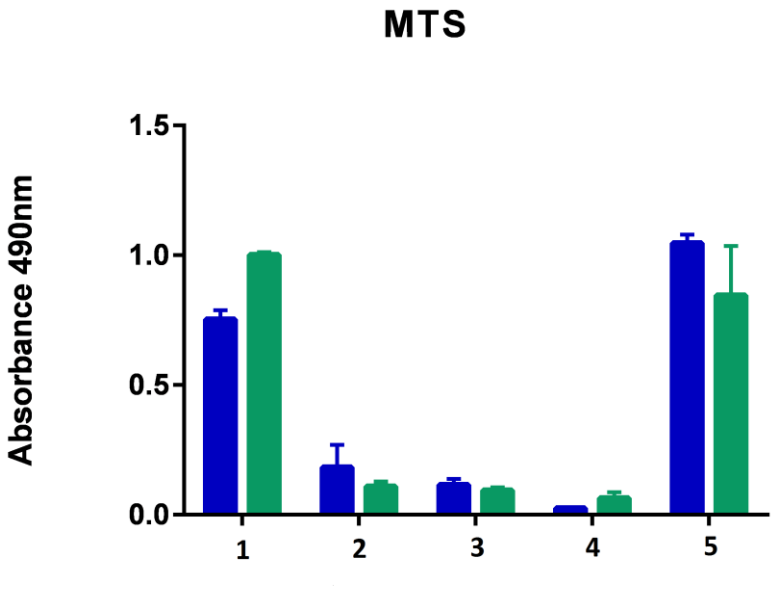


**Figure 22.** Absorbance measurements of formazan at 490 nm for metabolic activity assay. Blue bars represent cell seeding concentration of 4000 cells/µl and green bars represent the seeding concentration of 6000 cells/µl. 1: ELP coating 2: 3wt% 1:1.4 ELP hydrogel 3: 3wt% 1:0.7 ELP hydrogel 4: 1wt% 1:1.4 ELP hydrogel 5: Collagen coating.

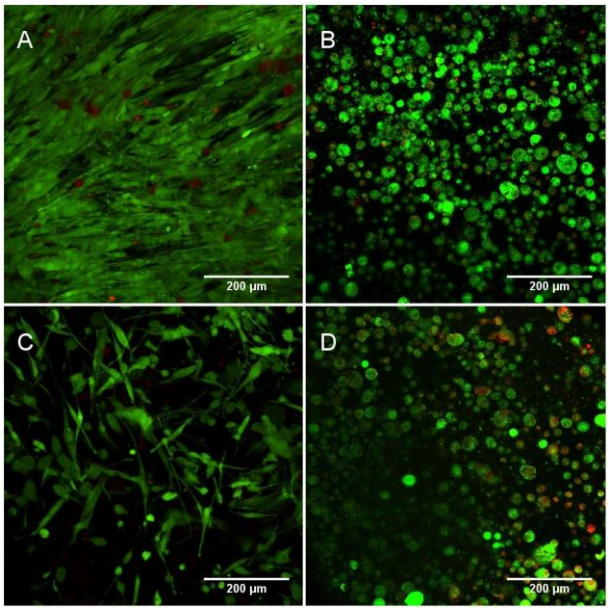


**Figure 23.** 20x confocal images of cells in ELP optimization trial. Calcein in green channel and EthD-1 in red channel. A: collagen coating. B: collagen coating with THPC added. C: ELP 3wt% 1:1.4 crosslinker ratio. D: 1wt% ELP 1:1.4. D is presentable for all other conditions with ELP except ELP 3wt% 1:1.4 crosslinker. (Scalebar: 200 µm, image sizes 710x710 µm)

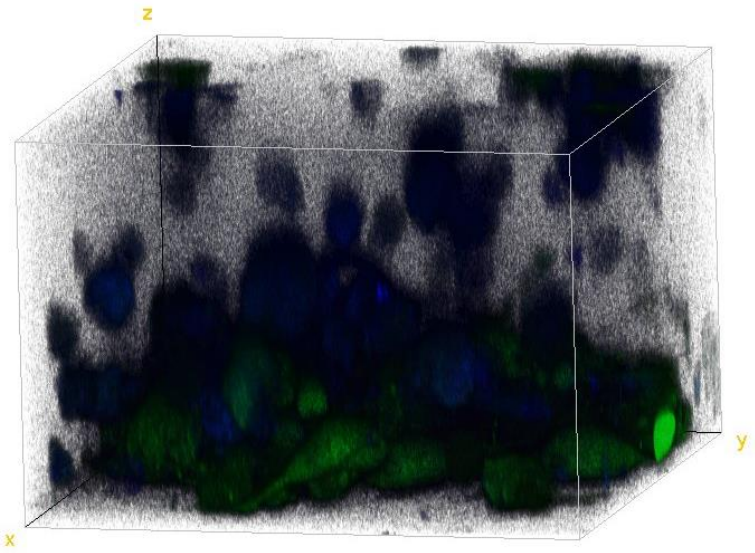


**Figure 24.** 40x multimodal image of cells that survived three days of culture in 3wt% ELP hydrogel with 1:1.4 ratio toward crosslinker. Image analyzed with trilinear interpolation in volume viewer (ImageJ). Calcein in green (MPEF) and EthD-1 in blue (MPEF). Scale x- and y-axis: 0-175 µm.

## 4.3. Second differentiation

This section presents the results of the second differentiation of hADSCs toward adipocytes and β-cells. Confocal and nonlinear images are presented and discussed together with cellular assays. Images from the immunocytochemical staining and bodipy staining are also included in this chapter.

### *4.3.1. ADIPOCYTE DIFFERENTIATION*

Knowledge gathered from the first experiment led to conclusions about changes that might enhance differentiation on ELP. Less stiff hydrogels are proposed where cells can spread at an early stage and expand during lipid accumulation if differentiation is achieved, and thereby avoiding obstruction of cell spreading. ELP with no crosslinker was investigated to examine the effect of ELP on differentiation without the cytotoxicity effects. Therefore ELP coating instead of collagen coating was performed as both a 2D control as well as an investigation of effects of ELP contra collagen coating. The viability of hADSCs on ELP coating has already been confirmed in the ELP optimization. A new hydrogel composed of collagen and ELP (explained in method section 3.1.2) was included in an effort to investigate ELP in hydrogels without the crosslinker cytotoxicity. This mix was then gelated with NaOH as prior collagen hydrogels with the hypotheseis that the adsorbed ELP would be incorporated and trapped inside the gel because of its size. The pure collagen I hydrogel (37 °C gelation temperature) from the first seeding was used as a positive control due to prior successful results. The crosslinking temperature of 37 °C for collagen was chosen over collagen 4 °C to ensure fast gelation times and thereby avoiding cell sinking. Results from measurements in CedexHiRes prior to seeding are stated in Appendix B.

With 3wt% ELP and lower concentration of crosslinker softer hydrogels than in prior investigations were prepared. Heilshorn *et al.* managed to promote neurite outgrowth in this more compliant matrix. Comparison with this successful outcome might not be guaranteed due to different cell type, but their results gave a direction in hydrogel matrix preparation

since both neurites and adipocytes are fragile cell types sensitive to stress and surrounding factors. There are many different fat compartments in the body with different properties[81] which makes conclusions from published literature on adipose tissue difficult to interpret. Adipose tissue of abdominal fat has been shown to have mechanical stiffness properties in the dimension of the elastic moduli of the prepared ELP hydrogels, giving strength to the used protocol.[81]

The three other factors changed in this second experiment were: cell incorporation inside hydrogels (instead of seeded on top), higher cell concentration and no coating prior to hydrogel seeding. These changes led to high hydrogel contraction resulting in small hydrogels with high cell density. This also led to many cells still being present outside of the hydrogel growing on a 2D surface composed of proteins from the hydrogel adsorbed to the glass surface during contraction, a conclusion made since cell attachment directly on glass surfaces with no coating is difficult to maintain.

#### 4.3.1.1. Time point day 2

Confocal images from day 2 (Figure 25) are comparable to that of the first seeding with few exceptions. Cellular morphologies are again spread on coated surface (ELP) and the two different collagen containing hydrogels whereas round cellular phenotypes are dominating in the hydrogels consisting of ELP with THPC. Live/dead staining show high cell viability on coating and in collagen hydrogels, and lower in hydrogels containing ELP. The ELP hydrogel where the cells were seeded on top were too opaque for visualization so images where taken outside of the hydrogel, on the glass surface. Subsequent non-linear images of cells seeded on top of the ELP hydrogel showed consistent round morphology (Figure 26). Cell spreading on ELP coating and collagen/ELP hydrogel show that ELP is supporting cell spreading when not crosslinked with THPC, as seen in the ELP optimization. Nonlinear images (Figure 26) show high confluence of cells on ELP coating with higher cell concentration compared to the first seeding, due to higher seeding concentration. Cells seeded on top of ELP hydrogel or encapsulated in ELP hydrogel show round morphology. That cells show different morphology when seeded on 2D ELP coating (Figure 26 A) and on top of ELP hydrogel (Figure 26 B), which should provide similar attachment for the cells suggest crosslinker toxicity. Morphology of cells incorporated inside the hydrogel (Figure 26 C) could except from crosslinker toxicity, also suffer from the inability to degrade the matrix and therefore not expand in the hydrogel. Figure 27 shows nonlinear image suggesting that the stiffness of the hydrogel is still too high for hADSCs to expand and that cellular degradation of the matrix is not present. Certainty that the results from the collagen hydrogel with adsorbed ELP are affected by the presence of ELP cannot be guaranteed since a molecular investigation of content in the hydrogel have not been performed.

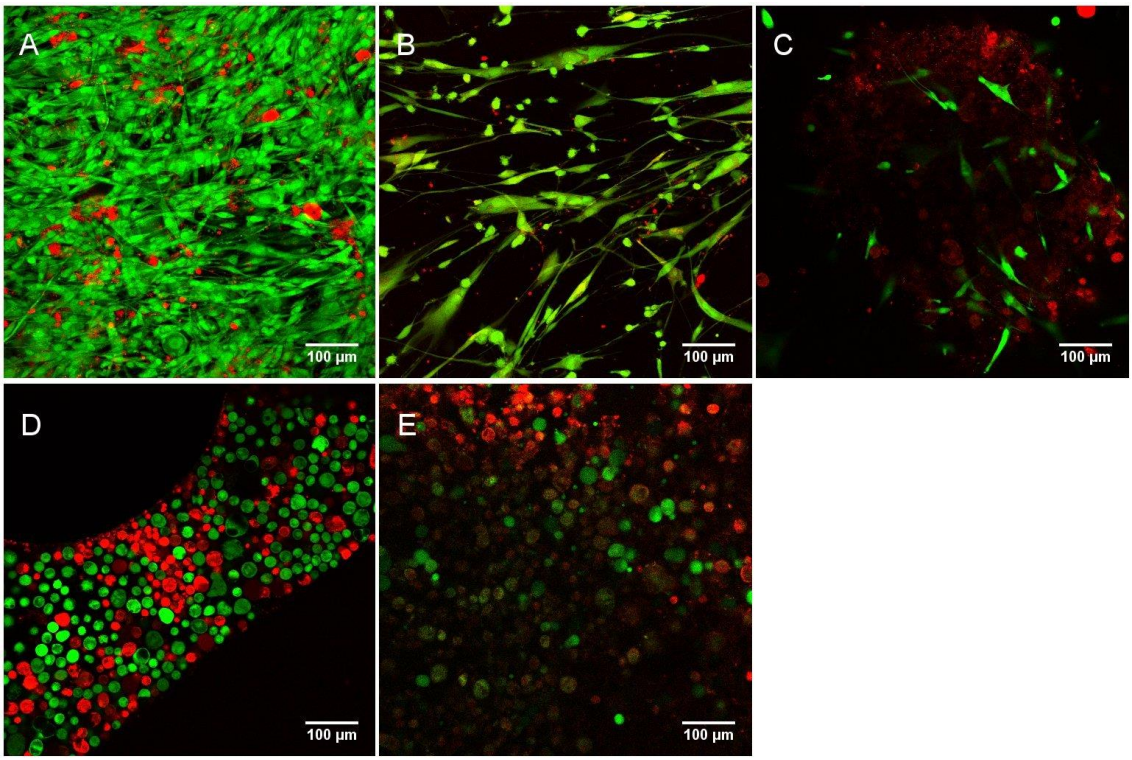


**Figure 25.** Confocal images of live/dead stained cells at day 14 with calcein in green and EthD-1 in red. A - ELP coating. B – Collagen hydrogel, C - collagen/ELP hydrogel. D – ELP hydrogel with cells seeded after gelation. E– ELP hydrogel with cells encapsulated inside. (Scalebar: 100µm, image sizes 710x710 µm)

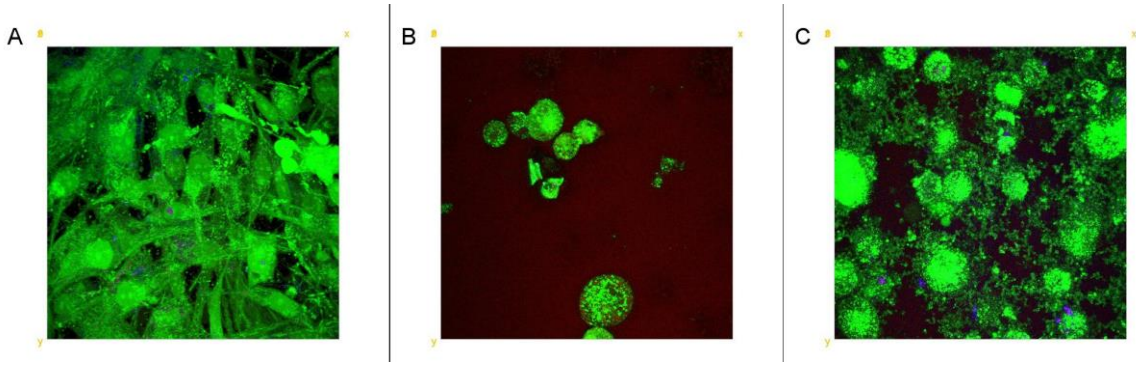


**Figure 26.** Nonlinear images of live/dead stained hADSCs on day 2 with calcein in green and EthD-1 in blue. A – ELP coating, B – ELP hydrogel, cells seeded on top, C – ELP hydrogel with encapsulated cells. Image size 171,9 x 171,9 µm.

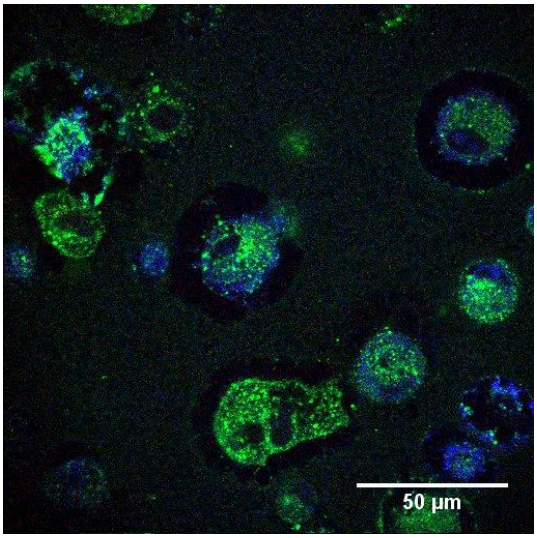


**Figure 27.** Nonlinear images of live/dead stained cells with calcein in green and EthD-1 in blue for ELP hydrogel 3wt% with crosslinker ratio 1:1.4.

When amount of live stain versus dead stain was calculated at day two, results consistent with the first seeding are obtained (Figure 28). A higher amount of dead cells are present in the hydrogels containing ELP crosslinked with THPC.

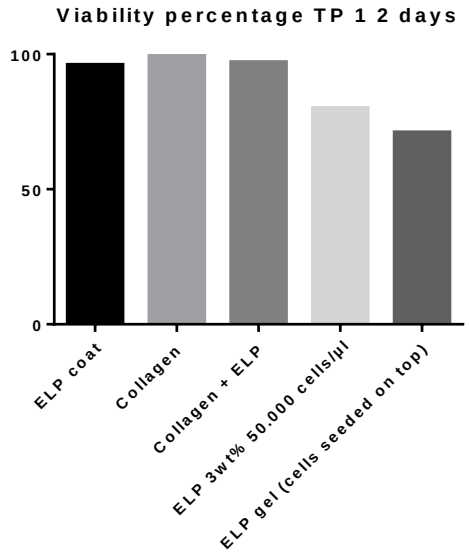


**Figure 28.** Live stain divided by total stain in confocal images at day 2.

## Metabolic activity assay

The MTS assay (Figure 29) shows that cells on 2D coating of ELP are most metabolically active at day 2, followed by collagen hydrogel and then lower in the ELP hydrogels crosslinked with THPC and the collagen/ELP hydrogel. When normalized to number of viable cells, determined with CEDEX cell counter, cells in ELP hydrogel showed highest value, though strongly varying between wells. Again, it must be pointed out that values in this assay are varying greatly. Problems with this assay combined with ELP hydrogels as mentioned earlier seem to be persistent and no conclusions will be based on these results. The low value of cells on ELP coating after normalization might depend on faster saturation on 2D surfaces since MTS tetrazolium does not need to penetrate into the hydrogel prior to conversion into formazan. A time dependent investigation of cells on 2D surfaces and cells incorporated in hydrogels could be of value to improve the assay.

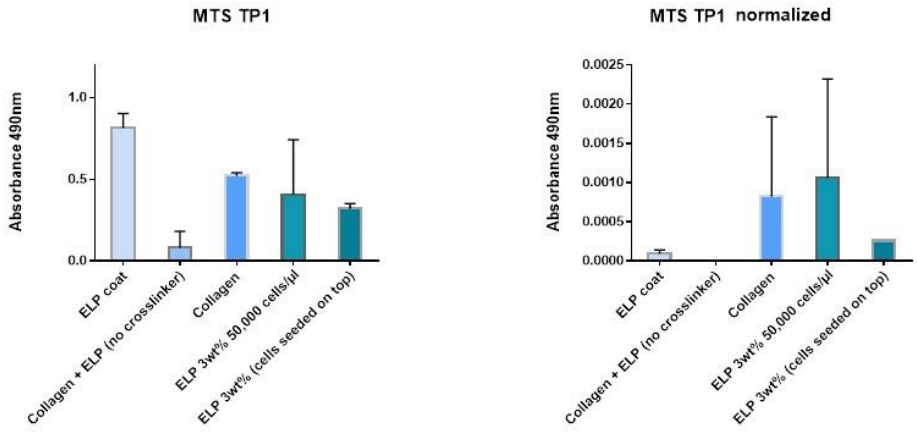


**Figure 29.** Metabolic activity at day 2**.** Overall average value/well and normalized value to viable cell number counted in CEDEX HiRes.

#### 4.3.1.2. Time point day 14

Confocal images with live/dead staining from day 14 are shown in Figure 30. Viable cells show a more contracted morphology compared to day 2 which is typical for adipocytes, giving strength to that differentiation has occurred. Cells on ELP coating have a higher amount of cells with ruptured membranes (red). A possible explanation to this is the high cell concentration that, on a coated surface, might give a too high cell density since the cells have no distribution in the z-axis (height). Cells in collagen hydrogel and collagen/ELP hydrogel have a high viable cell amount. Cells on and in ELP hydrogels with THPC have a higher amount of dead cells and the morphology of the cells is round. Figure 31 show nonlinear images of all conditions investigated. Lipid droplets in red (CARS) are apparent in all wells with ELP coating, collagen hydrogel and collagen/ELP hydrogel. No lipid droplets are visible in cells in ELP hydrogel or in cells seeded on top of ELP hydrogel.

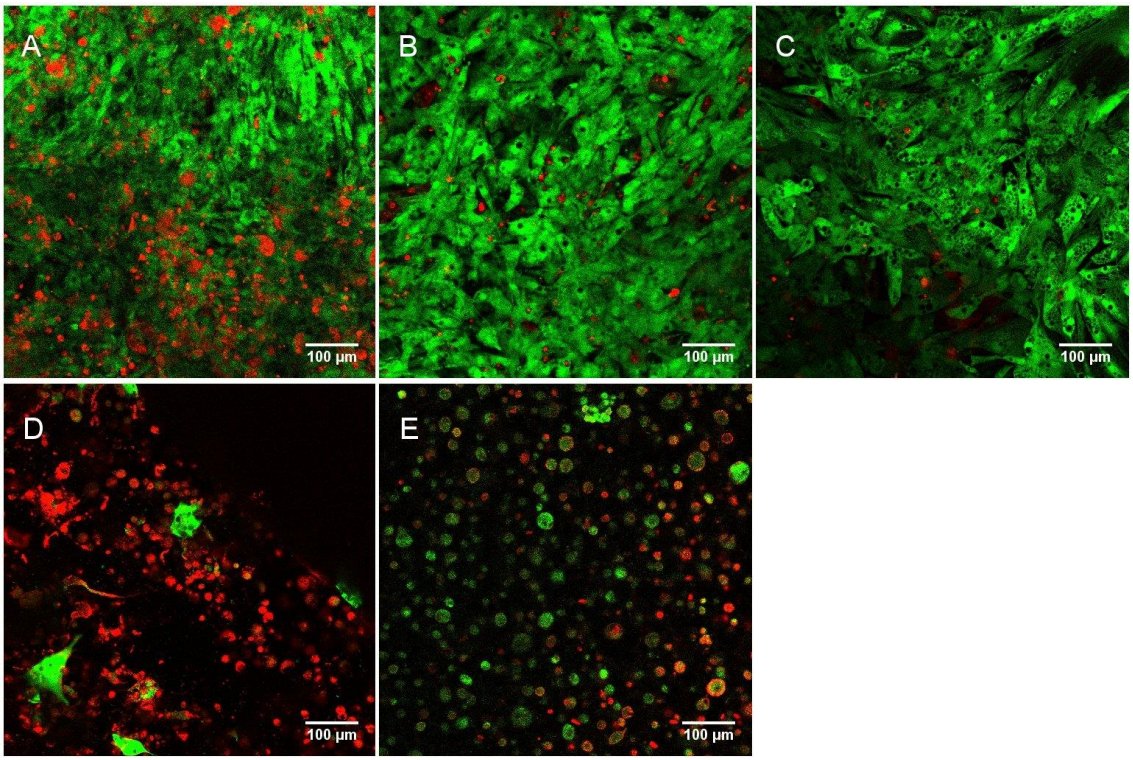


**Figure 30.** Confocal images of live/dead stained cells at day 14 with calcein in green and EthD-1 in red. A - ELP coating, B – collagen hydrogel C - collagen/ELP hydrogel. D - ELP hydrogel with cells seeded after gelation, E - ELP hydrogel with cells encapsulated inside. (Scalebar: 100 µm, image sizes 710x710 µm)

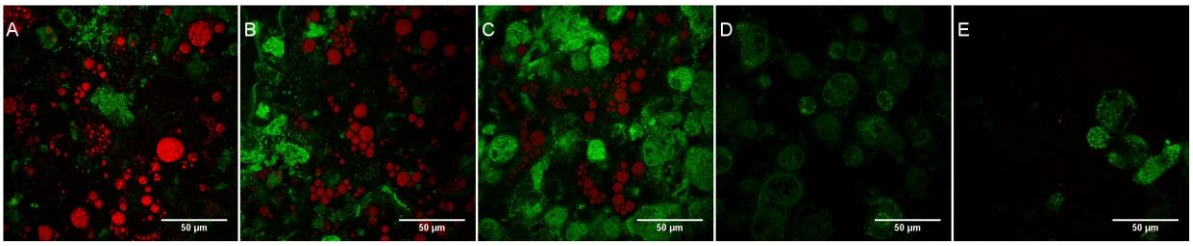


**Figure 31.** Nonlinear images of unstained cells at day 14 with lipid droplets in red (CARS) and autofluorescence in green (MPEF). A – ELP coating. B – Collagen/ELP hydrogel. C – Collagen hydrogel. D - ELP hydrogel. E – Cells on top of ELP hydrogel. Scalebar 50 µm, image sizes 180,1 x 180,1 µm

After 13 days the amount of live stained cells in hydrogels containing ELP crosslinked with THPC is very low compared to dead stained cells (Figure 32)

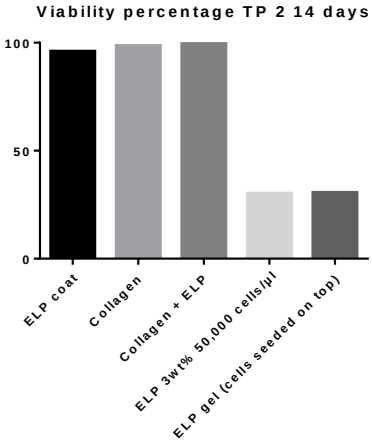


**Figure 32.** Live stain divided by total stain in confocal images at day 14.

## Lipid droplet analysis

A lipid droplet analysis of larger lipid droplets (above 4 µm) was performed. Larger lipid droplets are more interesting since they bear more resemblance to mature adipocyte lipid droplets. Cells that were outside of the hydrogel due to contraction were calculated separately because they have different external surroundings. A total of 50 lipid droplets per condition were investigated. Larger lipid droplets were found to range between 4 – 22 µm with most abundant ranges between 4 – 10 µm (Figure 33). Lipid droplets show little difference in size between the three conditions, although cells differentiated in collagen hydrogel have more lipid droplets in the range 6-8 µm where the other conditions have the most lipid droplets in the 4-6 µm range. Total amount of lipids/cell was calculated for three cells per condition as area of lipids divided by cellular outlines (example in Figure 33). This resulted in lipid percentages of 46% in ELP coating, 52.6% in collagen/ELP hydrogel and 42% in collagen hydrogel. These are higher values than calculated in the first seeding, suggesting that higher cell concentration promote higher lipid content. Lipid percentage is highest in the hydrogel containing ELP adsorbed to collagen. An analysis of amount of lipids droplets (> 4 µm) per cell in the different conditions was performed with the intent that lesser amount of lipid droplets versus total lipid content can assess the degree of differentiation. The number of lipid droplets per cell was on average 9.67 on ELP coat, 9.33 in collagen/ELP hydrogel and 11 in collagen hydrogels. This show that lipid droplets are fewest in collagen/ELP hydrogel as well as they take up the largest area in this condition, suggesting more similarities with mature adipocytes. Difficulties with estimating cell outlines inside hydrogels complicated the lipid per volume investigation, and that is the reason for few replicates (3 cells) in this calculation. The values may therefore not be representable for the whole well. Figure 34 shows comparative images of cells inside a hydrogel and cells outside of a hydrogel. Cell outlines are more clear and easily estimated (image B) when no disturbance from autofluorescence or cell debris is present (image A).

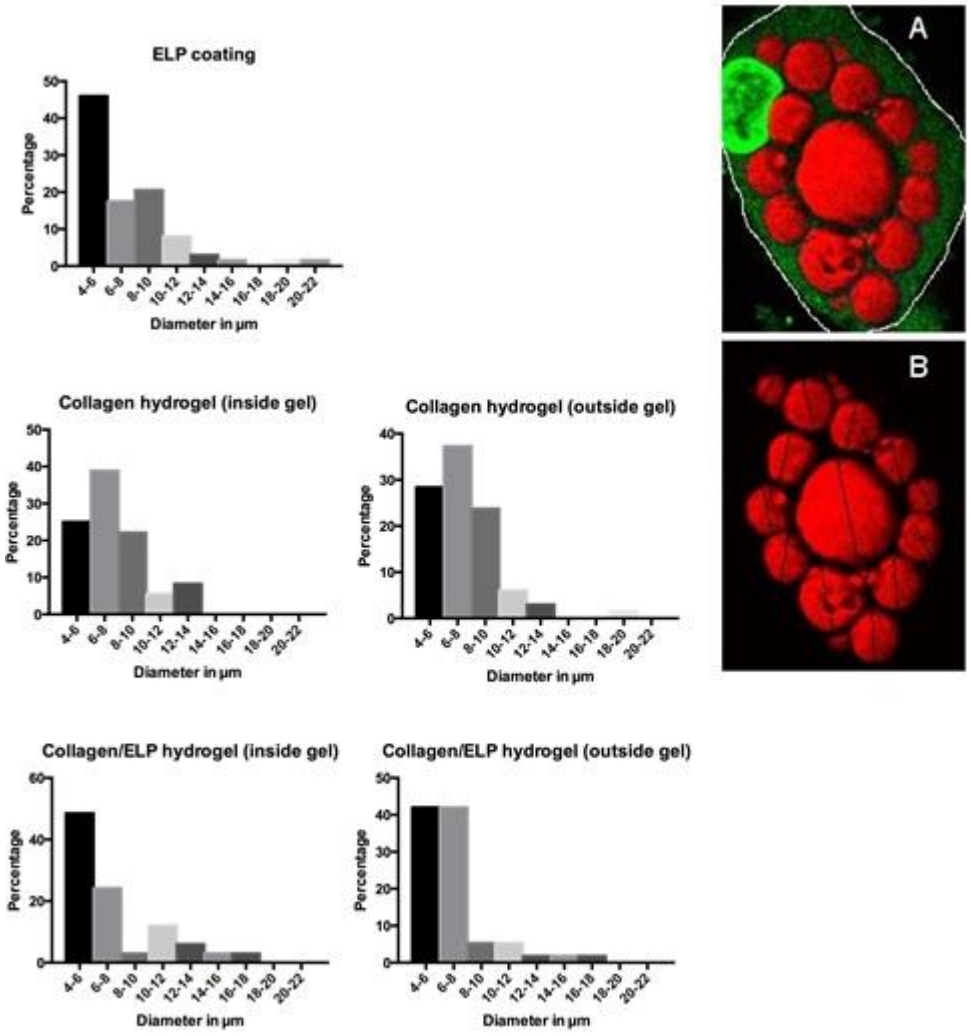


**Figure 33.** Histograms showing lipid droplet size. Cells growing outside of hydrogel due to contraction have been measured separately due to different external factors that might affect differentiation, even though seeded inside the hydrogel at day 0. Lipids smaller than 4µm are excluded. A – Example of cell outlines drawn by hand to calculate area with ImageJ with lipid droplets in red (CARS), cytoplasm in dark green (MPEF) and Hoechst staining in bright green (MPEF). B – Lipid droplets diameter drawn. Measured by hand with ImageJ. Cell from collagen/ELP hydrogel (outside gel)

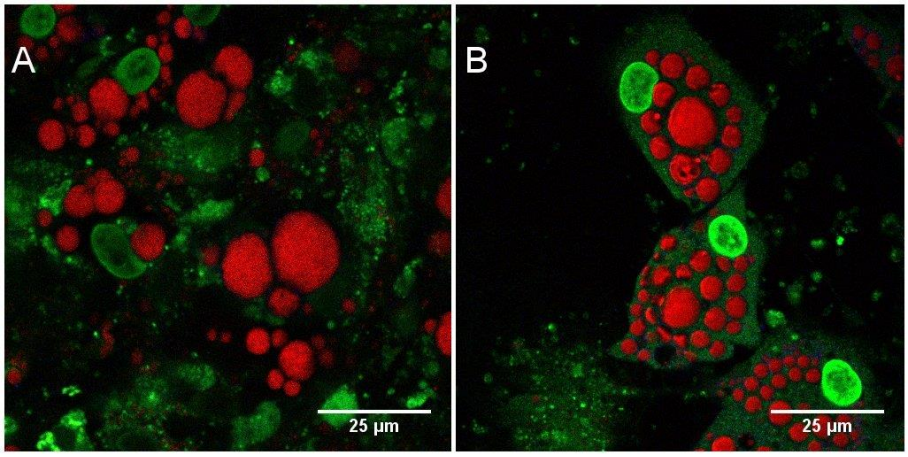


**Figure 34**. Comparison of cells inside hydrogel and outside hydrogel due to contraction. Nonlinear images with lipid droplets in red (CARS), Hoechst staining in green (MPEF), and autofluorescence in darker green (MPEF). A – cells inside collagen/ELP hydrogel. B – cells outside hydrogel with less disturbing fluorescence from surrounding cells and debris.

## Metabolic activity

After 14 days the metabolic activity assay indicates that metabolic activity of cells in ELP with crosslinker hydrogels have diminished to very low values, but that cells on ELP coated wells as well as in collagen hydrogel and collagen/ELP hydrogel have relatively high activity. The normalized values show much higher metabolic activity in cells in collagen and collagen/ELP hydrogels compared to ELP coating. A reason for this could be that when cells are counted in order to normalize the value, more cells detach from the ELP coated surface than from inside of the hydrogels, hence giving lower value according to absorbance divided by viable cells. The cells that are encapsulated inside the hydrogel cannot break out of the hydrogel prior to cell counting giving a lower, but false value on viable cell concentration. Problems with saturation as described earlier might also be present. This concludes that the MTS assay overall has many disadvantages when working with hydrogels of different composition when trying to compare values between the conditions.

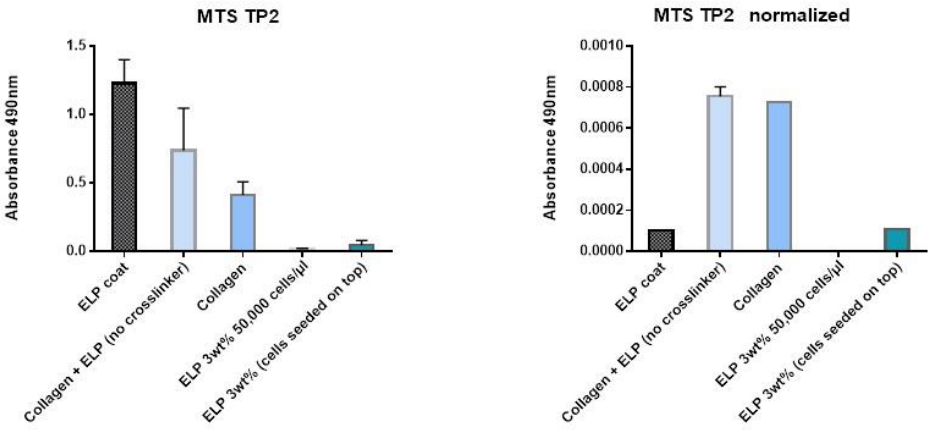


**Figure 35.** Metabolic activity at day 14. MTS values in total and normalized to number of viable cells. Cell counting was done with CEDEX HiRes.

## Adipogenic phenotype assessment

In this section, stem cell marker CD105, as well as lipid droplet associated protein perilipin are investigated. The neutral lipid stain bodipy is also examined.

## Surface marker for mesenchymal stem cells – CD105

CD105, or endoglin, is a surface protein of mesenchymal stem cells and should show strong presence in wells before differentiation is commenced.[82] Immunolabeling of this protein at day 2 (Figure 36), before differentiation, show presence of this protein pointing to that there in fact are stem cells (hADSCs)[83], and that the purity of the stem cells seem high. The strongly fluorescing cells in image A are stained with antibody versus CD105. Compared to unlabeled cells in image B presence of CD105 in A is determined. Image C is the same image as image B with increased gain to show that cells are present, but low fluorescing compared to A. Image D is CD105 and Hoechst stained and show strong signals versus image E which is the secondary antibody control (and Hoechst stained). At day 14 of differentiation lower presence of CD105 was detected in cells containing lipid droplets pointing towards that the transcription of CD105 is altered during differentiation (Figure 36, F).

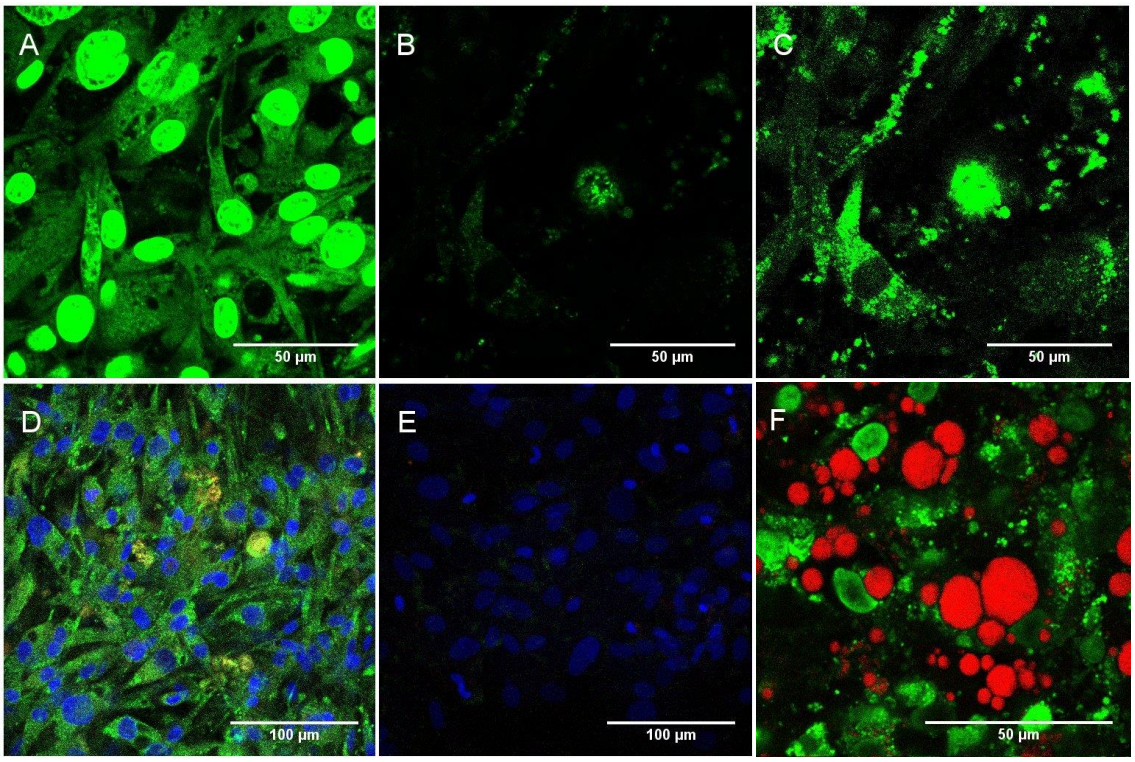


**Figure 36.** CD105 labeled cells at day 2 (A-E) and at day 13 (F). A - CD105/Hoechst stained cells (green) day 2. B - Unlabeled cells day 2. C - (B) again with higher gain to show cell presence. D - CD105 (green) and Hoechst staining (blue) in confocal microscope. E - Control stained only with secondary antibody and Hoechst (blue). F - Differentiated cells at day 13 with lipid droplets in red (CARS) show low fluorescence from CD105 compared to autofluorescence from cell debris.

## Adipogenic markers – Perilipin expression

Neutral lipids synthesized by adipocytes are stored in lipid droplets[84] and are only used in times of need, i.e. stress, starvation or similar. Perilipin is a protein present in adipocytes with the role of encapsulating lipid droplets, hindering lipases to break down the lipids in basal conditions.[85] Perilipin governs the hormonal storage and release of triglycerides where phosphorylation of perilipin by protein kinase A leads to lipolysis by hormone sensitive lipase and adipose triglyceride lipase.[86] Perilipin is primarily found in adipocytes [87] making it a good adipogenic differentiation marker to compare with results from nonlinear microscopy. Figure 12 shows perilipin present at the lipid droplet borders. Image D shows perilipin imaged with a 609/57 nm filter. When filter was changed to a 720 nm short pass filter (image F) perilipin intensity was increased due to factors from the microscopic setup. The dichroic mirror in the setup used is blocking most signals below 635 nm and this only permits a low amount of photons with lower wavelength to pass through. Since the short pass 720 nm filter permits all wavelengths between 650 nm and 720 nm more unspecific signals from the cells are also included. Imaging with filters in that high wavelength range is possible since Alexa Fluor 594 have broad emission ranging from 580 nm to 750 nm. Perilipin should primarily be found in differentiated adipocytes so immunolabeling of hADSCs at day 2 and adipocytes at day 14 should show difference in fluorescence at 580 nm-720 nm (emission spectra of Alexa 594). Interestingly there seem to be, even though low and not ordered, presence of perilipin in the undifferentiated cells (Figure 38). The gain in this image is increased compared to Figure 37 F, and not comparative in signal. Since the stem cells used are extracted from adipose tissue,

the finding that perilipin seems to be existing in the hADSCs before differentiation protocol towards adipocytes is started, might have importance regarding the hormonal state of the stem cells. If the hADSCs that are able to differentiate into several cell types such as osteoblast, chondrocytes[88] and β -cells have already started to commit to adipogenic fate, then research trying to assess these other cell types may have problems with successful differentiation. If endocrine signals are inducing perilipin transcription, then other adipogenic factors might also be present, which should be further investigated.

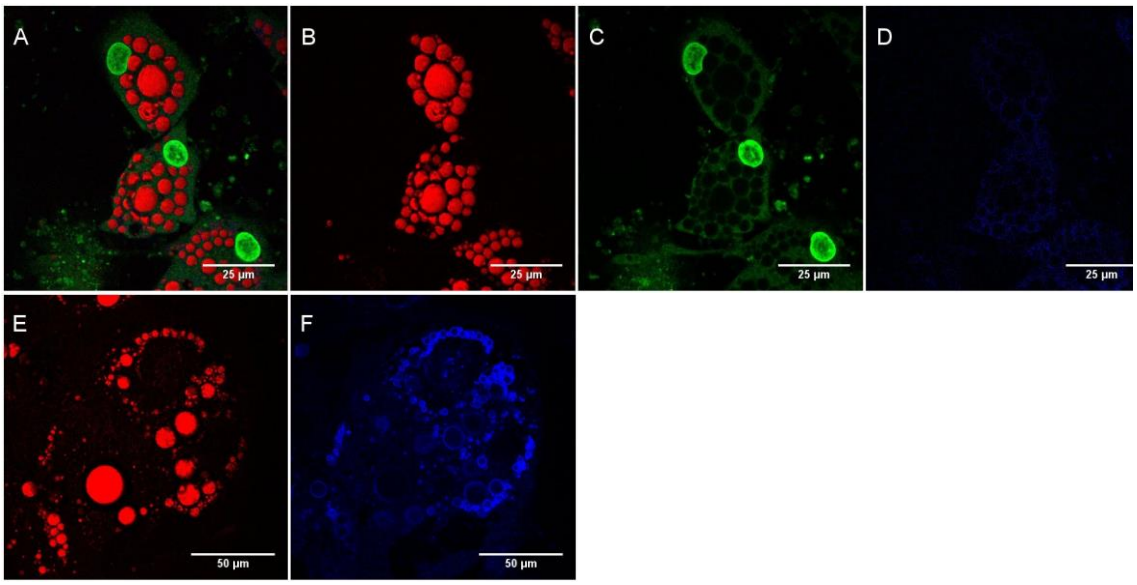


**Figure 37.** Hoechst stained and Perilipin antibodystained cells at day 13 with lipid droplets in red (CARS), Hoechst staining in bright green (MPEF), autofluorescence in darker green (MPEF) and perilipin in blue (MPEF). A – All channels. B - CARS at 661/20 nm. C - fluorescence at 514/30 nm. D – fluorescence at 609/57 nm (perilipin). Photon hits increased due to low signal at 609/57 nm due to dichroic blockage of wavelengths < 635 nm.
E- Lipid droplets (CARS). F – Perilipin imaged with short pass filter 720 nm yielded much stronger signals of perilipin but more unspecific signals from cells.

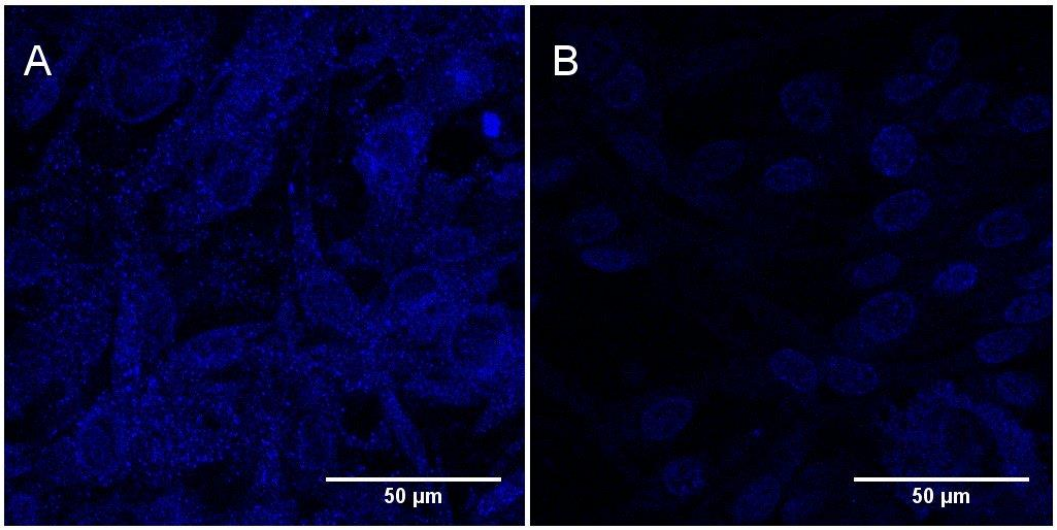


**Figure 38.** Nonlinear images of cells at day 2. A – Perilipin immunostaining in blue (MPEF) and Hoechst staining in blue (MPEF) leaking through filter. B – Hoechst staining for comparison to verify that signals in A is not unspecific Hoechst staining or autofluorescence. (only SP720 nm filter channel included for better visualization of difference.)

## Lipid droplet stain – Bodipy

Bodipy (D-3922) staining of neutral lipids is a common way to visualize lipid droplets. It is a very intensely fluorescing molecule making detection easy but also impairs possible other nearby signals due to its potency. To verify the non-linear microscopy setup of lipid imaging, bodipy staining was performed. This shows that lipid droplet location and size exactly corresponds to CARS signal (Figure 39). When working with adipocytes without access to non-linear microscopy, bodipy staining is a suitable method to image lipid droplets. Bodipy stain in hADSCs at day 2 prior to differentiation, where hypothesized to give low fluorescent signal since no lipid droplets should yet have been formed. Figure 40 confirms lower presence of bodipy stain but there seem to be a few small lipid droplets present also at this time point. This could strengthen the finding of perilipin being present in the hADSCs at day 2. Since many cell types have been found to store lipids in droplets, this discovery does not ensure that the stem cells have committed to adipogenic fate, but further investigation to assess the state of the hADSCs could be valuable.

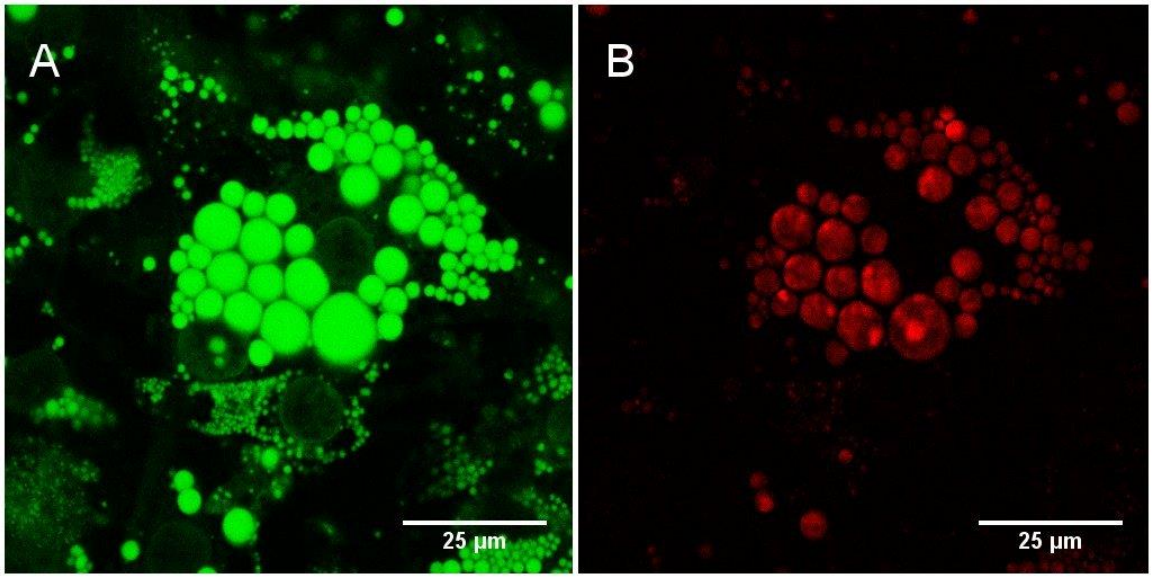


**Figure 39.** A- Bodipy stained cells imaged with filter 514/30 nm in green (MPEF). B – Same cells imaged with filter 661/20 nm in red (CARS).

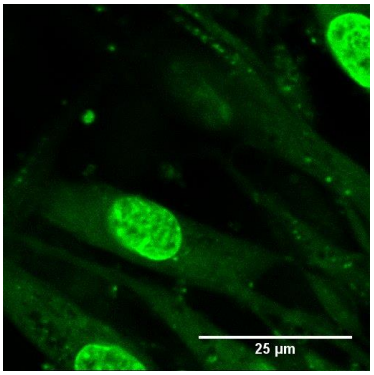


**Figure 40.** Bodipy and Hoechst stained hADSCs in green (MPEF) at day 2, showing small lipid droplets. Larger bright green is nucleus.

## Cellular distribution in hydrogels

All hydrogels in the second seeding were put in an incubator at 37 °C directly after seeding each condition to prevent cells from sinking to the bottom of the well and to reduce toxicity of the crosslinker. Despite this, a higher cell concentration was found near the bottom due to sinking (Figure 41). The interesting fact is that cells near the glass bottom had both more and larger lipid droplets and less undifferentiated cells (Figure 41). This suggests that cells prefer a solid surface to spread on, that the glass bottom provides, to improve differentiation. Another possible explanation is that the cells can spread more easily under the gel which is not covalently bonded to the glass bottom. It could also depend on lower nutrient availability in the middle of the hydrogel due to high cell density, however, the upper borders of the hydrogels also show less differentiation than the bottom reducing the strength to this assumption.

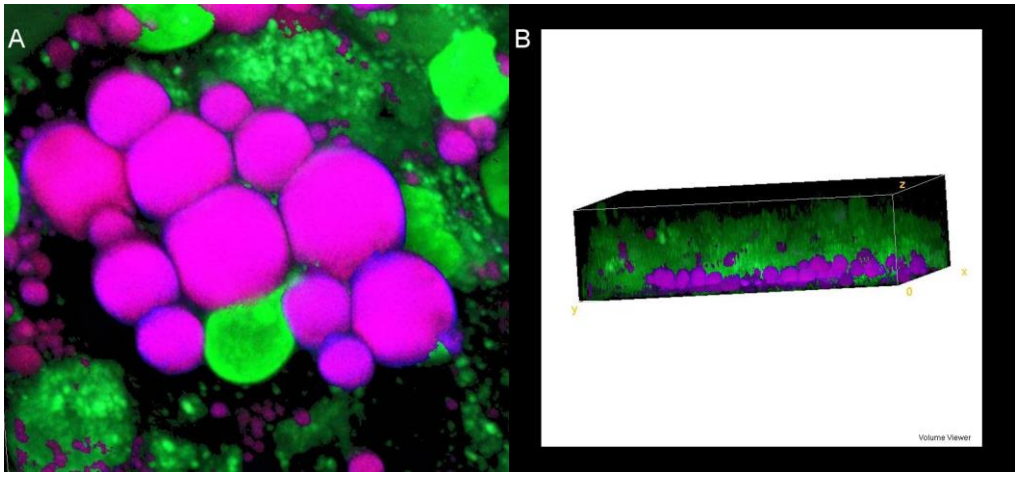


**Figure 41.** A – 3D rendering of cell near glass bottom in a collagen hydrogel. Lipid droplets in purple (CARS) and nuclei in green (cell outlines not visible). B - 3D rendering of adipocyte distribution in collagen hydrogel. Lipid droplets (purple) near bottom and increasing autofluorescing less differentiated cells (green) as height increases. Length of cell in A - 45,7 µm. Image size in B –180,1x180,1x51 µm

## Hydrogel degradation effect

The mechanical properties of a hydrogel matrix are as mentioned of high importance for the fate of the encapsulated stem cells. Properties similar to that of the natural ECM are suggested to favor differentiation. Results show that the successful differentiation in hydrogels composed of the natural ECM protein collagen is also dependent on the degradation of the matrix. The negative differentiation results from the ELP matrix are (together with crosslinker toxicity) assumed to depend on the inability to degrade the matrix, making cell spreading prior to anchoring impossible. Figure 42 shows the matrix degradation over time, where collagen fibers seem to have been completely degraded whereas the ELP remains similar over time. This is also presented earlier in Figure 27 where cells seem to have tried to grow, pushing onto the hydrogel, and then collapsed due to failure of expanding. Hydrogel degradation was assessed with nonlinear microscopy, where SHG was used to image collagen fibers (image A, B) and CARS to assess ELP structure (image C, D). That the cells show a morphology suggesting dead cells already at day two could explain the non-degraded ELP. If

the cells die early due to toxicity of the crosslinker, they can obviously not degrade the matrix. More experiments where the toxicity is reduced need to be carried out to ensure the degradation capabilities of ELP. A result that can be more surely obtained from this degradation assay is that the ELP is stable in wet condition at 37 °C during the two weeks of incubation.

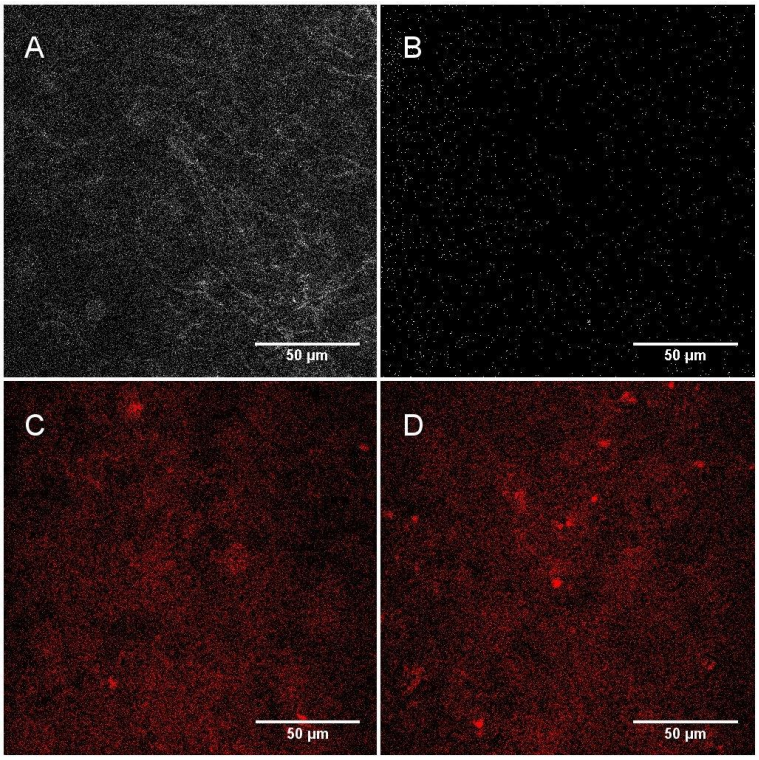


**Figure 42.** A – SHG signal from collagen fibers at day 2. B – SHG signal from day 14 shows degradation of collagen. C – CARS signal from ELP at day 2. D – CARS signal from day 14 shows no degradation of ELP.

### *4.3.2. β-CELL DIFFERENTIATION*

This section is devoted to the results obtained in the second differentiation of hADSCs toward beta-like cells. Initially, results from the metabolic activity assay will be presented and discussed. Later images of cells from the live/dead staining from both time points are displayed. These are followed by a discussion of the results obtained with non-linear microscopy. Subsequently, images from the Bodipy staining and an argument of the findings are given. As an important verification of β-like cells, GSIS and C-peptide ELISA assays were performed. Finally, images from the immunocytochemistry are presented for cells grown in LM 511 50 µg/ml hydrogel. Results from the other conditions can be found in APPENDIX G.

#### 4.3.2.1. Metabolic activity assay

The absorbance measurements at 490 nm of formazan for both time points are presented in Figure 43. The result is based on two measurements for each condition except for ELP coating at day 5 where only one measurement has been performed. An overall analysis of the chart reveals that the metabolic activity decreases with time but less variation between

conditions can be observed at day 16 in comparison to day 5. The fact that measurement from the first time point indicates quite large variation is probably due to the selected wells. At this time point the first and the last wells for each condition were selected. As a consequence of pipetting, the cell number in each well is probably not consistent and decrease as the hydrogels has been cast. For the second time point the wells chosen for examination were adjacent to each other and the results indicate less variation. In this time point the variation between conditions are also quite small when the results have not been normalized to cell number.

The number of cells in each well was counted with the Cedex cell counter and the results were used to normalize the absorbance values; results are presented in Figure 44. This procedure was performed since the proliferation assay does not take into account the actual cell number in each well, it only measure the amount of formazan produced by living cells. One problem which was raised during that procedure was hydrogel losses. The hydrogels were very loose and during the washing step some of the hydrogels were rinsed away resulting in an absorbance value for the proliferation assay but without any cells in the counting step. For that reason some of the values have been corrected by the average of the other hydrogels for these conditions. This approach might not be optimal but the result could provide a hint of the viability for that condition. One of the values that had to be adjusted was the cell number for the second measurement of LM 511 50 µg/ml which might be an explanation to the large error bar. For more information of which cell concentration that has been used, see APPENDIX H. However, when analyzing this chart some variation between the conditions can be observed, especially at day 16. It seems that the cells grown in LM scaffolds had the highest proliferation during day 5 time point. Another observation is that cells grown in LM 511 50 µg/ml have a tendency to higher proliferation than cells grown in LM 411 50 µg/ml hydrogels at day 16. The result for LM 411 10 µg/ml has a higher normalized value than LM 411 50 µg/ml. This could be a result of adjusted value for the hydrogel with lower concentration of LM but when comparing the result with the collagen hydrogel they seem to be similar. For that reason, an explanation is that the low concentration of LM in the hydrogel does not significantly affect the cellular viability, Another explanation to the result is that the LM has not sustained in the hydrogel throughout the differentiation and therefore been washed away in medium changes.

#### 4.3.2.2. Live/dead staining

The images from the Live/dead staining from both time points are visualized in Figure 45. All of these images have spread cells expressing calcein staining and no obvious difference can be seen between the images. Images K and L represent LM 411 10 µg/ml and ELP coating respectively at time point day 16. Comparison between 3D and 2D growth can be done by these images and both have satisfying cellular morphology and high viability. An interesting feature for the cell grown on ELP coated well is that they seem to form compartments. This might be because there is some artifact on the glass or that this formation is more beneficial for the cell cluster. During measurements in the confocal microscope a problem with the penetration depth occurred. Some areas of the hydrogels were too thick and could not be imaged. This is probably because the cells had contracted the hydrogel.

#### 4.3.2.3. Non-linear images

Pure hydrogels, without any entrapped cells, were cast and visualized with the non-linear microscope. The purpose with this experiment was to investigate if any signal could be detected from LM or if LM changed the structure of the collagen fibers within the hydrogels. The filters used during these experiments were chosen as 405/10 nm in forward, 514/30 nm in epi-side and 661/20 nm in epi-straight. With this setup, SHG signal from collagen can be

detected from 817 nm laser in forward direction and the filter of choice for epi-side collects autofluorescence that might arise during measurements. The results from these measurements are displayed in Figure 46 where the red signal is generated from the forward scattering and the green signal is generated from scattering in epi-side direction. The images show that the signals is mostly collected in the forward detector and that no obvious difference can be seen in hydrogels containing LM (B-F) and the collagen hydrogel (A). The signals that are generated also seem to be generated from fiber structures which mean that the signals most probably are generated from collagen and not LM.

The cells with live/dead staining were once again imaged, but this time with the non-linear microscope one day post staining. As can be seen in Figure 47 (A-D), the signal from calcein (green) is still present inside of the cells. However, the EthD-1 which binds DNA was supposed to be detected in the blue channel but instead some other features were revealed in this channel. The signal was not considered to be generated from EthD-1 since the nucleus inside the calcein stained cells was well imaged and the cells seemed to have intact cellular integrity. As can be seen in the images, the signals were also generated within the cytoplasm which indicates that it is not DNA bound EthD-1 in compromised cells which is imaged.

For that reason, unstained cells were examined with the same settings and the signal pattern is also visualized in these cells, as can be seen in images E-G. The presence of these features in unstained samples indicates that the signal is generated from endogenous structures within the cells. The signal was detected with the epi-straight detector which indicates that the signal is within the red spectra. The unstained cell images also clearly show that the signal came from features which were organized in a specific ring-shaped structure in the cytoplasm of the cells.

In order to specify the signal, it was examined in cells grown in the LM 411 50 µg/ml hydrogel from the time point at day 5. The results from these measurements can be seen in Figure 48. In image A, both beams were guided into the sample and the ring structure from the blue channel is clearly visible. However, in image B the 1064 nm laser was blocked and in image C the 817 nm laser was blocked. The beam blocking removes the signal in (B) and in (C) all signals are lost. This result indicates that the signal requires both beams simultaneously. The time decay from the signal when no beam was blocked was also investigated and is presented in image D. In this image, the low peak with stretched time decay is collected from the green channel and the shape of the histogram is typical for autofluorescence.[89] The signal from the blue channel has faster time decay and generates a sharp peak in the histogram. The time decay of this signal is approximately sub nanosecond and based on previously published data this is the typical time decay for a CARS signal.[90]

The structure was examined by zooming in on one of the cells in the lower right corner of image A in Figure 48. A z-stack revealed that the structure was composed of several small, round, granules. A slice of this stack is presented in Figure 49. The diameter of 15 granules, that could clearly be distinguished, was measured and the results of these measurements and the average diameter is presented in Table 11. The diameters ranging between 770-1244 nm are roughly the same length as the wavelengths of the lasers used (817 nm and 1064 nm). Their quite small size also conforms with the fact that scatter from small object should give a strong CARS signal in epi detection.[91]

With these results in mind, it was of high relevance to investigate if the granules increased in size over time. An enlargement in size could indicate that the cells were actually differentiating towards another cell type than the aiming β-like cells. For that reason, cells from each condition were also investigated at day 16 of differentiation and a comparison to the cells from time point at day 5 is presented in Figure 50. In these images the red signal is SHG from collagen which indicated that the images were taken inside of the hydrogel. However, some of the hydrogels were very dense due to contraction and the collagen fibers

were difficult to image. An enlarged image of cell grown in LM 411 10 µg/ml hydrogel is presented in image K and is considered to be representable for all hydrogels at day 16. The other enlarged image, image L, visualizes cells grown on ELP coating. Neither of these images reveals a notable enlargement of the granule size over time.

In order to dismiss this finding being solely hydrogel related cells grown outside of the hydrogels were examined and presented in Figure 51. Result from the collagen hydrogel is displayed in image A of Figure 51 and cells grown on ELP coating are once again displayed in image B. An image comparison reveals that the distinct structure also is generated in cells grown outside of the contracted hydrogel and therefore the structure is not due to the hydrogel composition.

#### 4.3.2.4. Neutral lipid staining- Bodipy

The cells used in this project are derived from human adipose tissue and therefore one explanation to these granules is that they are small lipid droplets which also would explain the CARS signal. For that reason, cells differentiated to day 16 were stained with the fluorescence dye Bodipy which visualizes neutral lipids. Hoechst staining was also included in the experiment in order to visualize the nucleus, the result can be seen in Figure 52. Cells with Bodipy staining (grey) can be seen in all conditions. A zoomed in image of a cell in the LM mix 50 µg/ml hydrogel is displayed in image H. The small lipid droplets can clearly be distinguished and they seem to be located at the same position as from where the CARS signal was generated in the cells examined in the multimodal microscope. These findings of neutral lipids in small clusters inside of the cells indicate that the lipids are stored and might not interfere with the cellular function.

#### 4.3.2.5. C-peptide ELISA assay

The calibration curve which was included in for the C-peptide ELISA was too high ranged for the intensity values measured from the samples. For that reason, the calibration curve was modified by removing the two highest concentrations and adding the blank as a calibrator. Further, the regression model was constrained at 4.71 pmol/L which was the concentration for the first original calibrator. This might not be an optimal approach for analyses. However, it was considered as the best suited approach for these analyses under the circumstances given.
A comparison between the original and modified regression model can be seen in APPENDIX F.

The results generated from the measurements are presented in Figure 53. In this figure the intensity is not normalized to cell number. A first observation is that some of the conditions have negative concentration which is an error that most probably has to do with the regression model. The bars in the chart are based on two measurements which generated quite large standard deviation. It might be that the incubation time needs to be increased during the GSIS so that the glucose has enough time to diffuse into the hydrogel and thereafter for the C-peptide produced after pre-insulin cleavage to diffuse out to the supernatant. Further the detection limit for the assay is 2.5 pmol/L which means that all measurement of 2.5 pmol/L and below should be considered as noise rather than actual results. As can be seen in the diagram, all values except for the EndoC-βH1cells which was included as positive controls are measured below detection limit.

With this knowledge in mind, the conditions that gave a positive response to glucose were still normalized to viable cell number to investigate if any condition indicated a tendency of increased insulin response upon increased glucose concentration. The results from the normalization are displayed in Figure 54. Due to hydrogel losses and undetected C-peptide in many of the conditions it was unfeasible to investigate the response in these conditions. However, the results indicate that the hydrogel which gives the highest response is the laminin

mixes. Results from the LM mix 10 µg/ml hydrogel even gives an increase of C-peptide upon increased glucose level which was the aiming result.

#### 4.3.2.6. Immunocytochemistry assay

Results from the ICC assay were first analyzed with 40x multimodal microscope since MPEF should provide high depth of focus and reduces the photo-damage and bleaching of the fluorophore.

Typical results from these images are presented in Figure 55 where Images A-C and D-F are from the same cells but with different filters and staining. Image A and D are detected in forward with 452/45 nm filter which was used to visualize nucleus with Hoechst staining. Images B and E visualizes Insulin and Sox17 respectively with Alexa Fluor 488 as secondary antibody, detected in epi-side with 514/30 nm filter. C and F are images of PDX1/alexa594 detected in epi-straight with 720 nm shortpass filter. Hoechst, PDX1 and Sox17 were all expected to be found in the nucleus since they are nuclear staining and transcription factors. However, problems arose during the measurements due to excitation overlap of Hoechst and Alexa Flour 488 which made it impossible to conclude the origin of the signal in the 514/30 nm filter. An additional complication during these measurements was the autofluorescence from endogenous structures within cells which also were transmitted in the 514/30 nm filter. This fact made it challenging to distinguish between signal from the Alexa Flour 488 flourophore in the nucleus and autofluorescence in the cytoplasm.

In order to overcome these problems, the cells from the day 16 time point were reimaged 9 days post staining using a confocal microscope. In this microscope three different lasers are being used subsequently to excite the fluorophores separately, which enables more direct excitation and collection. Images were taken on cells which had grown both outside and inside the hydrogel. The results for cells grown in LM mix 50 µg/ml were considered as typical results for all conditions and are presented in Figure 56; other results can be seen in Appendix F. The fact that the unstained cells in image A give signal within the nucleus is probably due to Hoechst staining which has leaked through the cover of the well plate during incubation time or transport. All images are composed of ten images with 1 µm steps which have been z-projected in order to enhance overall signal of the cells. When analyzing the cells stained for insulin and PDX1, image B and E, it can be seen that the cells grown inside the hydrogel seems to give rise to less distinguishable signal than the cells grown outside of the hydrogel. This result may be because the contracted hydrogel became too dense for the cells and not as favorable for differentiation. Other explanations might be that scattering inside the hydrogel reduced the signal or that the position of the cells causes less distinguishable results. When analyzing the signals from cells stained for Sox17 (green) and PDX1 (red) in 2D, image C, some signal of Sox17 was detected even in the cytoplasm of the cells. This result was not expected since Sox17 is a transcriptional factor which should be detected in the nucleus. Investigation of the same staining within the hydrogel showed no obvious co-localization of the signals within the nucleus, image F. However, when comparing image F to the unstained cells in image D, a lot of signal seems to be coming from uncontrolled autofluorescence.

The signals from the cells grown on 2D were also analyzed with the different channels separately, the result from these analyses are presented in Figure 57 together with results from hADSCs at passage 0. These cells were included as controls and has been treated the same as the other cells but without primary antibody. By comparing the control cells, image J-K, to cells treated with antibodies, images B-C and F-G, the majority of the detected signal seems to be originating from bound secondary antibody. However, the control cells indicate some unspecific binding. In the cells stain for PDX1/INS, image A-D, the signal from insulin can be detected in the cytoplasm but the signal from PDX1 which is supposed to be in the nucleus

also seems to be expressed in the cytoplasm. Furthermore, when analyzing the SOX17 staining, image F, there seem to be an enhanced signal co-localized with the Hoechst staining in image E. However, even though the fluorescence in the cytoplasm was less than for the insulin staining, it was still significantly higher than for the control cells. Even in this staining the signal from PDX1, image G, collected in the cytoplasm which indicates that the some of the signal is due to unspecific binding of the Alexa Flour 594 antibody. If there would have been autofluorescence then it should have been detected at the unstained cells in Figure 56. The dislocated PDX1 expression in both staining might be because the primary antibody in this case is a polyclonal antibody and might bind other epitopes which is not investigated in this project.

The signals from cells grown inside of the hydrogel have also been investigated separately and are displayed in Figure 58. Image B and F indicate that some of the cells express insulin. For the Sox17 staining, image C and G, the conclusion is not that obvious since the signal should have been originated from the nucleus. The cells in image F-H seem to be quite round which indicates unhealthy cells and these cells can accumulate endogenous fluorophores which might contribute to the signal. The PDX1 staining is difficult to distinguish in both hydrogels.

Even though the results from the ICC gave a lot of additional information one aspect was not achieved. The results from time point day 16 were supposed to be compared with results from time point day 5. However, since complications arose in the multimodal microscope and time past before the cells were reimaged in the confocal microscope, the cells from the time point at day 5 were not in condition for imaging. The desired result after comparison would have been to seen a decrease of the endodermic marker Sox17 and a regulation of the pancreatic endoderm marker PDX1.

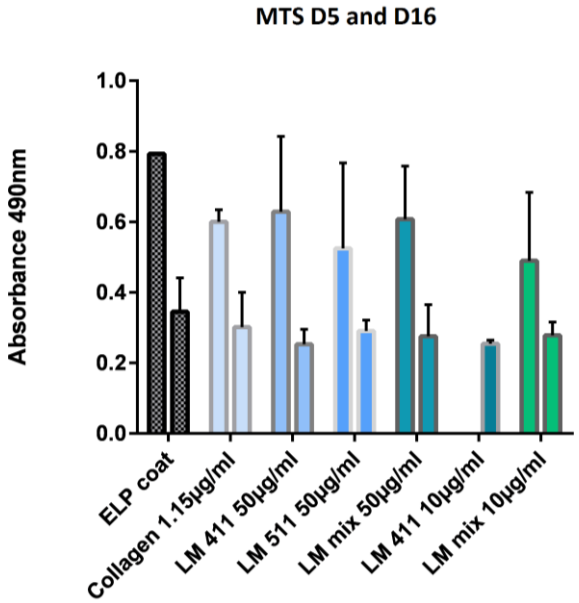


**Figure 43.** Absorbance measurement at 490nm of formazan, a product of MTS tetrazolium. Blank has been subtracted from all measurements. The first and second bar represents measurements at time point day 5 and day 16 respectively.

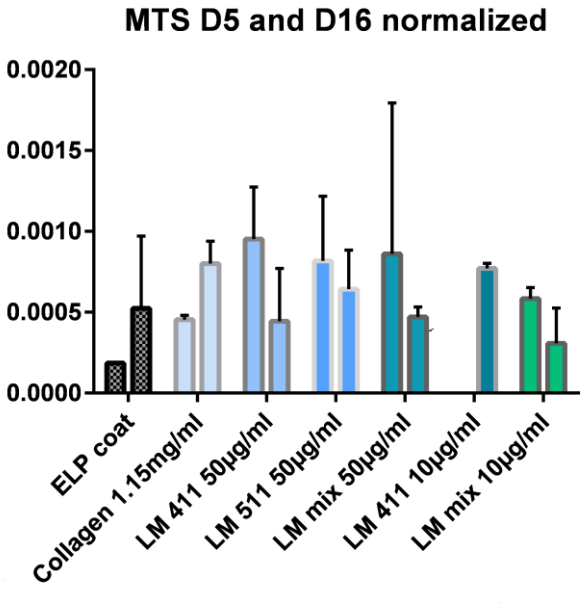


**Figure 44.** Data from metabolic activity assay normalized with cell number counted in Cedex cell counter. The first bar for each condition represent data from time point day 5 and the second bar represent the time point at day 16.

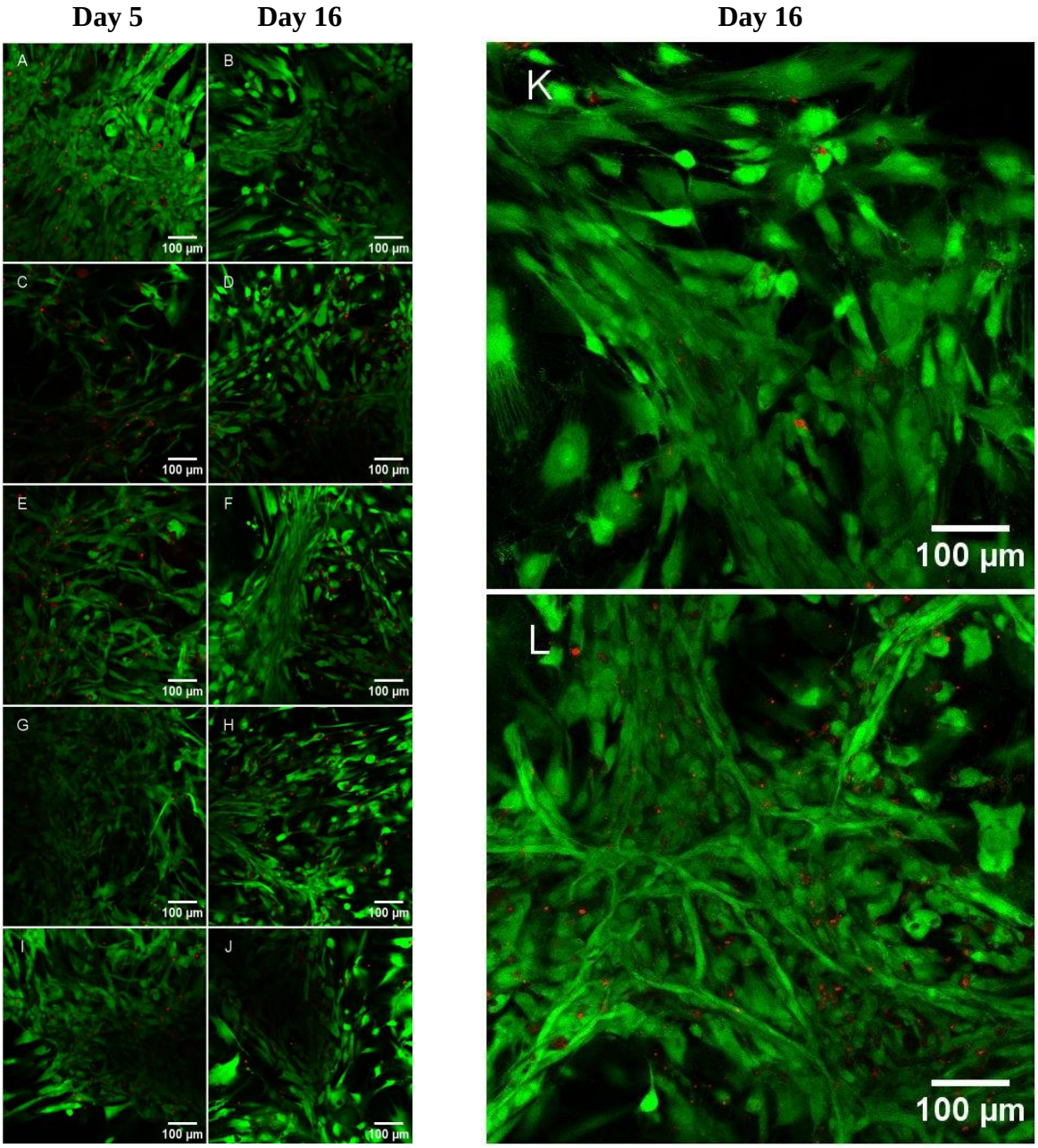


**Figure 45**. 20x confocal images of hADSC at time point day 5 and day 16 of differentiation toward β-like cells. Cells are stained with live/dead staining, Calcein (green) and EthD-1 (red). A-B: Collagen 1.15 mg/ml, C-D: Laminin 411 50 µg/ml, E-F: Laminin 511 50 µg/ml, G-H: Laminin mix 50 µg/ml, I-J Laminin mix 10 µg/ml, K: Laminin 411 10 µg/ml, L: ELP coating. All images are fixed to a gain of 0-4095 counts per pixel for both channels. Images A, C, E, G, I are taken at time point on day 5 of differentiation. B, D, F, H, J, K, L are imaged at day 16 of differentiation. Scalebar in all images are 100 µm.

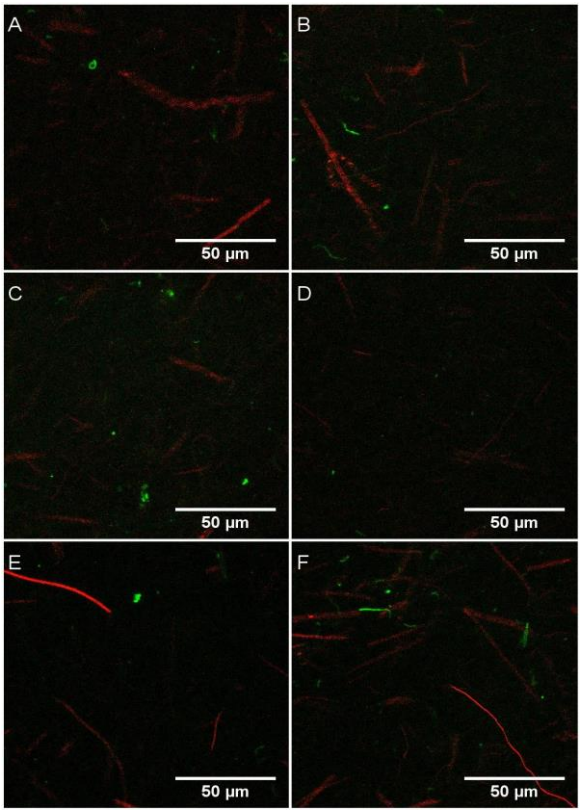


**Figure 46.** 40x multimodal images of hydrogels without cells. Collagen fibers detected in forward direction seen in red (SHG) and in epi-side (MPEF) A: Collagen 1.15 mg/ml, B: Laminin 411 50 µg/ml, C: Laminin 511 50 µg/ml, D: Laminin mix 50 µg/ml, E: Laminin 411 10 µg/ml, F: Laminin mix 10 µg/ml. Laser powers 817 nm: 100 mW, 1064 nm: 120 mW, average: 8, pixeldwell: 5.04 µs, fieldzoom: 143.8 µm, stepsize: 1 µm. All images have the same gain of green: 0.26, red: 0-5 counts per pixel and have been z-projected during analysis.

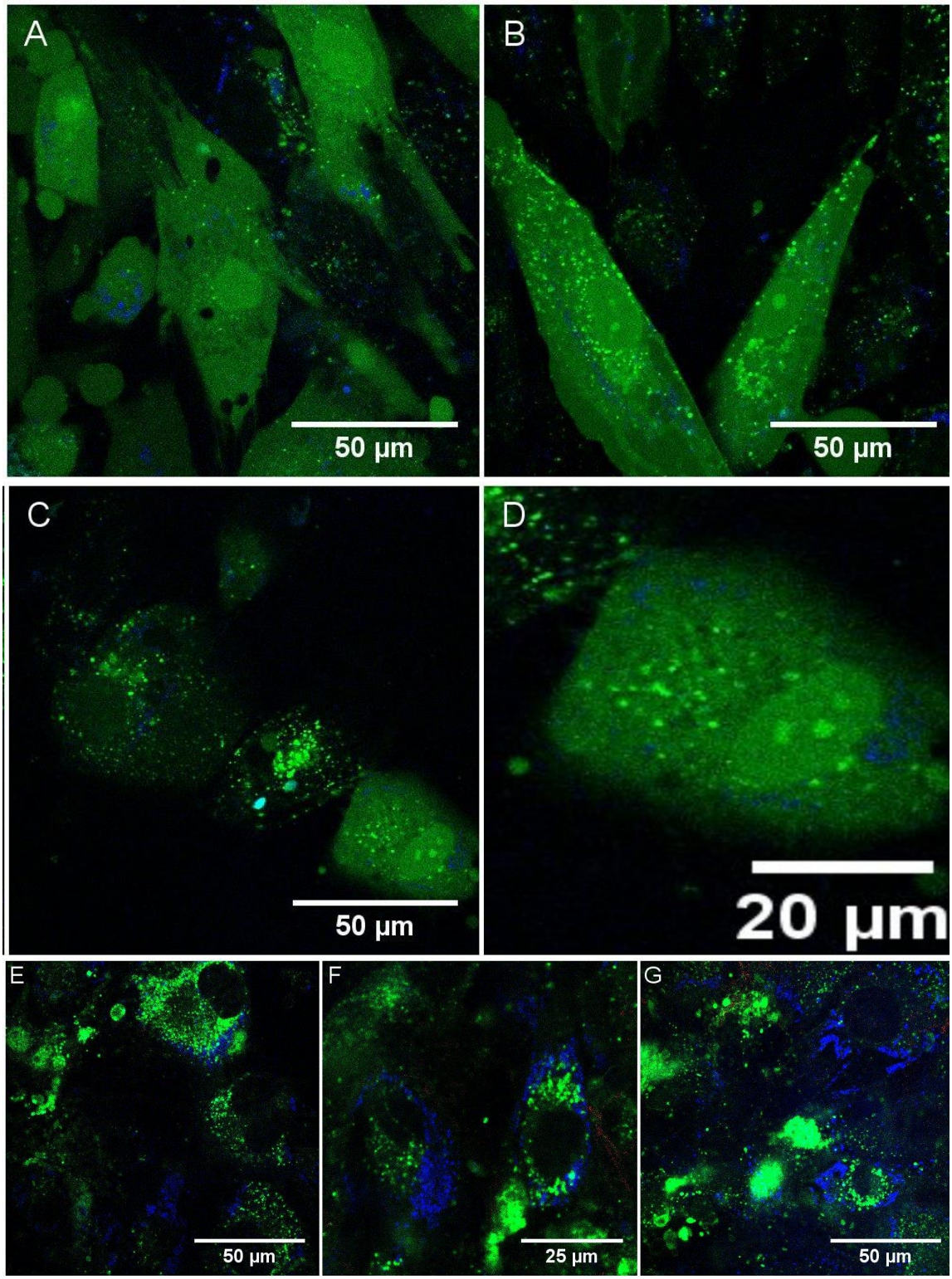


**Figure 47.** 40x Multimodal microscope images of cells from day 5 time point. A-D cells imaged one day post live/dead staining. A: collagen 1.15 mg/ml, B: Laminin mix 10 µg/ml, C-D: Laminin mix 50 µg/ml, D is an enlargement from cell visualized in lower right corner of C. Forward detection of collagen fibers with 405/10 nm filter seen in red (SHG), Epi-straight detection of granules with 661/20 nm filter seen in blue (CARS), Epi-side detection of calcein and autofluorescence with 514/30 nm filter seen in green (MPEF). All four are normalized to same gain, R: 0-1, G: 0-53, B: 0-15 photon counts. E-F cells imaged without staining. E: collagen 1.15 mg/ml, F: Laminin mix 10 µg/ml, G: Laminin mix 50 µg/ml. The gain for each image has been adjusted separately to visualize granules.

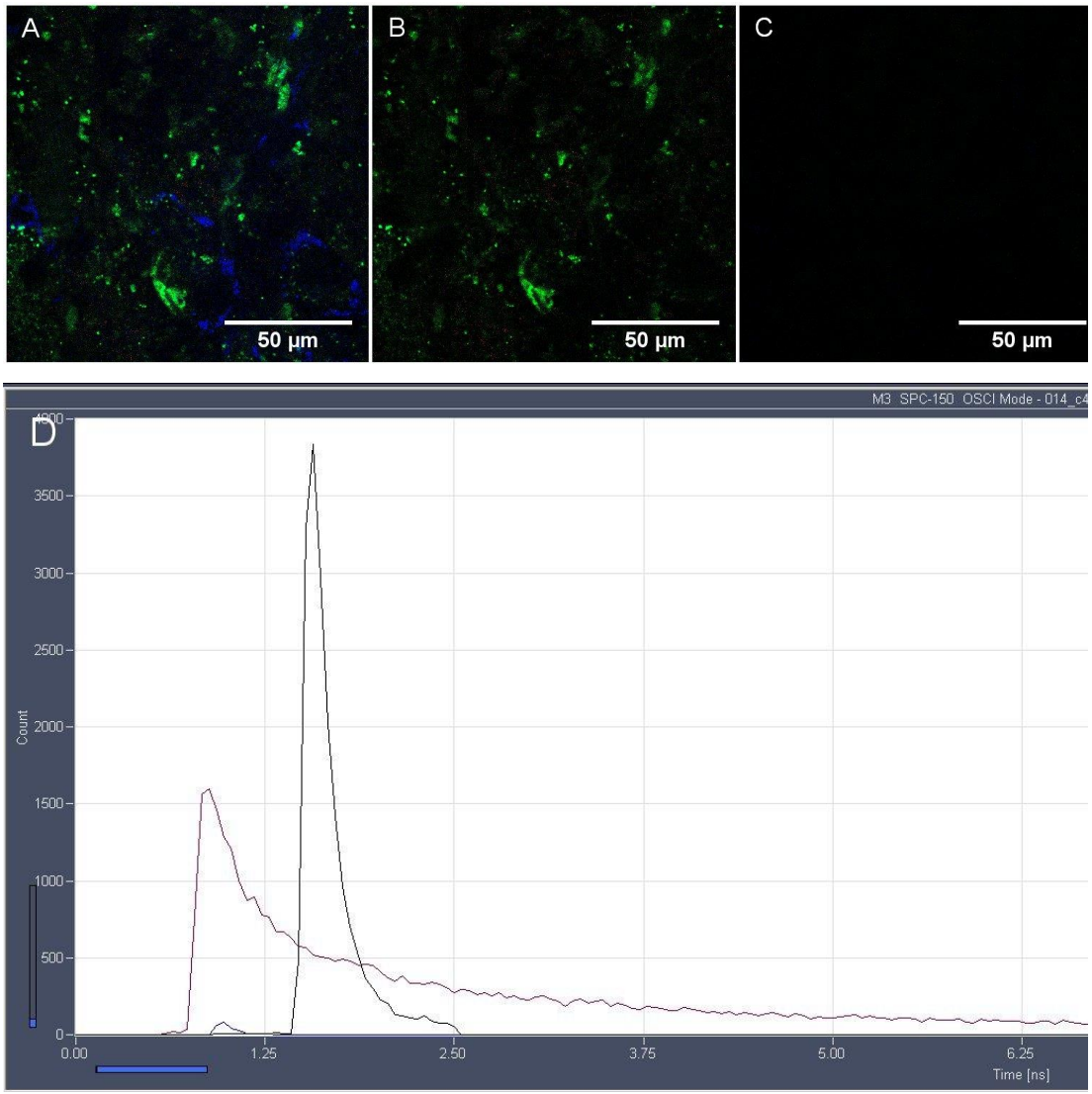


**Figure 48.** 40x multimodal image of cells from time point day 5, grown in laminin 411 hydrogel 50 µg/ml. A: Image generated with both laser beams (817 nm and 1064 nm), B: Image generated with 1064 nm blocked and C: Image generated with laser beam 817 nm blocked. Epi-straight detection of granules with 661/20 nm filter seen in blue (CARS), Epi-side detection of autofluorescence with 514/30 nm filter seen in green (MPEF). Image D visualizes the time decay of the counts in each modal from picture A. The sharp peak correlates to the blue signal and has a maximum at approximately 3800 counts. The second peak correlates to the green signal and has a maximum of approximately 1600 counts. Laser powers: 817 nm 100 mW, 1064 nm 120 mW.

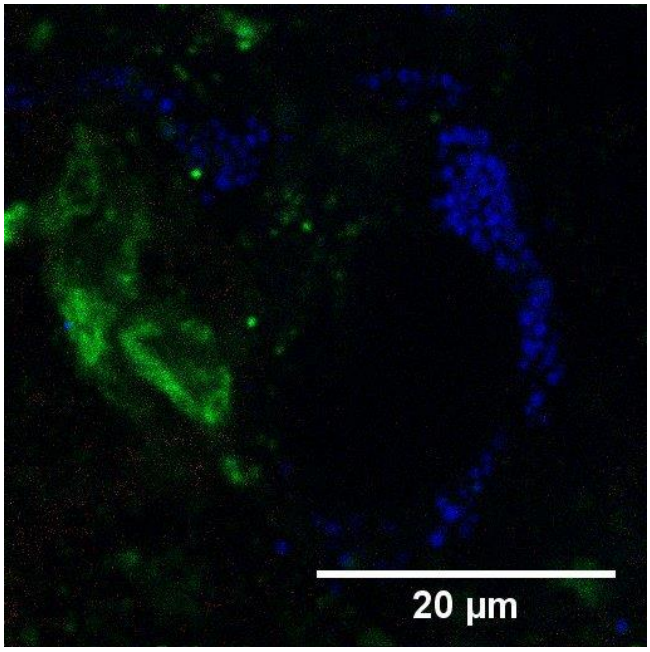


**Figure 49.** 40x multimodal image of cell from time point day 5, grown in laminin 411 hydrogel 50µg/ml. Zoomed in imaged of cell in Figure 48 (A). Measurement of average diameter is based on these granules. Epi-straight detection of granules with 661/20 nm filter seen in blue (CARS), Epi-side detection of autofluorescence with 514/30 nm filter seen in green (MPEF).

**Table 11. Measurement of granular diameter from cell grown in laminin 411 50 µg/ml hydrogel. (n=15)**

| Measurement | Diameter (µm) |
|---|---|
| 1 | 0.912 |
| 2 | 1.051 |
| 3 | 0.984 |
| 4 | 0.886 |
| 5 | 0.984 |
| 6 | 0.926 |
| 7 | 0.770 |
| 8 | 0.815 |
| 9 | 0.939 |
| 10 | 1.214 |
| 11 | 1.244 |
| 12 | 1.162 |
| 13 | 1.013 |
| 14 | 1.073 |
| 15 | 1.132 |
| **Average** | **1.007** |

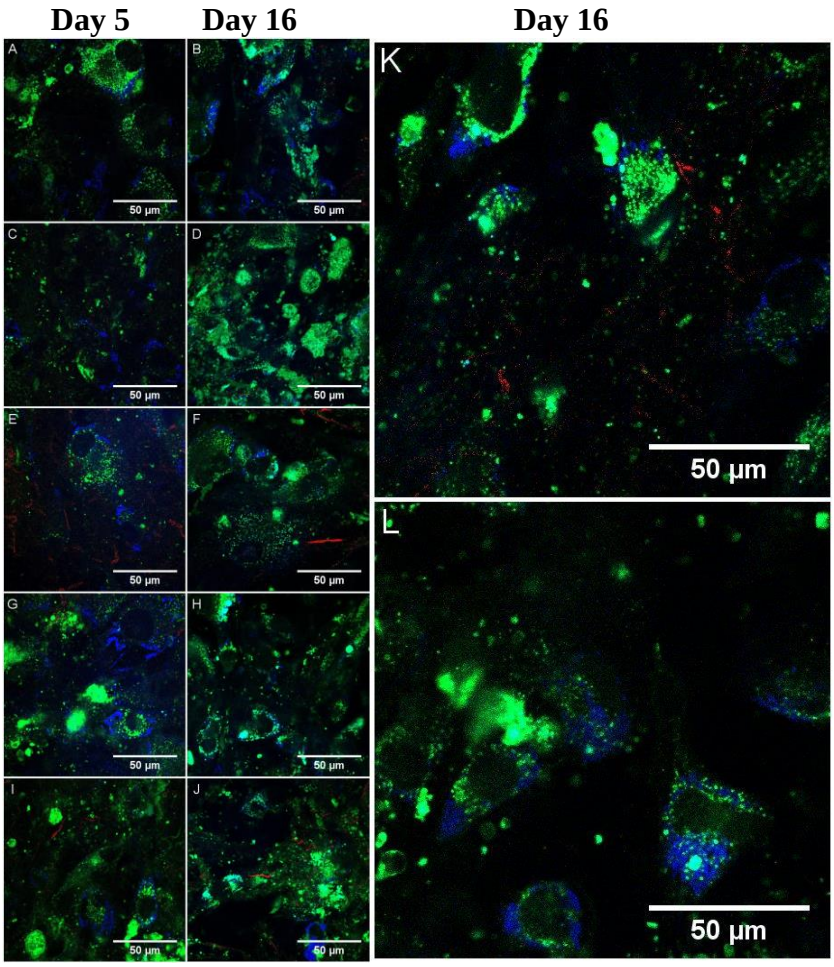


**Figure 50.** 40x multimodal microscopic images of unstained cells at day 5 and day 16. A-B: Collagen 1.15 mg/ml, C-D: Laminin 411 50 µg/ml, E-F: Laminin 511 50 µg/ml, G-H: Laminin mix 50 µg/ml, I-J: Laminin mix 10 µg/ml, K: Laminin 411 10 µg/ml, L: ELP coating. A, C, E, G, I are images from day 5 time point and B, D, F, H, J, K, L are images taken from day 16 time point. Forward detection of collagen fibers with 405/10 nm filter seen in red (SHG), Epi-straight detection of graunles with 661/20 nm filter seen in blue (CARS), Epi-side detection of autofluorescence with 514/30 nm filter visualized in green (MPEF). Gains time point day 5: A (R: 0-2, G: 0-17, B: 0-5), C (R: 0-1, G: 0-32, B: 0-20), E (R: 0-1, G: 0-3, B: 0-25), G and I (R: 0-1, G: 0-30, B: 0-13). All images from day 16 timepoint have the same gain (R: 0-1, G: 0-53, B: 0-15) with the exception of L, which does not have any red signal.

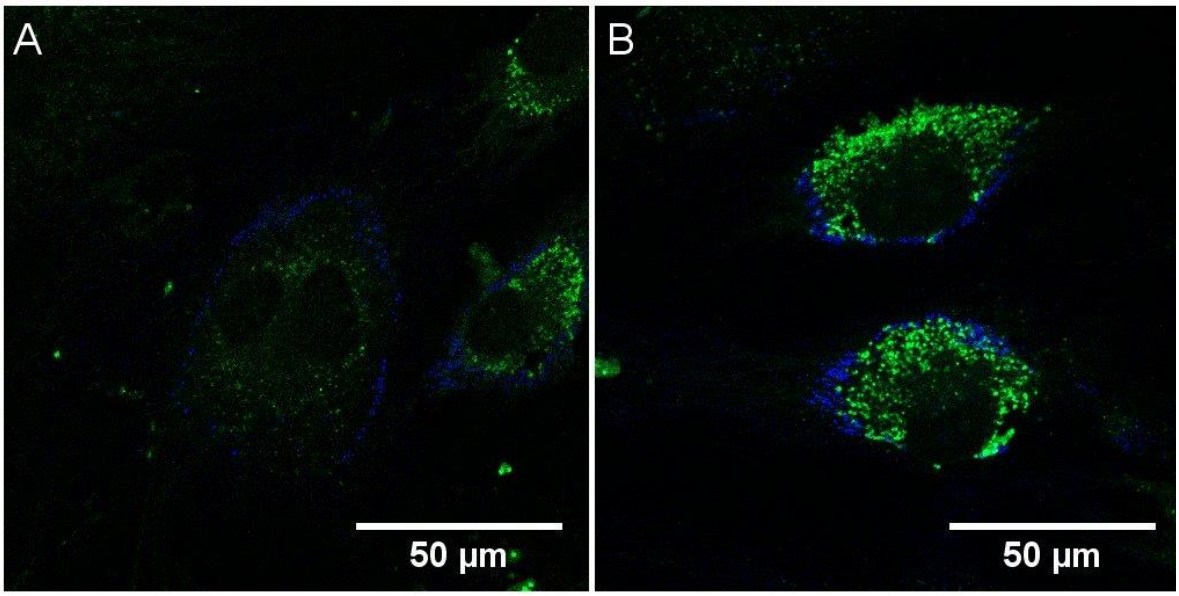


**Figure 51.** 40x multimodal microscopic images of unstained cells taken outside of gel at day 16. A: Collagen 1.15 mg/ml, B: Laminin mix 10 µg/ml. Epi-straight detection of granules with 661/20 nm filter visualized in blue (CARS), Epi-side detection of autofluorescence with 514/3 nm filter seen in green (MPEF). Both have the same gain for the blue modal (0-13) but differs for the green modal, A: 0-30, B: 0-70 counts.

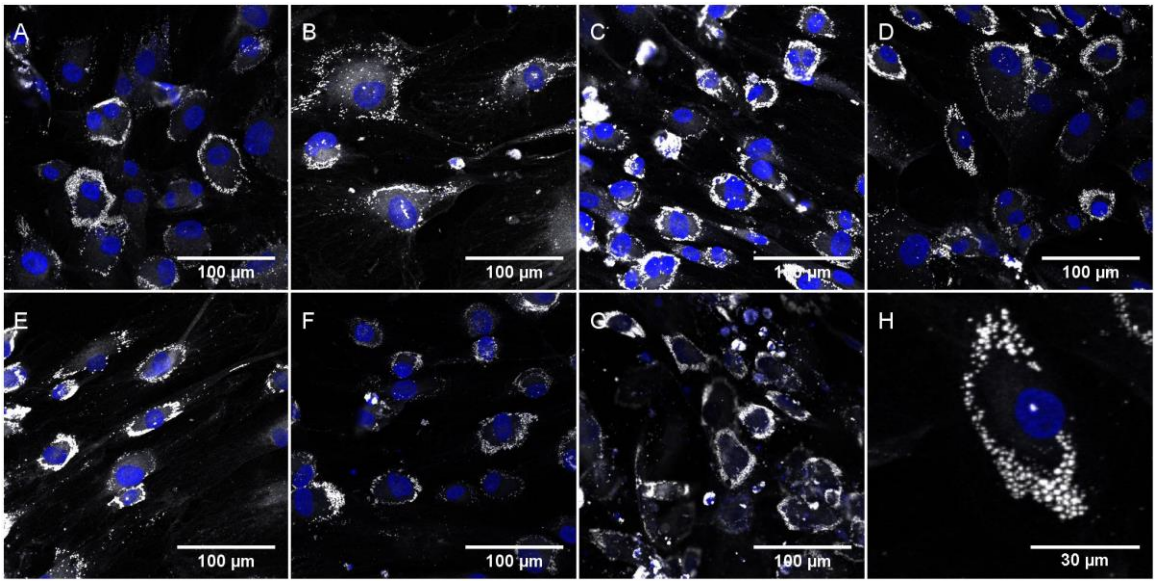


**Figure 52.** 20x confocal images of cells stained with Bodipy (gray) and Hoeschst (blue). A: Collagen 1.15 mg/ml, B: LM 411 50 µg/ml, C: LM 511 50 µg/ml, D: LM mix 50 µg/ml, E: LM 411 10 µg/ml, F: LM mix 10 µg/ml, G: ELP coating, H: zoomed image of cell in D, scalebar: 30 µm. All images are normalized to the same gain.

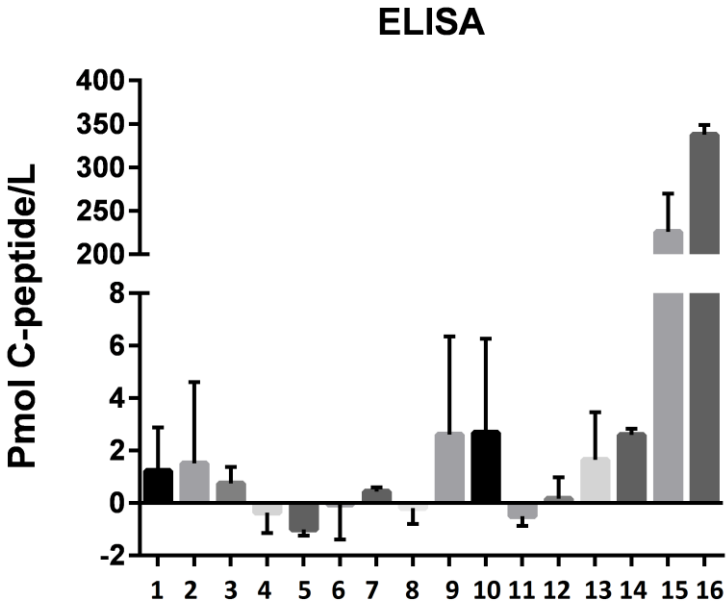


**Figure 53.** The results from the ELISA assay. Each concentration has been measured twice and results are based on regression model, see APPENDIX F. 1: ELP 2.8 mM, 2: ELP 28 mM, 3: Collagen 2.8 mM, 4: Collagen 28 mM, 5: LM 411 50 µg/ml 2.8 mM, 6: LM 511 50 µg/ml 2.8 mM, 7: LM 511 50 µg/ml 28mM, 8: LM 511 50 µg/ml II 2.8 mM, 9: LM 511 50 µg/ml II 28 mM, 10: LM mix 50 µg/ml 2.8 mM, 11: LM mix 50 µg/ml 28 mM, 12: LM 411 10 µg/ml 28 mM, 13: LM mix 10 µg/ml 2.8 mM, 14: LM mix 10 µg/ml 28 mM, 15: EndoC-βH1 2.8 mM (control), 16: EndoC-βH1 28 mM (control).

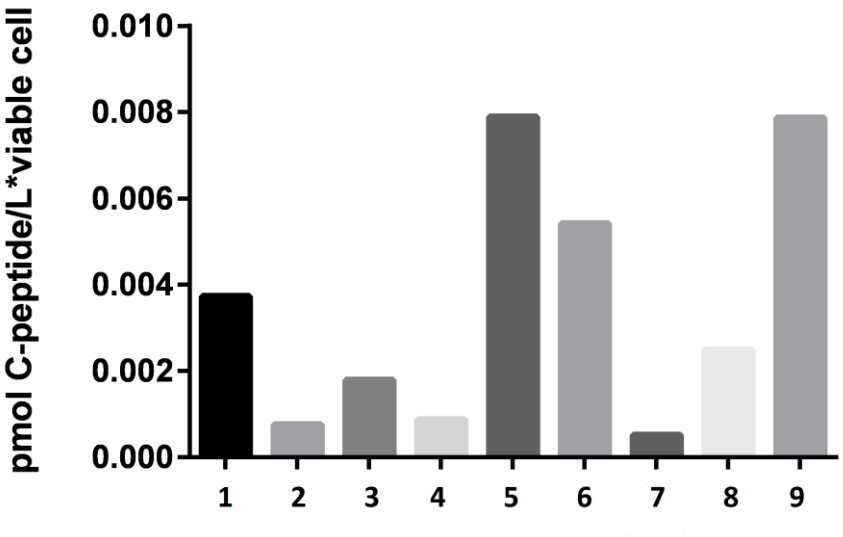


**Figure 54.** Positive concentrations from ELISA assay normalized to viable cell count obtained with CEDEX cell counter. 1: ELP 2.8 mM, 2: ELP 28 mM, 3: Collagen 2.8 mM, 4: LM 511 50 µg/ml 28 mM, 5: LM mix 50 µg/ml 2.8 mM, 6: LM mix 50 µg/ml 28 mM, 7: LM 411 10 µg/ml 28 mM, 8: LM mix 10 µg/ml 2.8 mM, 9: LM mix 10 µg/ml 28 mM

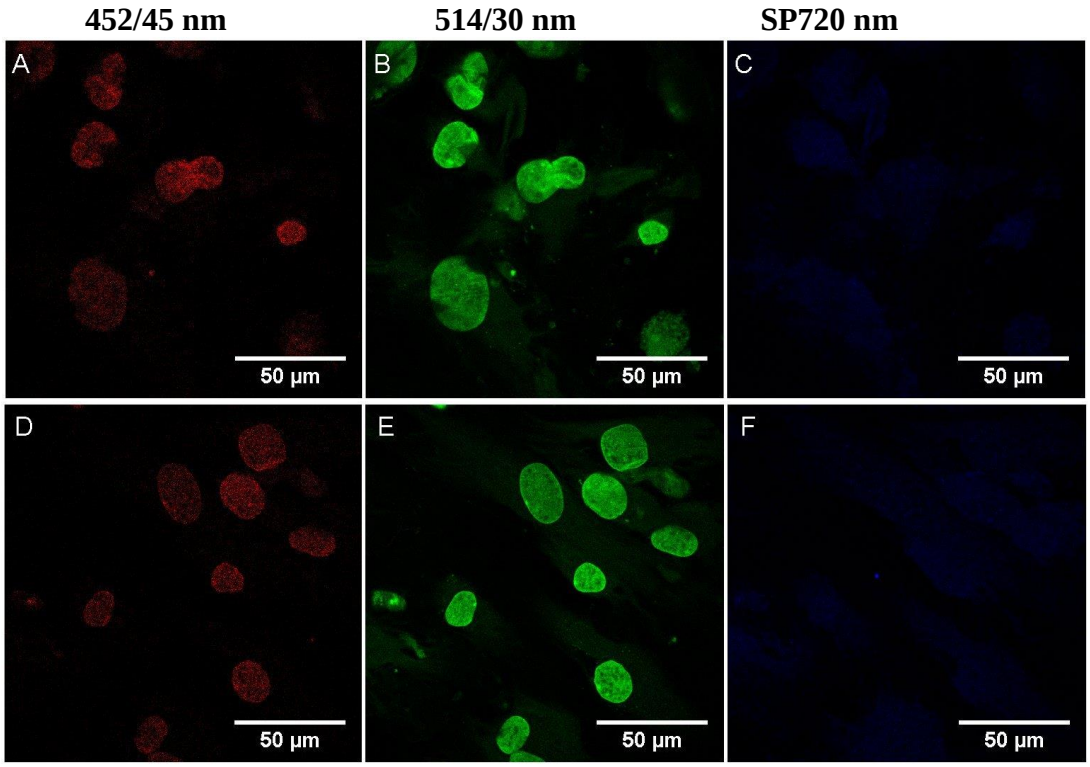


**Figure 55.** 40x multimodal microscopic images of immunolabeled cells taken outside of LM 511 50 µg/ml hydrogel. Images A-C are from the same cells but with different filters. D-F are images of the same cells but with different filters. A and D: Hoechst detected in forward with 452/45 nm bandwidth filter, B: Insulin/Alexa Flour 488 detected in epi-side with 514/30 nm bandwidth filter, C and F: PDX1/Alexa Fluor 594 deteted in epi-straight with 720 nm shortpass filter, E: Sox17/Alexa Flour 488 detected in epi-side with 514/30 nm bandwidth filter.

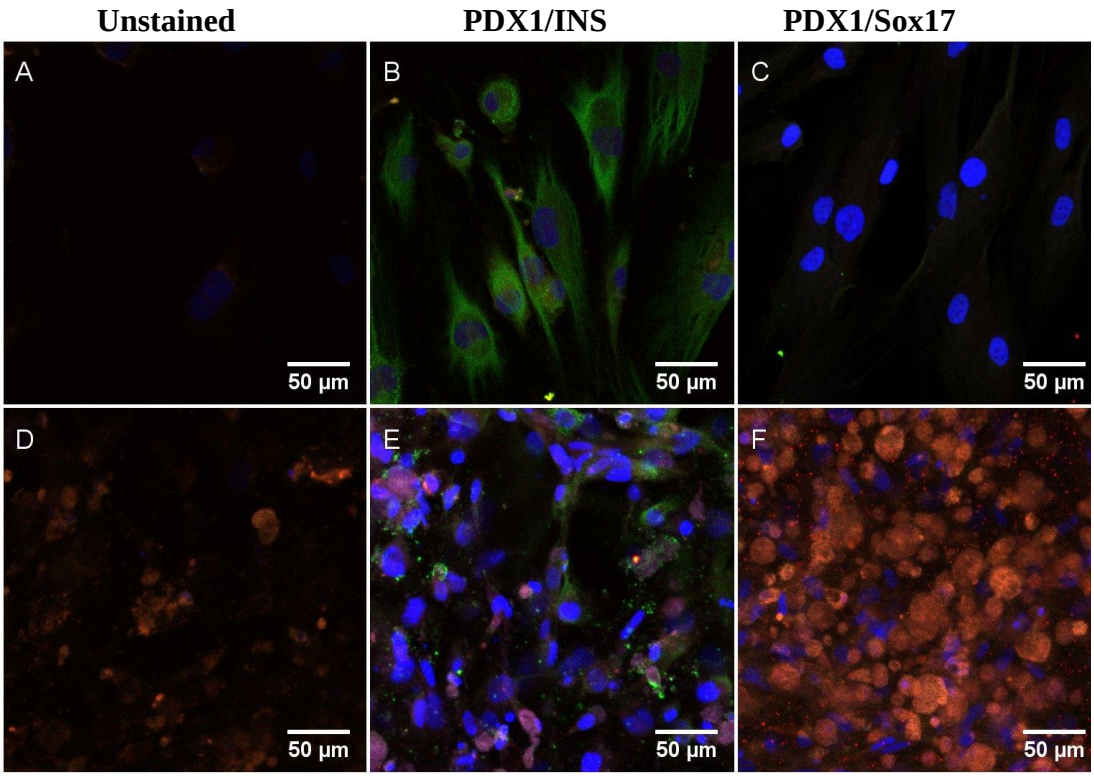


**Figure 56.** 20x confocal images from Immunocytochemisty assay of cells grown in collagen LM Mix 50 µg/ml hydrogel for 16 days. Cells imaged 9 days post staining. Hoechst staining visualized in blue, Alexa Fluor 488 in green and Alexa Fluor 594 in red. A-C are images taken outside of gel. D-F are images from cells grown inside hydrogel. All images have been z-projected in ImageJ.

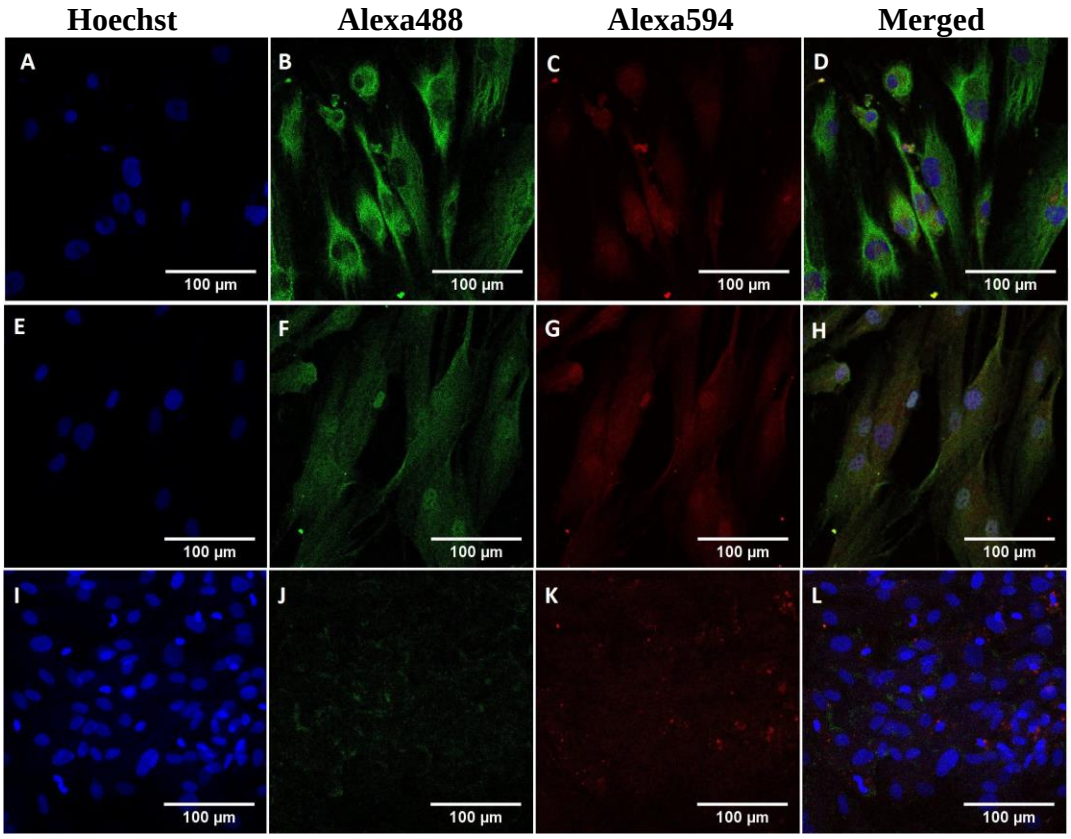


**Figure 57.** 20x confocal images of cells grown outside of collagen LM Mix 50 µg/ml hydrogel for 16 days. A-D: cells with nuclear staining (A) and stained for insulin (B) and PDX1 (C) Image D is a merged image of A-C. E-H: cells with nuclear staining (E) and stained for Sox17 (F) and PDX1(G). Image H is a merged image of E-G. I-L: Control cells (hADSCs P=0) stained nuclear stainin (I) and secondary antibodies Alexa Flour 488 (J) and Alexa Flour 594 (K). Image L is a merge image of I-J.

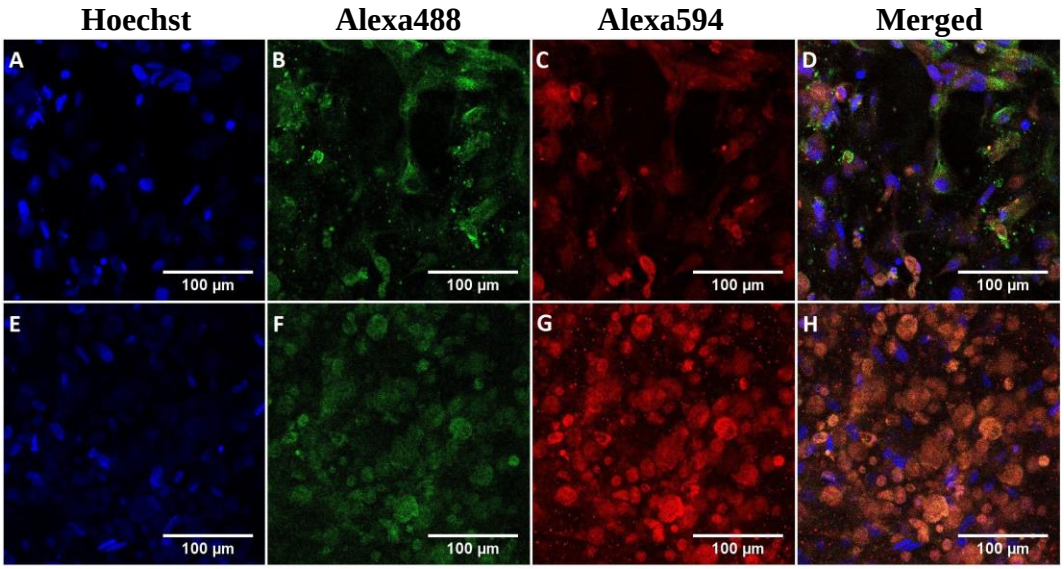


**Figure 58.** 20x confocal images of cells grown inside of collagen LM Mix 50 µg/ml hydrogel for 16 days. A-D: cells with nuclear staining (A) and stained for insulin (B) and PDX1 (C) Image D is a merged image of A-C. E-H: cells with nuclear staining (E) and stained for Sox17 (F) and PDX1(G). Image H is a merged image of E-G

## 4.4. Crosslinker toxicity

In order to investigate if other common crosslinkers might be less toxic, hADSCs were cultured for three days in hydrogels with these compounds. The results from this seeding are presented in this section.

When analyzing the metabolic activity of the toxicity seeding, presented in Figure 59, the value obtained from the THP crosslinked ELP hydrogel is similar to the ELP coating control. This result seems very satisfying since the absorbance value is even higher than the collagen hydrogel control. However, the high metabolic activity of these cells is probably due to degradation of the crosslinker caused by long storage time. This assumption was attained by the fact that no hydrogel was present in the well and that the cells seemed to grow on a 2D surface similar to the ELP coating. ELP crosslinked with THPC show relatively high metabolic activity, but also here, no hydrogels were present making interpretation difficult. The collagen hydrogel without crosslinker does also show relatively high metabolic activity consistent with earlier results. ELP with glutaraldehyde indicate no metabolic activity.
THPC in collagen hydrogel decreases the metabolic activity drastically which indicates high toxicity of THPC. This finding is aligned with the previous results presented in this report and strengthens the argument of crosslinker toxicity in these seedings.

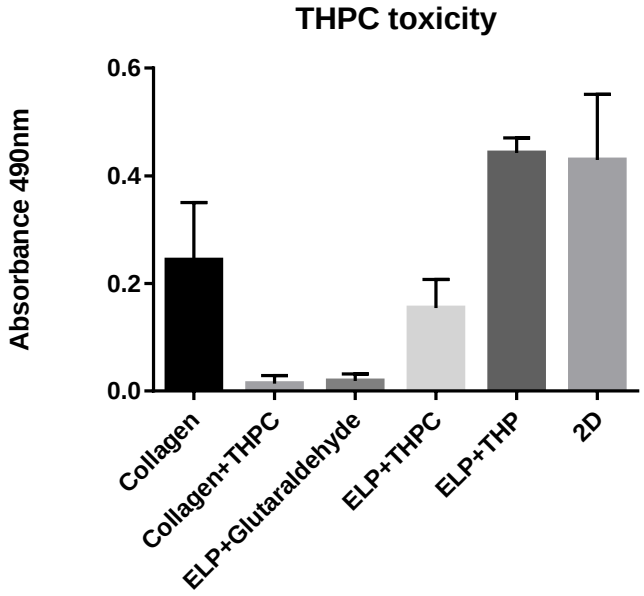


**Figure 59.** In this table results from the proliferation assay of experiment with different crosslinkers are presented. Absorbance has been measured at 490 nm.

# 5. CONCLUSIONS AND OUTLOOK

This section presents conclusions that have been obtained throughout the thesis. First, conclusions from the adipocyte differentiations are presented followed by conclusions from the β-cell differentiations. The main conclusions from the ELP optimization and THPC toxicity trials are also presented.

## 5.1. Adipocyte differentiation

This section discusses the most important findings and conclusions of the work performed and newly developed materials for possible upcoming differentiation experiments are mentioned.

### *5.1.1. First and second seeding*

All results gathered throughout the conducted experiments suggests that ELP crosslinked with THPC in the concentration range that was tested is not suitable for hADSCs and do not provide a good basis for differentiation towards adipocytes. The lowering of ELP concentration as well as THPC ratio did not improve viability or differentiation. Since differentiation has been successful on the other platforms with the same chemical differentiation protocol there is no reason to doubt that this is in fact a suitable working solution for hADSCs toward adipocytes. Instead it is concluded that it is the toxicity of the crosslinker as well as the inability to degrade the ELP matrix during early cell spreading that is causing these results. The ELP hydrogels might also hinder the growth factors from reaching the cells at the same degree as in the 2D and collagen hydrogels due to a denser network of proteins. If this is the case, a higher growth factor concentration might improve differentiation. The fact that hADSCs both spread and differentiate on ELP coated surface but not when seeded on top of an ELP hydrogel indicates that there is THPC molecules present, affecting the cells.

Further experiments with other ways of crosslinking and where a more degradable matrix is used needs to be investigated and new hydrogels are currently developed at our collaboration group at Stanford University (Heilshorn Biomaterial Group). SHIELD is a biodegradable alternative where no chemical crosslinker is needed.[92] Instead a mild physical crosslinking depending on thermoresponsive formation of hydrogel is implemented. MITCH is another biodegradable hydrogel where no crosslinker is needed. This material is "self-healing" with non-covalent bonds with possibilities to disassemble its network making injections possible, where after crosslinking can re-occur, which reshapes the hydrogel network.[93] Adipose derived stem cell survival after injection in mice have been reported using this material.[93] To further improve the differentiation on collagen hydrogels it is likely favorable to include more factors that can mimic the ECM of adipose tissue. It has been shown that adipocytes are surrounded by basal lamina mainly consisting of collagen IV, that is thought to protect the sensitive cells from disrupting the large lipid droplet that constitute almost all of the cellular cytoplasm.[94] That cells differentiate at higher degree if they have contact with the glass bottom suggest that the cells need a stiff contact point in one dimension to differentiate. To investigate cell differentiation without the influence of the glass bottom, seeding the cells in hydrogels on top of cell free hydrogels that have already gelated is suggested. Then the cells would have soft material in all dimensions, even if sinking occurs. A method to solve the problem with contracting hydrogels that increases cell density and thereby complicates investigations of this kind, is to embed the hydrogel with short collagen fibers.[95] E. Gentleman *et al.* successfully differentiated adipocytes in these scaffolds which contracted less and had higher total cell number due to minimized loss of cells.

The live/dead staining has repeatedly shown high live cell presence also in cells with morphology that indicated dead cells. This led to questions to what is possible to conclude from live/dead staining as a viability assay. Knowledge about cell type and morphology can be crucial to be able to discard or accept results correctly.

For the metabolic activity assay, a thorough protocol where material differences in absorbance and hydrogel properties for diffusion are investigated should be made, to attain more consistent results.

The non-linear microscopy methods have proven applicable in investigating adipocytes in hydrogels where several features have been imaged. Lipid droplets and ELP structure have mainly been detected with CARS microscopy and collagen I fibers have been visualized with SHG. The ease of taking the plate from incubator directly to the microscope for imaging, with no need for inconvenient preparations such as staining, have provided good understanding of the benefits with non-linear microscopy.

Collagen I hydrogels and Collagen I / ELP hydrogels have provided the best scaffolds for the continued research regarding of adipocyte differentiation. The presence of ELP adsorbed to collagen in this hydrogel has not been demonstrated and analytical chemical measurements of the composition of this hydrogel are proposed to determine exact constituents.

As final conclusions it have been shown that cells can differentiate in 3D scaffolds, at least to similar degree as on 2D substrates. To obtain fully mature adipocytes *in vitro*, resembling mature native adipocytes, material development in the production of hydrogels with improved properties could be of great importance.

## 5.2. β-cell differentiation

In this section the conclusions that have been obtain in the first and second differentiation of hADSCs toward β-cells are presented.

### 5.2.1. First seeding

Based on the results from the first seeding the most promising hydrogel constituent is collagen. However, since results from the other hydrogels indicate that the gelation time needs to be faster, collagen 37 °C is the most favorable. The time for the metabolic activity assay should be increased since the conversion to formazan might require longer time when cells are encapsulated in hydrogels. A longer incubation time might also decrease the variation between different wells of the same condition. The low metabolic activity of cells encapsulated in ELP hydrogels can be seen already after 5 days of differentiation suggesting that the cells in these hydrogels becomes necrotic and die which is also confirmed in non-linear images.

The picogreen assay did not provide the information which was desirable since no dsDNA was detected in ELP composed hydrogels. This is most probably because the linear regression has too much error in the low range. For that reason the method should be changed to cell counting in CedexHiRes in further studies.

It can be concluded from results of the live/dead stained images and non-linear images that collagen provides a matrix where cells can survive and spread. This result together with the batch-to-batch variation of matrigel supports the decision to exclude matrigel from the experimental setup.

### 5.2.2. Second seeding

Normalization of the absorbance value from the proliferation assay with the cell number from Cedex cell counter seems to give more reliable results than the picogreen assay in first seeding. However, some hydrogels were lost between measurement of absorption and cell counting. It was concluded that this problem is probably due to the hydrogel contraction and that the degree of contraction would be lower if the cell concentration was lower. Lower cell concentrations would give more stable hydrogels and as long as the cells still are in contact with each other this would also give more reliable results for the normalized proliferation assay. However, the result that LM 511 seems to generate better normalized value than LM 411 with 50 µg/ml also agrees with the fact that LM 511 is the isoform which is found in the vascular BM in human islets. Verification of LM in the hydrogels should be performed to fully conclude that the LM is still entrapped within the hydrogels. Nidogens could also be included in the hydrogel composition as crosslinker between the collagen fibers and the LM.

The imaging with non-linear microscopy did not provide any information about the LM inside the hydrogels. The fact that other research groups also have tried to find SHG signals from LM but not succeed[67] strengthen the believe that the signal is solely generated from the collagen fibers.

The non-linear images reveal CARS signals from small lipids within the cells which are also confirmed by Bodipy staining. However, these droplets do not increase in size over times and the ICC indicates that the cells produce insulin. For that reason, the conclusion to these droplets is that they are probably energy stores rather than a sign of wrong differentiation. This conclusion of native lipid droplets inside of cells that are not adipocytes are also confirmed by a study of macrophages inside adipose tissue done by Urasaki *et al.*.[96]

Recommendations for future work would be to passage the cells once prior to seeding. This treatment would hopefully be less harsh to the cells then seeding directly after thawing and would therefore increase the cellular survival throughout the differentiation. Since the pancreatic marker in the ICC (PDX1) seemed to be detected also in the cytoplasm it would be of interest to investigate other pancreatic markers e.g. NKX6.1 to see if this one provides satisfying results within the nucleus. Lastly, all work with collagen has been performed with

collagen I but the most abundant isoform in the pancreas is collagen IV. For that reason it would be interesting to investigate if hydrogels with collagen IV enhances β-cell differentiation and increases the cellular survival.

### 5.3. ELP optimization

We conclude that ELP concentration and THPC ratio does not improve cell viability, suggesting crosslinker toxicity even at lower concentrations. However, a few cells in the 3wt% ELP with 1:1.4 ratio crosslinker density and 6000 cells/µl survived and were considered as successful results. Even though no explanations could be provided to why these cells survived, this condition was determined to be investigated further in upcoming experiments.

### 5.4. Toxicity evaluation

The evaluation of toxicity between different crosslinkers did not provide any alternatives with properties better than THPC. The problems that occurred with gelation surely affected the outcome of this experiment. Conclusions that can be made are that glutaraldehyde is not suitable for hADSC proliferation and that the effect of THP needs to be re-evaluated with fresh THP that is not degraded. A lower ratio of THPC was used in this experiment and this may have been a factor causing the low gelation for ELP hydrogels.

## CONTRIBUTIONS

In this thesis, two main projects have been performed simultaneously. Maria Åström has been performing the β-cell differentiation and therefore also written the texts in this report which involves this differentiation. Additionally, she has been writing the introduction and the background sections, the human pancreas, laminins and Multiphoton excitation fluorescence. Robin Dahlén has been performing the adipocyte differentiation and hence written the text about this differentiation. He has also been the main author for the background sections, collagen, elastin-like protein and coherent anti-Stokes raman scattering.

All other sections not mentioned have been performed and written by both parts with equal contribution. Correction reading and writing has been performed by both parts throughout the report regardless of main project.

## ACKNOWLEDGEMENTS

We would like to express our greatest gratitude toward our supervisors Alexandra Paul and Diana Ribeiro for their guidance, inputs and valuable consultations throughout this thesis as well as for their useful comments and remarks on the thesis writing. Additionally, we would like to thank the molecular microscopy group at Chalmers University of Technology for taking their time supporting us with valuable knowledge in non-linear microscopy. Furthermore, we would like to thank Heilshorn Biomaterials Group at Stanford University for providing us with the bioengineered elastin-like protein. Lastly, we would like to address our sincere gratitude to Anna Forslöw and Annika Enejder for providing us with these projects as well as their precious time consulting us during this thesis.

# REFERENCES


1. World Health Organization. *The Global Eradication of Smallpox: Final Report of the Global Commission for the Certification of Smallpox Eradication, Geneva, December 1979. History of international public health* **4,** (1980).

2. World Health Organization. WHO/UNICEF coverage estimates 2013 revision. (2014). at <http://apps.who.int/immunization_monitoring/globalsummary/timeseries/tswucoveragedtp3.html> (Web: 10 March 2015)

3. Lacy, E. P. *et al.* New Hypothesis of Insulin Secretion. *Nature* **219,** 1177–1179 (1968).

4. Simoni, R., Hill, R. & Vaughan, M. The discovery of insulin: the work of Frederick Banting and Charles Best. *J. Biol. Chem.* **277,** 1–3 (2002).

5. Nobelprize.org Nobel Media AB. The Discovery of Insulin. (2014). at <http://www.nobelprize.org/educational/medicine/insulin/discovery-insulin.html> (Web: 8 December 2014)

6. World Health Organization. *Global Health Estimates: Death by Cause, Age, Sex and Country 2000-2012*. (World Health Organization, 2014).

7. International Diabetes Federation. Complications of diabetes. (2014). at <http://www.idf.org/complications-diabetes> (Web: 10 December 2014)

8. Atkinson, M. A, Eisenbarth, G. S. & Michels, A. W. Type 1 diabetes. *Lancet* **383,** 69–82 (2014).

9. Royal Collage of Physicians (UK). *Type 2 Diabetes: National Clinical Guideline for Management in Primary and Secondary Care (Update)*. (Royal college of physicians, 2008).

10. American Diabetes Association. Type 2 diabetes in children and adolescents. *Pediatrics* **105,** 671–680 (2000).

11. Brännmark, C. *et al.* Increased adipogenesis of human adipose-derived stem cells on polycaprolactone fiber matrices. *PLoS One* **9,** e113620 (2014).

12. WHO. Obesity and overweight. (2014). at <http://www.who.int/mediacentre/factsheets/fs311/en/> (Web: 3 November 2014)

13. Kahn, S. E., Hull, R. L. & Utzschneider, K. M. Mechanisms linking obesity to insulin resistance and type 2 diabetes. *Nature* **444,** 840–846 (2006).

14. Lindgiirde, E. Prevention of Type 2 (non-insulin-dependent) diabetes mellitus by diet and physical exercise. *Diabetologica* **2,** 891–898 (1991).

15. Nathan, D. M. *et al.* Medical management of hyperglycemia in type 2 diabetes: A consensus algorithm for the initiation and adjustment of therapy. *Diabetes Care* **32,** 193–203 (2009).

16. Vachharajani, V. & Granger, D. N. Adipose tissue: A motor for the inflammation associated with obesity. *IUBMB Life* **61,** 424–430 (2009).

17. Lee, J., Cuddihy, M. J. & Kotov, N. a. Three-dimensional cell culture matrices: state of the art. *Tissue Eng. Part B. Rev.* **14,** 61–86 (2008).

18. Straley, K. S. & Heilshorn, S. C. Independent tuning of multiple biomaterial properties using protein engineering. *Soft Matter* **5,** 114 (2009).

19. Aizawa, Y., Owen, S. C. & Shoichet, M. S. Polymers used to influence cell fate in 3D geometry: New trends. *Prog. Polym. Sci.* **37,** 645–658 (2012).

20. Kaido, T. *et al.* Regulation of human β-cell adhesion, motility, and insulin secretion by collagen IV and its receptor α1β1. *J. Biol. Chem.* **279,** 53762–53769 (2004).

21. Otonkoski, T. *et al.* Unique basement membrane structure of human pancreatic islets: implications for beta-cell growth and differentiation. *Diabetes. Obes. Metab.* **10,** 119–127 (2008).

22. Michael E. Symonds. *Adipose tissue biology*. (Springer, 2012).

23. Kahn, B. B. & Flier, J. S. Obesity and insulin resistance. *J. Clin. Invest.* **106,** 473–481 (2000).

24. Trayhurn, P. & Beattie, J. H. Physiological role of adipose tissue: white adipose tissue as an endocrine and secretory organ. *Proc. Nutr. Soc.* **60,** 329–339 (2001).

25. Xu, H. *et al.* Chronic inflammation in fat plays a crucial role in the development of obesity-related insulin resistance. *J. Clin. Invest.* **112,** 1821–1830 (2003).

26. Wellen, K. E. & Hotamisligil, G. S. Obesity induced inflammatory changes in adipose tissue. *J. Clin. Invest.* **112,** 1785–1788 (2003).

27. Lim, J. G. & Atala, A. in *Tissue Engineering From Lab to Clinic* (eds. Pallua, N. & Suschek, V. C.) 521–536 (Springer, 2011).

28. Jain, R. & Lammert, E. Cell-cell interactions in the endocrine pancreas. *Diabetes. Obes. Metab.* **11,** 159–167 (2009).

29. D'Amour, K. A. *et al.* Production of pancreatic hormone-expressing endocrine cells from human embryonic stem cells. *Nat. Biotechnol.* **24,** 1392–1401 (2006).

30. Brissova, M. *et al.* Assessment of human pancreatic islet architecture and composition by laser scanning confocal microscopy. *J. Histochem. Cytochem.* **53,** 1087–1097 (2005).

31. Nikolova, G., Strilic, B. & Lammert, E. The vascular niche and its basement membrane. *Trends Cell Biol.* **17,** 19–25 (2007).

32. Jain, R. & Lammert, E. Cell-cell interactions in the endocrine pancreas. *Diabetes. Obes. Metab.* **11,** 159–167 (2009).

33. Alberts, B. *et al.* in *Molecular Biology of THE CELL Fifth Edition* (eds. Anderson, M. & Granum, S.) 1165–1167 (Garland Science, 2008).

34. Myllyharju, J. & Kivirikko, K. I. Collagens and collagen-related diseases. *Ann. Med.* **33,** 7–21 (2001).

35. Lodish, H. *et al.* in *Molecular Cell Biology* (ed. Tenney, S.) 979–981 (W.H. Freeman and Company, 2000).

36. Antoine, E. E., Vlachos, P. P. & Rylander, M. N. Review of Collagen I Hydrogels for Bioengineered Tissue Microenvironments: Characterization of Mechanics, Structure, and Transport. *Tissue Eng. Part B. Rev.* **20,** 1–14 (2014).

37. Drury, J. L. & Mooney, D. J. Hydrogels for tissue engineering: Scaffold design variables and applications. *Biomaterials* **24,** 4337–4351 (2003).

38. Chen, X. *et al.* Second harmonic generation microscopy for quantitative analysis of collagen fibrillar structure. *Nat. Protoc.* **7,** 654–69 (2012).

39. Timpl, R. *et al.* Laminin-A Glycoprotein from Basement Membranes *. *J. Biol. Chem.* **254,** 9933–9937 (1979).

40. Aumailley, M. *et al.* A simplified laminin nomenclature. *Matrix Biol.* **24,** 326–332 (2005).

41. Durbeej, M. Laminins. *Cell Tissue Res.* **339,** 259–268 (2010).

42. Miner, J. H. *et al.* The Laminin α Chains: Expression, Developmental Transitions, and Chromosomal Locations of α1-5, Identification of Heterotrimeric Laminins 8–11, and Cloning of a Novel α3 Isoform. *J. Cell Biol.* **137,** 685–701 (1997).

43. Biolamina AB. General Laminin Information. at <http://www.biolamina.com/general-laminin-information-1> (Web: 14 December 2014)

44. Lampe, K. J., Antaris, A. L. & Heilshorn, S. C. Design of three-dimensional engineered protein hydrogels for tailored control of neurite growth. *Acta Biomater.* **9,** 5590–5599 (2013).

45. Rodin, S. *et al.* Clonal culturing of human embryonic stem cells on laminin-521/E-cadherin matrix in defined and xeno-free environment. *Nat. Commun.* **5,** 1–13 (2014).

46. Pierschbacher, M. D. & Ruoslahti, E. Cell attachment activity of fibronectin can be duplicated by small synthetic fragments of the molecule. *Nature* **309,** 30–33 (1984).

47. Hern, D. L. & Hubbell, J. A. Incorporation of adhesion peptides into nonadhesive hydrogels useful for tissue resurfacing. *J. Biomed. Mater. Res.* **39,** 266–276 (1998).

48. Wang, H. *et al.* Hybrid Elastin-like Polypeptide − Polyethylene Glycol (ELP-PEG) Hydrogels with Improved Transparency and Independent Control of Matrix Mechanics and Cell Ligand Density. *Biomacromolecules* **15,** 3421–3428 (2014).

49. Ruoslahti, E. & Pierschbacher, M. D. New perspectives in cell adhesion: RGD and integrins. *Science* **238,** 491–497 (1987).

50. Locke, M., Windsor, J. & Dunbar, P. R. Human adipose-derived stem cells: Isolation, characterization and applications in surgery. *ANZ J. Surg.* **79,** 235–244 (2009).

51. Zuk, P. A. *et al.* Human Adipose Tissue Is a Source of Multipotent Stem Cells. *Mol. Biol. Cell* **13,** 4279–4295 (2002).

52. Rosen, E. D. & MacDougald, O. A. Adipocyte differentiation from the inside out. *Nat. Rev. Mol. Cell Biol.* **7,** 885–896 (2006).

53. Rosen, E. D. *et al.* C/EBPα induces adipogenesis through PPARγ: a unified pathway. *Genes Dev.* **16,** 22–26 (2002).

54. Farmer, S. R. Regulation of PPARγ activity during adipogenesis. *Int. J. Obes.* **29,** S13–S16 (2005).

55. Rodriguez, A.-M. *et al.* Adipocyte differentiation of multipotent cells established from human adipose tissue. *Biochem. Biophys. Res. Commun.* **315,** 255–263 (2004).

56. Chandra, V. *et al.* Islet-like cell aggregates generated from human adipose tissue derived stem cells ameliorate experimental diabetes in mice. *PLoS One* **6,** 1–12 (2011).

57. Baer, P. C. *et al.* Human adipose-derived mesenchymal stem cells in vitro: evaluation of an optimal expansion medium preserving stemness. *Cytotherapy* **12,** 96–106 (2010).

58. Murtaugh, L. C. Pancreas and beta-cell development: from the actual to the possible. *Development* **134,** 427–438 (2007).

59. Cherif, H. *et al.* Effects of taurine on the insulin secretion of rat fetal islets from dams fed a low-protein diet. *J. Endocrinol.* **159,** 341–348 (1998).

60. Rezania, A. *et al.* Enrichment of human embryonic stem cell-derived NKX6.1-Expressing pancreatic progenitor cells accelerates the maturation of insulin-secreting cells in vivo. *Stem Cells* **31,** 2432–2442 (2013).

61. Lakowicz, R. J. in *Principles of Fluorescence Spectroscopy* 5–6 (Springer US, 2006).

62. Alberts, B. *et al.* in *Molecular Biology of THE CELL Fifth Edition* (eds. Anderson, M. & Granum, S.) 590–592 (Garland Science, 2008).

63. White, J. G., Amos, W. B. & Fordham, M. An Evaluation of Confocal Versus Conventional Imaging of Biological Stmctures by Fluorescence Light Microscopy. *J. Cell Biol.* **105,** 41–48 (1987).

64. König, K. Multiphoton microscopy in life sciences. *J. Microsc.* **200,** 83–104 (2000).

65. Shuhua Yue, Mikhail N. Slipchenko, and J.-X. C. Nonlinear, Multimodal Microscopy, Optical. **5,** (2013).

66. Monici, M. Cell and tissue autofluorescence research and diagnostic applications. *Biotechnol. Annu. Rev.* **11,** 227–256 (2005).

67. Zipfel, W. R. *et al.* Live tissue intrinsic emission microscopy using multiphoton-excited native fluorescence and second harmonic generation. *Proc. Natl. Acad. Sci. U. S. A.* **100,** 7075–7080 (2003).

68. Tkaczyk, T. S. in *Field guide to Microscopy* (ed. Greivenkamp, J. E.) 111 (SPIE, 2010).

69. Evans, C. L. *et al.* Chemical imaging of tissue in vivo with video-rate coherent anti-Stokes Raman scattering microscopy. *PNAS* **102,** 16807–16812 (2005).

70. Evans, C. L. & Xie, X. S. Coherent anti-stokes Raman scattering microscopy: chemical imaging for biology and medicine. *Annu. Rev. Anal. Chem. (Palo Alto. Calif).* **1,** 883–909 (2008).

71. Volkmer, A., Cheng, J.-X. & Xie, X. S. Vibrational Imaging with High Sensitivity via Epidetected Coherent Anti-Stokes Raman Scattering Microscopy. *Phys. Rev. Lett.* **87,** 2–5 (2001).

72. Zumbusch, A., Holtom, G. R. & Xie, X. S. Three-Dimensional Vibrational Imaging by Coherent Anti-Stokes Raman Scattering. *Phys. Rev. Lett.* **82,** 4142–4145 (1999).

73. Campagnola, P. J. in *Second Harmonic Generation Imaging* (eds. Pavone, F. S. & Campagnola, P. J.) 125–150 (Taylor & Francis Group, 2014).

74. McGilp, J. F. A review of optical second-harmonic and sum-frequency generation at surfaces and interfaces. *J. Phys. D. Appl. Phys.* **29,** 1812–1821 (1999).

75. Raub, C. B. *et al.* Noninvasive assessment of collagen gel microstructure and mechanics using multiphoton microscopy. *Biophys. J.* **92,** 2212–2222 (2007).

76. Chung, C., Lampe, K. J. & Heilshorn, S. C. Tetrakis(hydroxymethyl) Phosphonium Chloride as a Covalent Cross- Linking Agent for Cell Encapsulation within Protein-Based Hydrogels. *Biomacromolecules* **13,** 3912–3916 (2012).

77. Greenwood-Goodwin, M., Teasley, E. S. & Heilshorn, S. C. Dual-stage growth factor release within 3D protein-engineered hydrogel niches promotes adipogenesis. *Biomater. Sci.* **2,** 1627–1639 (2014).

78. Wu, X. *et al.* Preparation and assessment of glutaraldehyde-crosslinked collagen-shitsan hydrogels for adipose tisse engineering. *J. Biomed. Mater. Res. A* **April,** 59–65 (2007).

79. Romano, N. H., Madl, C. M. & Heilshorn, S. C. Matrix RGD ligand density and L1CAM-mediated Schwann cell interactions synergistically enhance neurite outgrowth. *Acta Biomater.* **11,** 48–57 (2015).

80. Rodin, S. *et al.* Clonal culturing of human embryonic stem cells on laminin-521/E-cadherin matrix in defined and xeno-free environment. *Nat. Commun.* **5,** 1–13 (2014).

81. Gefen, A. & Haberman, E. Viscoelastic properties of ovine adipose tissue covering the gluteus muscles. *J. Biomech. Eng.* **129,** 924–930 (2007).

82. Gronthos, S. *et al.* Surface protein characterization of human adipose tissue-derived stromal cells. *J. Cell. Physiol.* **189,** 54–63 (2001).

83. Zhao, Y., Gao, J. & Lu, F. Human adipose-derived stem cell adipogenesis induces paracrine regulation of the invasive ability of MCF-7 human breast cancer cells in vitro. *Exp. Ther. Med.* **6,** 937–942 (2013).

84. Brasaemle, D. L. *et al.* Proteomic analysis of proteins associated with lipid droplets of basal and lipolytically stimulated 3T3-L1 adipocytes. *J. Biol. Chem.* **279,** 46835–46842 (2004).

85. Greenberg, A. S. *et al.* Perilipin, a major hormonally regulated adipocyte-specific phosphoprotein associated with the periphery of lipid storage droplets. *J. Biol. Chem.* **266,** 11341–11346 (1991).

86. Brasaemle, D. L. Thematic review series: adipocyte biology. The perilipin family of structural lipid droplet proteins: stabilization of lipid droplets and control of lipolysis. *J. Lipid Res.* **48,** 2547–2559 (2007).

87. Servetnick, D. a. *et al.* Perilipins are associated with cholesteryl ester droplets in steroidogenic adrenal cortical and Leydig cells. *Journal of Biological Chemistry* **270,** 16970–16973 (1995).

88. Kimata, Y. *et al.* Genetic Evidence for a Role of BiP / Kar2 That Regulates Ire1 in Response to Accumulation of Unfolded Proteins. *Mol. Biol. Cell* **14,** 2559–2569 (2003).

89. Schneckenburger, H. *et al.* Autofluorescence lifetime imaging of cultivated cells using a UV picosecond laser diode. *J. Fluoresc.* **14,** 649–654 (2004).

90. Volkmer, A., Book, L. D. & Xie, X. S. Time-resolved coherent anti-Stokes Raman scattering microscopy: Imaging based on Raman free induction decay. *Appl. Phys. Lett.* **80,** 1505–1507 (2002).

91. Cheng, J.-X., Volkmer, A. & Xie, X. S. Theoretical and experimental characterization of coherent anti-Stokes Raman scattering microscopy. *J. Opt. Soc. Am. B* **19,** 1363–1375 (2002).

92. Cai, L., Dewi, R. E. & Heilshorn, S. C. Injectable Hydrogels with In Situ Double Network Formation Enhance Retention of Transplanted Stem Cells. *Adv. Funct. Mater.* **25,** 1–8 (2015).

93. Parisi-Amon, A. *et al.* Protein-engineered injectable hydrogel to improve retention of transplanted adipose-derived stem cells. *Adv. Healthc. Mater.* **2,** 428–432 (2013).

94. Mariman, E. C. M. & Wang, P. Adipocyte extracellular matrix composition, dynamics and role in obesity. *Cell. Mol. Life Sci.* **67,** 1277–1292 (2010).

95. Gentleman, E. *et al.* Allowing Development of Adipocytic Soft Tissue In Vitro. **12,** (2006).

96. Urasaki, Y. *et al.* Imaging immune and metabolic cells of visceral adipose tissues with multimodal nonlinear optical microscopy. *PLoS One* **7,** 1–8 (2012).

# APPENDIX A

Results from Cedex measurements prior to first seeding of hADSC towards adipocytes.

| | |
|---|---|
| Viable cell concentration (cells/ml) | $2.34*10^5$ |
| Viability (%) | 94.6 |
| Diameter (µm) | 17.48 |
| Aggregate (%) | 26.7 |

# APPENDIX B

Results from Cedex measurements prior to second seeding of hADSC towards adipocytes.

| | |
|---|---|
| Viable cell concentration (cells/ml) | $2.91*10^5$ |
| Viability (%) | 82.8 |
| Diameter (µm) | 17.29 |
| Aggregate (%) | 34.7 |

# APPENDIX C

Results from Cedex measurements prior to first seeding of hADSC towards β-cells.

| | |
|---|---|
| Viable cell concentration (cells/ml) | $2.45*10^5$ |
| Viability (%) | 91.9 |
| Diameter (µm) | 17.61 |
| Aggregate (%) | 27.5 |

# APPENDIX D

Results from Cedex measurements prior to second seeding of hADSC towards β-cells.

| | |
|---|---|
| Viable cell concentration (cells/ml) | $2.91*10^5$ |
| Viability (%) | 82.8 |
| Diameter (µm) | 17.39 |
| Aggregate (%) | 34.7 |

# APPENDIX E

Results from Cedex measurements prior to seeding for the toxicity evaluation

| | |
|---|---|
| Viable cell concentration (cells/ml) | $1.30*10^5$ |
| Viability (%) | 81.3 |

| | |
|---|---|
| Diameter (µm) | 17.14 |
| Aggregate (%) | 34 |

# APPENDIX F

Regression model with original calibrators and modified regression model for ELISA assay.

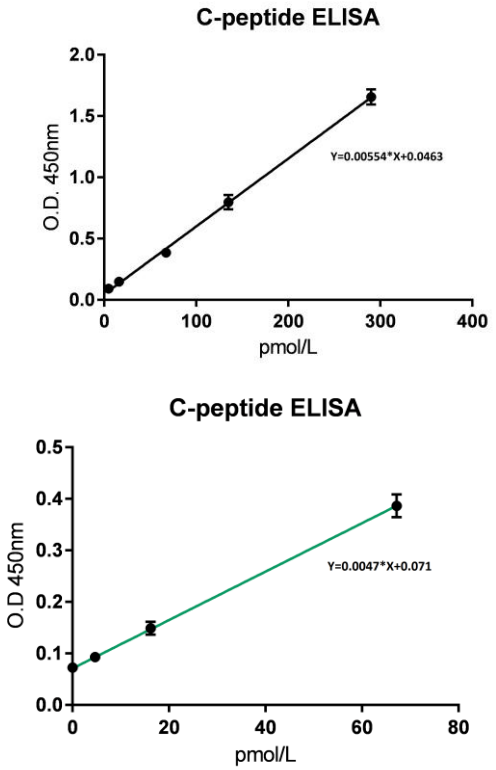


The original calibration curve (top) generated the regression model Y=0.00554*X+0.0463 and the modified (bottom) generated Y=0.0047*X+0.071.

# APPENDIX G

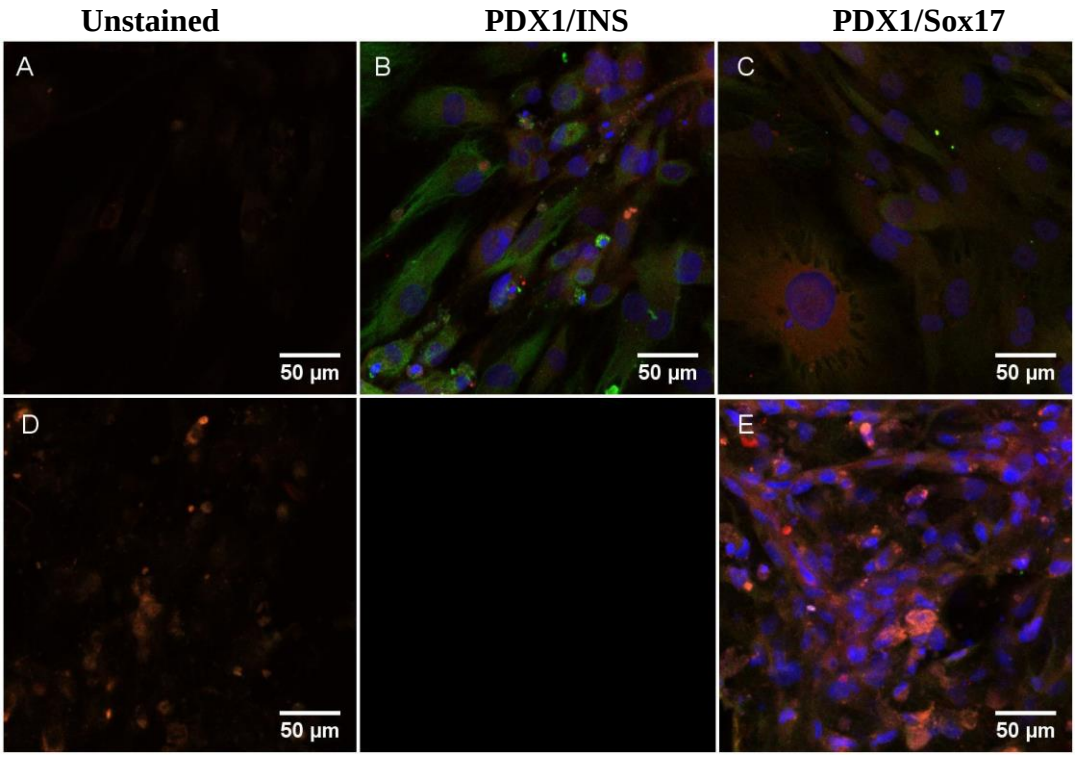


Images from Immunocytochemisty assay of cells grown in collagen 1.15 mg/ml hydrogel for 16 days. A-C are images taken outside of gel. D-E are images from cells grown inside hydrogel. No gel was found for PDX1/INS stained cells. All images are z-projected in ImageJ.

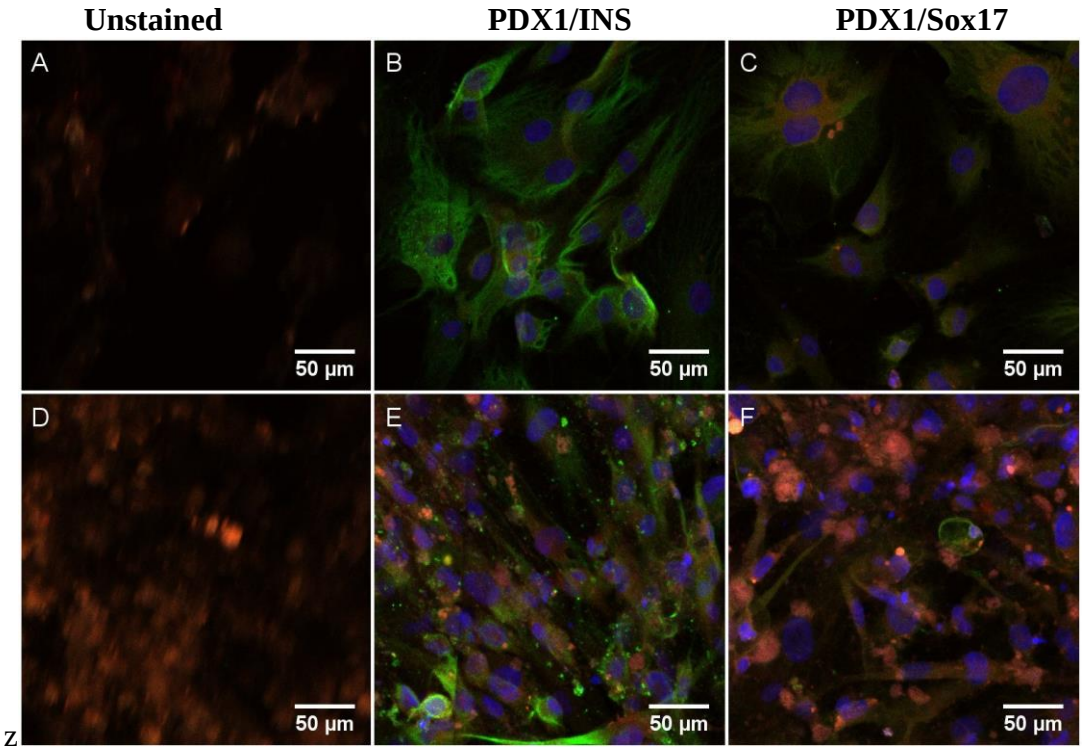


Images from Immunocytochemisty assay of cells grown in Lm 411 50 µg/ml hydrogel for 16 days. A-C are images taken outside of gel. D-F are images from cells grown inside hydrogel. All images are z-projected in ImageJ.

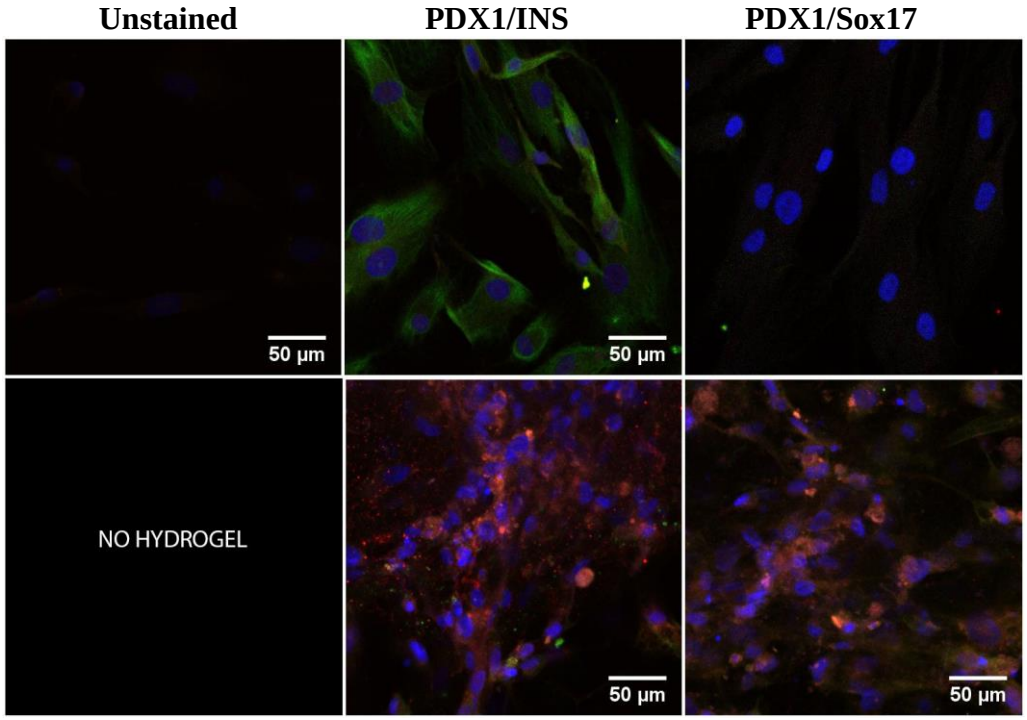


Images from Immunocytochemisty assay of cells grown in LM 511 50 µg/ml hydrogel for 16 days. A-C are images taken outside of gel. D-F are images from cells grown inside hydrogel. No gel was found for unstained cells. All images are z-projected in ImageJ.

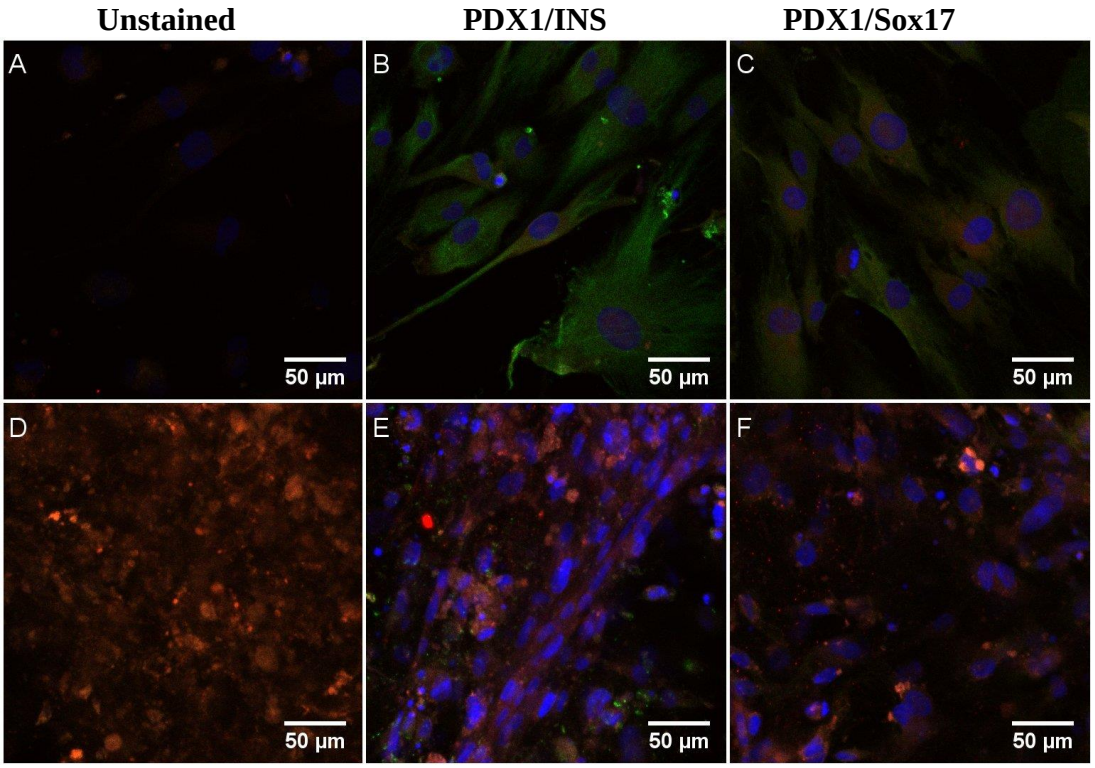


Images from Immunocytochemisty assay of cells grown in LM 411 10 µg/ml hydrogel for 16 days. A-C are images taken outside of gel. D-F are images from cells grown inside hydrogel. All images are z-projected in ImageJ.

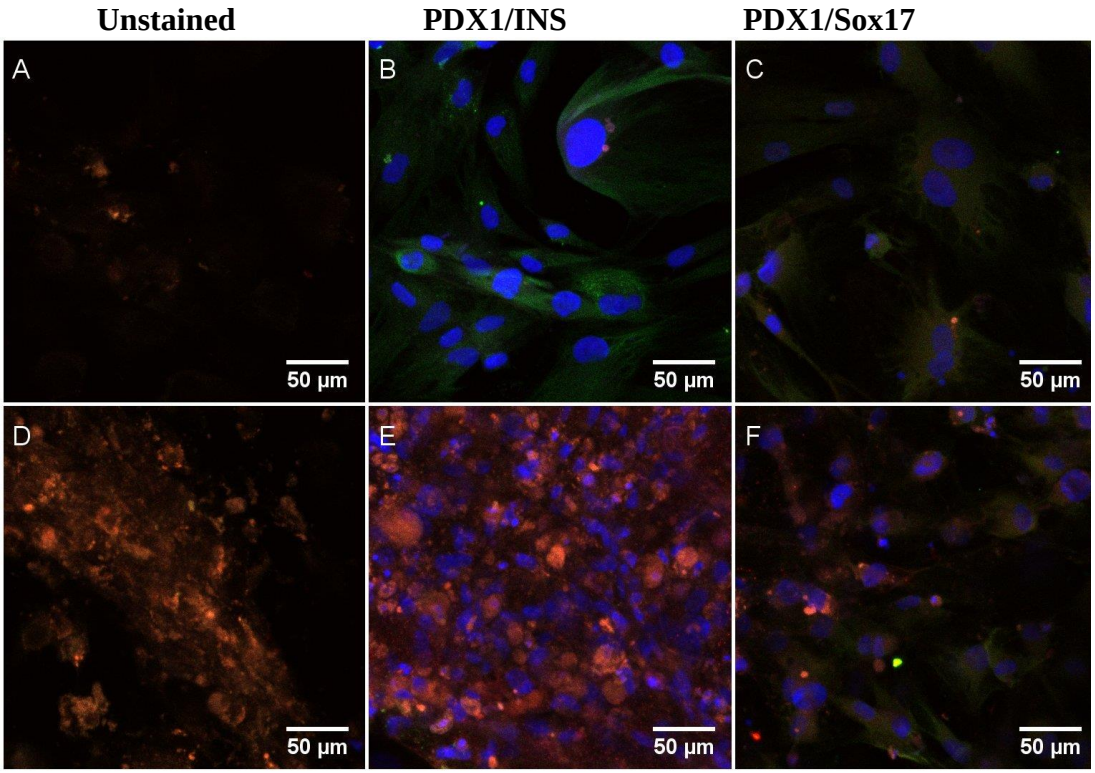


Images from Immunocytochemisty assay of cells grown in LM Mix 10 µg/ml hydrogel for 16 days. A-C are images taken outside of gel. D-F are images from cells grown inside hydrogel. All images are z-projected in ImageJ.

## APPENDIX H

| Condition | Abs. 490nm-average blank | Viable cells / sample | Viable cells (average/condition) | Comment |
|---|---|---|---|---|
| **Time point day 5** | | | | |
| ELP coating | 0.7930 | 4290 | | |
| Collagen I | 0.5753 | 1320 | | |
| Collagen I | 0.6241 | 1320 | | |
| Collagen I +LM 411 50 ng/ml | 0.7798 | 660 | | |
| Collagen I +LM 411 50 ng/ml | 0.4779 | 660 | | |
| Collagen I +LM 511 50 ng/ml | 0.6961 | - | 660 | Hydrogel lost, Average cell number of the condition used |
| Collagen I +LM 511 50 ng/ml | 0.3534 | 660 | | |
| Collagen I +LM mix 50 ng/ml | 0.7140 | 3960 | | |

| | | | | |
|---|---|---|---|---|
| Collagen I +LM mix 50 ng/ml | 0.5005 | 330 | | |
| Collagen I +LM mix 10 ng/ml | 0.6268 | 990 | | |
| Collagen I +LM mix 10 ng/m | 0.3530 | 660 | | |
| **Time point day 16** | | | | |
| ELP coating | 0.2773 | 330 | | Hydrogel lost, viable cells are for GSIS measurements |
| ELP coating | 0.4129 | 1980 | | Hydrogel lost, viable cells are for GSIS measurements |
| Collagen I | 0.2315 | 330 | | |
| Collagen I | 0.371 | - | 413 | Hydrogel lost, Average cell number of the condition used |
| Collagen I +LM 411 50 ng/ml | 0.2229 | 330 | | |
| Collagen I +LM 411 50 ng/ml | 0.2828 | 1320 | | |
| Collagen I +LM 511 50 ng/ml | 0.2682 | 330 | | |
| Collagen I +LM 511 50 ng/ml | 0.3125 | 660 | | |
| Collagen I +LM mix 50 ng/ml | 0.2117 | - | 495 | Hydrogel lost, Average cell number of the condition used |
| Collagen I +LM mix 50 ng/ml | 0.339 | 660 | | |
| Collagen I +LM 411 10 ng/ml | 0.2618 | 330 | | |
| Collagen I +LM 411 10 ng/ml | 0.2469 | - | 330 | Hydrogel lost, Average cell number of the |

| | | | | |
|---|---|---|---|---|
| | | | | condition used |
| Collagen I +LM 511 50 ng/ml | 0.2762 | - | 330 | Hydrogel lost, Average cell number of the condition used |
| Collagen I +LM 511 50 ng/ml | 0.2313 | 330 | | |
| Collagen I +LM mix 10 ng/ml | 0.2516 | 1650 | | |
| Collagen I +LM mix 10 ng/m | 0.3047 | - | 660 | Hydrogel lost, Average cell number of the condition used |